

Energy Research Programme

(Energieforschungsprogramm)

Publishable Final Report

Programme Steering Committee:

Climate and Energy Fund
(Klima- und Energiefonds)

Programme Administration:

Austrian Research Promotion Agency
(Österreichische Forschungsförderungsgesellschaft mbH (FFG))

Final Report

created 2020-02-28

Dynamic Collector Array Test (D-CAT)

FFG project name: MeQuSo

FFG project number: 848766

Citation (APA):

Ohnewein, P., Tschopp, D., Hausner, R., Doll, W. (2020). Dynamic Collector Array Test (D-CAT). Final Report FFG Project 848766 - MeQuSo. Development of methods for quality assessment of large-scale solar thermal plants under real operating conditions. Gleisdorf, AEE INTEC

Call	Energy Research Programme – 1 st submission
Project start	2015-08-01
Project end	2019-06-30
Project duration	47 months
Project coordinator	AEE INTEC
Contact person	DI Philip Ohnewein
Address	Feldgasse 19, A-8200 Gleisdorf
Phone	+43 (0) 3112-5886-0, ext. 255
Fax	+43 (0) 3112-5886-18
E-mail	p.ohnewein@aee.at
Website	www.aee-intec.at

Dynamic Collector Array Test (D-CAT)

MeQuSo. Development of methods for quality assessment of large-scale solar thermal plants under real operating conditions

Authors:

DI Philip Ohnewein
DI Daniel Tschopp, MA BSc
DI Robert Hausner
DI Werner Doll, MSc



Source: Picfly.at Thomas Eberhard



The project MeQuSo was supported by the Austrian Climate and Energy Fund and carried out as part of the Energy Research Programme (FFG 848 766). It addresses the submission focus area “Renewable Energies” (Erneuerbare Energien) with subarea “Solar thermal technologies” (Solarthermie, Schwerpunkt: 3.3). It also addresses focus area “Intelligent Networks” (Intelligente Netze) with subarea “Thermal grids” (Thermische Netze, Schwerpunkt: 4.2). Results have been contributed to IEA SHC Task 55 “Towards the Integration of Large SHC Systems into District Heating and Cooling (DHC) Networks”.

Contents

Abstract	7
1 Introduction	9
1.1 Methodology and structure of this report	9
1.2 Market overview of large solar thermal systems	9
1.3 Necessity of quality assessment	10
1.4 Responsibilities and risk sharing for plant performance	12
2 Existing test procedures and modeling approaches	14
2.1 Scope and use case	14
2.2 Laboratory test procedures for collectors	14
2.3 In-situ testing for collectors and collector arrays	18
2.4 In-situ performance evaluations from operators' perspective	21
2.5 Research need and challenges	23
3 Measurement of test plant “Fernheizwerk” (FHW)	25
3.1 Plant description	25
3.2 Measurement setup	29
3.2.1 Measurement points and sensors	29
3.2.2 On-site installation	29
3.2.3 Calibration and fluid test	32
3.3 External Shading	34
3.4 Continuous quality assurance	35
3.5 Measurement uncertainty	36
4 Overview of the Dynamic Collector Array Test (D-CAT) method	39
4.1 Aim and scope	39
4.2 Main features and characteristics	39
4.3 Use cases	40
4.4 System boundaries and measurement setup	41
4.5 Building blocks	42
5 Plant configuration and data preparation	45
5.1 Data acquisition	45
5.2 Plant configuration	47
5.3 Data pre-processing	50
6 Collector array modeling	52
6.1 Grey box modeling approach	52
6.2 Guidelines in model development	52
6.3 QDT model	54
6.4 D-CAT 1-N model	55
6.5 D-CAT 2-N model	57
6.6 Model validity	60
6.7 Numerical model solution	65

6.8	Model and parameter initialization	66
7	Auxiliary models	70
7.1	Radiation models	70
7.1.1	Overview	70
7.1.2	Internal and external shading of beam irradiance	71
7.1.3	Radiation Decomposition Model (RDM)	72
7.1.4	Horizontal plane to tilted surface irradiance models	74
7.1.5	Tilted sensor model (TSM) and tilted collector model (TCM)	75
7.2	Heat exchanger model	78
7.3	Pipe model	79
8	Parameter estimation	80
8.1	System test and condition monitoring	80
8.2	Optimal data selection	80
8.3	Problem formulation	86
8.4	Optimization	90
9	Application and validation	92
9.1	Practical optimization results	92
9.2	Example results for model behavior	98
9.3	Example results for radiation modeling	102
9.4	Solar yield guarantee	106
10	Discussion and conclusion	108
10.1	Discussion and lessons learned	108
10.2	Conclusion	109
11	Outlook	112
12	Appendix	116
12.1	List of abbreviations	116
12.2	List of symbols	117
12.3	List of figures	120
12.4	List of tables	125
13	References	126
14	Contact	136

Abstract

Large solar thermal plants ($> 500 \text{ m}^2$ collector area, $> 350 \text{ kW}$ thermal power) are an important technology to provide renewable heat. The market has experienced considerable growth in the last decade, with solar district heating (SDH) applications in Denmark as the driving force. Austria has successfully established a market for large solar thermal plants and is home to one of the leading flat plate collector producers in the world.

Building new large solar thermal plants requires high initial capital investment, which is paid back over the lifetime of the plant (typically 20 to 25 years) with the revenue from the produced solar heat. To ensure consistently high solar energy yields over the lifetime of the plant, both quality assurance at the start of the operation phase (commissioning) and on-going surveillance of the collector array performance are essential. If the solar yield is below expectations, possible reasons (weather conditions, malfunctioning components, soiling and dust, plant design, control strategy, inaccurate solar yield simulation) need to be distinguished to identify the responsible party and assess costs and benefits of optimization measures.

The main outcome of the project MeQuSo is a proof of concept of a new in-situ collector array test method called D-CAT (Dynamic Collector Array Test). The method is able to characterize a collector array with a set of parameters that describe the collectors' behavior, based on real-world operating conditions (measurements directly at the installation). D-CAT provides a parameter-based characterization of collector arrays in the field, much like what the quasi-dynamic/Solar Keymark test does for single collectors in the laboratory.

Performance relevant factors which concern the collectors as a component (e.g. soiling, broken insulation, faulty foil tension etc.) are reflected in the test parameters. For instance, collectors with broken insulation or faulty foil tension will have higher heat loss coefficients. The D-CAT method disentangles collector factors from other factors that do not accrue to the collector as a component (e.g. weather conditions, operating conditions, collector array geometry etc.).

The D-CAT method can be used at plant commissioning (comparison with the data sheet), for on-going surveillance (changes in collector characteristics), improved model-based/model-predictive control and to build systematic knowledge on the collector performance under real-world conditions. D-CAT can be used in combination with thermal power and energy yield guarantees to offer clarity between collector manufacturers and plant operators. D-CAT is applicable to collector arrays with flat plate collectors using measurement data from the normal, fully dynamic plant operation without the need to run special test sequences, and without interfering with system control in any way. The test can be run fully automatically and can be repeated easily at periodic intervals, or before and after important plant events.

The "FHW" large solar thermal plant is located in Graz (Austria) and feeds solar thermal energy into the Graz district heating system. In the MeQuSo project, the FHW plant has been equipped with high-precision measurement instrumentation and monitored for three years. Six separate collector arrays consisting of high-efficiency flat plate collectors of five European manufacturers were measured and analyzed.

In MeQuSo, two dynamic collector array models have been developed; these models adapt to the specific needs of collector arrays (vs. single collectors), explicitly modeling the fluid transport along the main flow direction. The models have been validated against experimental data from the FHW plant. The model parameters are estimated using a grey-box approach. In the estimation process, a statistically optimal data selection method is used to obtain those data intervals which contain maximum information for the estimation of the model parameters (lowest-variance and best-separable parameters). The estimation process is based on a global optimization algorithm. The D-CAT method

also has a radiation model which allows calculation of the average beam and diffuse irradiance on the collector array, using only total tilted irradiance as input. This makes the method applicable to typical measurement setups for large solar thermal plants, when only the total tilted irradiance is available. Steps for future work include applying the D-CAT method to a larger number of LST plants and gain experience with D-CAT based KPI calculations as well as long-term performance evaluations. Developing D-CAT as an open source software tool would help to make D-CAT available to other scientific institutes for collaborative development on a European level and disseminate D-CAT on the solar thermal market.

How to read this report: The report starts with an introduction on quality assessment of large solar thermal plants in chapter 1 and then gives an overview of existing test procedures and performance check methods to define the research need in chapter 2. Chapter 3 is dedicated to the measurement of the FHW plant. Chapters 4 to 8 contain a detailed description of the D-CAT method, and chapter 9 shows the application and validation of the method. Chapters 10 and 11 conclude with a summary of the main outcomes, a discussion of lessons learned and an outlook towards further research and applications.

1 Introduction

1.1 Methodology and structure of this report

- This chapter gives a market overview of large solar thermal systems and an introduction on quality assessment.
- The development of the D-CAT method started with an analysis of existing collector (array) models and test procedures to define the research need as described in chapter 2.
- In the MeQuSo project, a large solar thermal plant in Graz, Austria, was equipped with high-precision measurement instrumentation to gain measurement data over the years 2017 to 2019. These data were used in MeQuSo for the development and validation of the D-CAT method. The FHW plant and measurement concept are summarized in chapter 3.
- Chapter 4 gives an overview of the D-CAT method. Chapter 5 explains how to set up the interface in order to apply the D-CAT to a collector array.
- Chapter 6 describes the grey box modeling approach and the model development process that are at the core of the D-CAT method, including numerical model solution and model initialization.
- Chapter 7 explains auxiliary models (most importantly radiation models) used to calculate those inputs for the collector array models that are not directly available as plant measurement data.
- Chapter 8 explains the parameter estimation procedure including optimal data selection an the optimization process.
- In chapter 9, the validation and an exemplary applications of the D-CAT method, as available at this time, are shown.
- Chapter 10 is the discussion and conclusion, and chapter 11 gives an outlook on further developments and research directions.

1.2 Market overview of large solar thermal systems

Solar thermal systems are an important technological solution to provide renewable heat. By the end of 2018, the total installed capacity amounted to 480 GW nominal thermal power (686 million m² collector area) with an estimated annual energy yield of 396 TWh [1]. System sizes range from small installations for single-family houses, medium scale systems for multi-family houses, smaller heating networks and process heat plants, to large-scale systems [2]. Large solar thermal (LST) plants are defined as systems with more than 500 m² collector aperture area or 350 kW nominal thermal power [1] (a factor of 0.7 kW thermal power per m² collector aperture area is commonly used to convert collector area to nominal power [3]).

Worldwide, 339 large solar thermal systems with a capacity of 1.2 GW (1,747,200 m² collector area) were in operation end of 2018 [1]. Although the total installed capacity is small compared to small-scale solar thermal systems, large-scale systems are quickly gaining importance. While the solar thermal market shrunk by 2.8% annually between 2010 and 2018, the market for large-scale systems had an average 15.5% increase per year in the main markets of Denmark, China, Germany and Austria in the same period [4]. Solar district heating (SDH) applications in Denmark have been the driving force for large solar thermal installations. By the end of 2018, a total of 118 plants with a capacity of

970 MW were in operation, making up 63% of the capacity worldwide [1]. Austria has an installed capacity of 27 MW and 23 systems, ranking number four in the world if the two big solar process heat plants in Oman (104 MW) and Chile (28 MW) are not considered [1]. Besides heat supply to district heating networks, the main applications are heat supply to local heating networks with residential, commercial and public buildings and solar process heat [1].

The basic feature of investments in LST plants is a high initial capital investment, which is payed back over the lifetime of the plant (typically 20 to 25 years) with the revenue from the produced solar heat. LST systems make use of economies of scale and can reach specific costs below 200 €/m_{gr}² for ground-mounted collectors [2]. Operation and maintenance (O&M) costs are very low: An estimate based on Austrian experiences sets O&M costs to 0.5% of the investment cost for LST collector arrays [5]. The revenue of large scale solar thermal systems is typically based on a fixed price per produced kilowatt hour solar heat, which the costumer pays to the plant owner, plant operator or energy service company. Achieving low levelized cost of heat (LCOH) is the key success factor for LST plants [6]. Low LCOH requires high solar energy yields, while keeping investment and O&M costs low. It is also crucial to have an accurate prediction of the solar yield during the engineering phase, in order to minimize the investment risk and reduce risk premiums which have a negative impact on the competitiveness of the technology.

1.3 Necessity of quality assessment

Quality assessments for LST plants are used during commissioning and operation to check the condition of the plant and its components, to assess the control strategy and to determine if the plant performance and solar yield matches the expectations. Methods to assess the solar yield date back to the 1980s, when the first LST plants were engineered and built in Sweden and Denmark [7]. The main challenge for quality assessment methods for the solar yield lies in the multitude of factors influencing the solar yield, and the fact that some of these factors are stochastic in nature and expensive to measure with good precision (e.g. solar radiation). The solar yield essentially depends on design, components and operation of the plant, on the customer-side load (thermal power demand and temperature levels) and environmental conditions (solar radiation, ambient temperature, wind), and their interdependencies.

There are a number of possible reasons that lead to deviations between the predicted solar yield/predicted financial profit as calculated in the planning phase and the measured solar yield/financial profit at system operation. The following influencing factors may cause such target/actual deviations (see also figure 1):

- 1) The prediction of the solar yield at the planning stage is done with simulation programs, such as TRNSYS [8] and PolySun [9]. The simulation model needs to be a close enough to the actual plant design.
- 2) Crucial inputs are the efficiency parameters of the components, mainly the deployed collectors. The efficiency parameters of collectors are obtained by testing a collector under standard laboratory test conditions according to ISO 9806 [10], which offers a stationary and quasi-dynamic test procedure and is certified under the Solar Keymark certificate [11]. In recent years, the quasi-dynamic test procedure has gained popularity as its efficiency parameters describe the collector more accurately under non-stationary conditions than the stationary test and consider variable shares of direct and diffuse irradiance. But the conditions of the collectors tested in the laboratory and their operation in the field can be considerably different (soiling of glass cover, less-than-ideal stress of convection barrier foil, vegetation, etc.) and the test results themselves are subject to uncertainties as round-robin tests show [12].

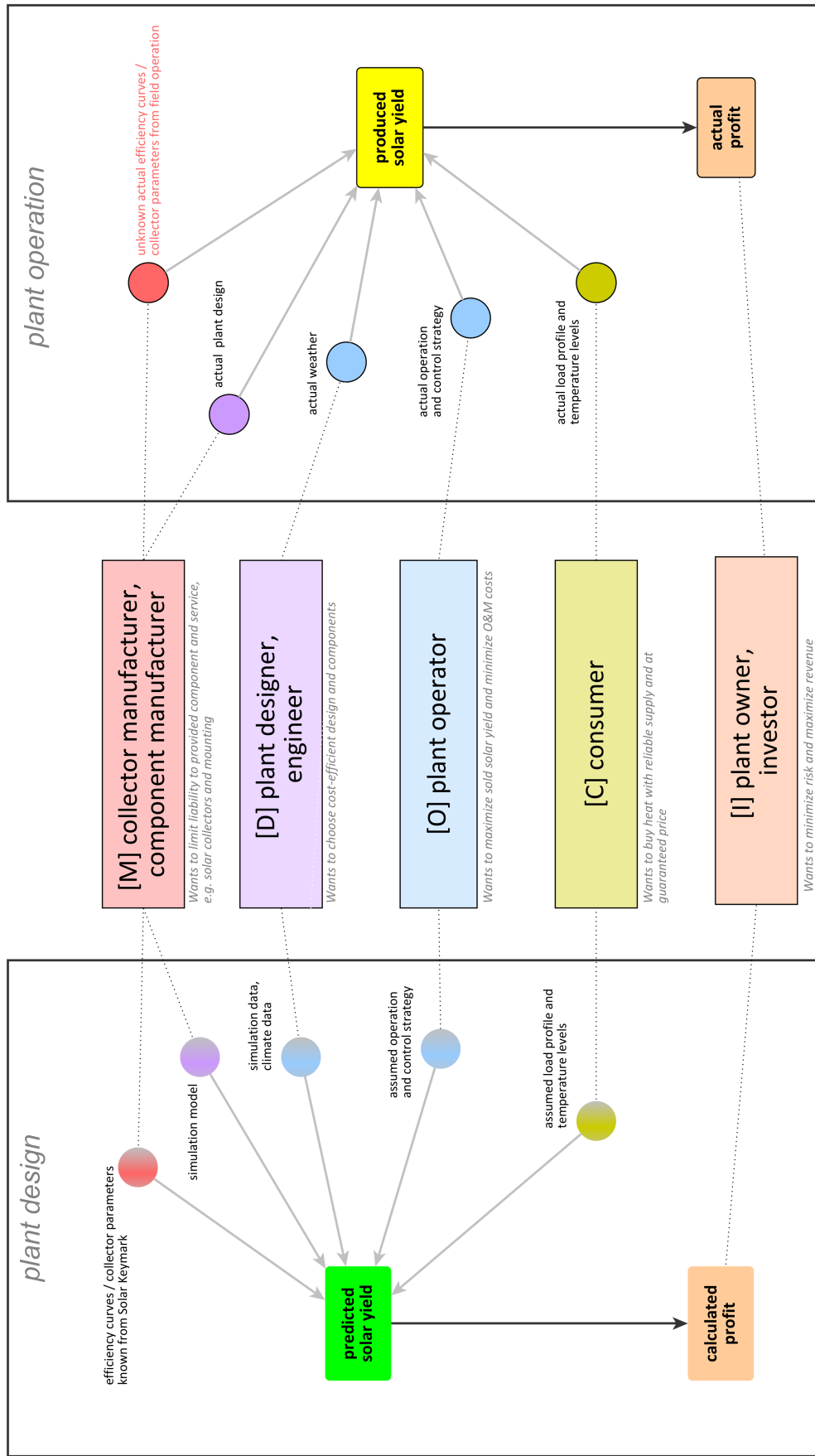


Figure 1: Risk sharing in large solar thermal projects: The main parties involved in the realization and operation of a large solar thermal plant (operator, investor, heat consumer etc.) interact in many ways along the project steps from planning phase to ongoing operation. This figure displays their interests and responsibilities.

- 3) The quality of climate data needs to be thoroughly investigated [13]. Climate stations typically only measure the horizontal global radiation and the decomposition in its direct and diffuse part and the conversion to the tilted surface requires radiation modeling [14]. Climate data are long-term averages and do not account for yearly variations. Many countries face a slow increase of the available solar radiation in recent years compared to standard long-term data for periods like 1961-1990 [15].
- 4) Actual control strategy and operation typically also differs, as the control strategy is usually simplified in simulation tools and the control strategy needs to be adapted to the local conditions.
- 5) Accurate assumptions on the heat demand and return temperatures often poses a problem for large solar thermal systems, despite the existence of various load forecasting methods [16]. The load profile and return temperatures impact the operation temperatures and also the useful solar heat. For example, a low demand in the summer months can lead to more stagnation.

1.4 Responsibilities and risk sharing for plant performance

Quality assessment for LST plants requires separating the factors influencing the solar yield as best as possible, in order to answer questions such as: “Is the solar yield lower than expected because the load is lower (or customer-side temperatures higher) than assumed during plant design? Or do the collectors not perform as indicated by the data sheet? Was it just a year with low irradiance? Are there engineering problems concerning plant design or control strategy?”. These challenges are typical for renewable energy systems where the weather as a stochastic boundary condition has a strong influence on the performance. Besides solar thermal technologies, also PV plants [17] or wind plants [18] are affected by this problem.

Such questions aim not only to pinpoint the causes for possible target/actual deviations, but also ask for a clear division of responsibilities and risk sharing, which is the basis of all performance guarantee procedures. The lack of stringent quality assessment methods that take real operating and weather conditions into account make it harder to share the risk regarding weather conditions between plant operator, designer and plant owner, and D-CAT aims at overcoming this gap. The parties/stakeholders involved in an LST project want to limit their responsibility to their specific task in the realization and operation of the project (see figure 1).

- **[M] Component manufacturers**, mainly collector manufacturers, want to limit their responsibility to the provided components and services (e.g. collectors and mounting); they do not want to be made liable for the way their components are actually operated (e.g. high/low temperatures) or deployed (e.g. row spacing, tilt) within a field installation. Collector manufacturers usually only guarantee the thermal power output under restrictive conditions, but not the energy yield of the LST plant or the collector array.
- **[D] Plant designers (engineering, consulting)** are eager to choose a cost-efficient system design and the best collectors and assume responsibility for the overall plant design. Designers typically only give a guarantee on the solar yield when they also act as plant operators. Designers want to claim against component manufacturers if components do not meet the agreed specifications (e.g. based on data sheet values).
- **[O] Plant operators** want to restrict their liability to the operation. In case operators guarantee the solar yield, they want to regress on the plant designer and require the customer to stick to specified technical condition (e.g. minimum thermal load, load profile, or upper limit for

the return temperature). The risk regarding weather conditions may be attributed to the plant operator, designer or owner, or shared among these parties.

- **[C] Heat consumers** require a reliable heat supply, want to pay a fixed heat price (€ ct/kWh) and limit their responsibility to meeting the agreed load profile requirements.
- **[I] Investors / plant owners** carry the financial risk and want to claim against the operator or designer if the plant is not designed or operated well if this leads to reduced profit or reduced plant lifetime.

Parties can also have multiple roles. Here are some practical examples:

- **[M D O]** Companies like Arcon-Sunmark A/S, Savosolar or Ritter XL Solar act as both collector manufacturer, plant designer and operator.
- **[D O I]** The Austrian company SOLID Solar Energy Systems GmbH¹ takes responsibility for the investment and plant design and acts as an Energy Service Company (ESCo), operating plants and selling heat to housing facility owners and/or district heating utilities, who pay a contracted price [19].
- **[O I]** Danish district heating utilities also often act both as investors and operators [20].

¹formerly S.O.L.I.D. Gesellschaft für Solarinstallation und Design mbH

2 Existing test procedures and modeling approaches

2.1 Scope and use case

According to the ISO/IEC directives, measurement and test methods aim to “specify the procedure for determining the values of characteristics or for checking conformity to stated requirements” [21]. Test methods need to ensure high validity and reliability of the results. Test validity is the extent to which a test actually measures what it intends to measure. High reliability means, that the test has similar results under consistent conditions [22]. Standardized test methods lead to comparability of results [21].

For testing collectors (and to some extend for collector arrays), numerous methods have been developed, covering thermal performance, reliability, durability and safety issues. This analysis is limited to test methods for the thermal performance. Short term testing of the thermal performance has little overlap with reliability and durability tests, although long term testing of the thermal performance can give indications on the reliability and durability [23]. Typical uses case for thermal performance tests are:

- 1) Commissioning
- 2) Surveillance (comparison over time)
- 3) Control
- 4) Testing at different locations (comparison for different locations)
- 5) Certification of collectors

The D-CAT method focuses on use cases 1) to 4), which are described in more detail in chapter 4.3. Use case 5) is linked to quality labels. The main quality label for solar thermal products is the Solar Keymark [24], which is the basis for most European supporting schemes and tendering, and is also increasingly recognized worldwide and harmonized with other labels through the GSCN (Global Solar Certification Network) [25]. Certification of solar thermal collectors according to Solar Keymark requires testing of collectors according to ISO 9806 [26]. Testing of solar thermal collectors enables description of the collector with collector efficiency parameters.

Criteria to classify existing test procedures, including the specifications of the D-CAT method, are described in table 1. Possible system boundaries are shown in figure 2. The description of existing test procedures uses this classification scheme in the background.

2.2 Laboratory test procedures for collectors

Numerous test methods have been developed for collectors. A systematic experimental and theoretical evaluation of dynamic test procedures developed till the year 2000 is provided by [27]. In the following, two test procedures are presented in more detail. The first method is the Quasi-Dynamic Test (QDT), which is the most widespread procedure for solar thermal collectors today. The second method is the New Dynamic Method (NDM), which has currently no widespread application, but has an interesting modeling approach which shares similarities to the D-CAT 1-N model.

The **Quasi-Dynamic Test (QDT)** was developed by Bengt Peres in the 1990s [28] [29] [30]. The procedure was made a European standard EN 12975 [31] in 2000, which became the international

Table 1: Criteria for test procedure classification (D-CAT specifications in red italics).

<i>Criteria</i>	<i>Typical specifications</i>
Use case	<i>Commissioning (performance guarantee), surveillance, control, testing at different locations</i> , certification of collectors
Test site	Laboratory indoor, laboratory outdoor, <i>in-situ (at installation site)</i>
Performance boundaries	Single collector(s), <i>collector array without distribution pipes</i> , collector array with distribution pipes, collector array including pipes and heat exchanger
Collector types	<i>Flat plate</i> , parabolic trough, compound parabolic concentrator, evacuated tube collector
Key performance indicators	(Normative) <i>collector parameters, target/ actual comparison</i>
Scope	<i>Thermal power, solar yield</i>
Collector (array model)	Explained variable: thermal power output, <i>outlet temperature</i> . Model: no model, steady state, dynamic model, <i>fully dynamic; 1-N model, 2-N model</i>
Additional models	No additional models, <i>effective direct and diffuse radiation, distribution pipes, heat exchanger</i>
Required sensors	Precision: high precision, <i>low precision</i> Measurands: <i>mass flow/volume flow, inlet temperature, outlet temperature, total tilted irradiance</i> , beam irradiance, <i>ambient temperature</i>
Duration of measurement	<i>4-5 days, up to 6 months</i>
Test data	Used data: defined test sequence, <i>normal plant operation</i> Data pre-processing: <i>filtering criteria</i> , averaging Sampling rate: 1 s, <i>10 s</i> , 1 min., 15 min., 1 h
Main boundary conditions	Stable inlet, outlet and mass flow rate; stable inlet and mass flow rate, <i>fully dynamic conditions</i> , minimal thermal power, <i>no external shading, no internal shading</i> , no high wind

standard ISO 9806 in 2013. The current version is ISO 9806:2017 [10]. The original QDT procedure was intended both for laboratory and in-situ application, but in-situ testing is only allowed since the latest ISO revision in 2017. In 2019, the Solar Keymark Rules added a new Appendix P5.5 which described the procedure for in-situ certification according to Solar Keymark [32]. At the time of writing, no in-situ applications of ISO 9806 [10] are known to the authors. The use case of the QDT method is the certification of new solar thermal collectors. It is applicable to all types of fluid heating solar collectors and air heating solar collectors.

The collector model of the QDT method has a lumped capacity term which is related to the mean fluid temperature. The QDT model and its differences to the D-CAT model are explained in chapter 6.3. The outcome of the model are normative collector parameters (peak collector efficiency, incidence angle modifier, heat losses, etc.). For the execution of the test, the method prescribes that the collector mounting shall be such that the lower edge is not less than 0.5 m above the local ground surface. The QDT method is typically applied outdoors. The method also requires high precision measurements of the hemispherical solar radiation and diffuse irradiance or beam irradiance, ambient temperature, wind speed, volume flow (or mass flow) and inlet and outlet temperature. Test sequences use a constant volume flow of 0.02 kg/s per square meter of collector gross area or according to the

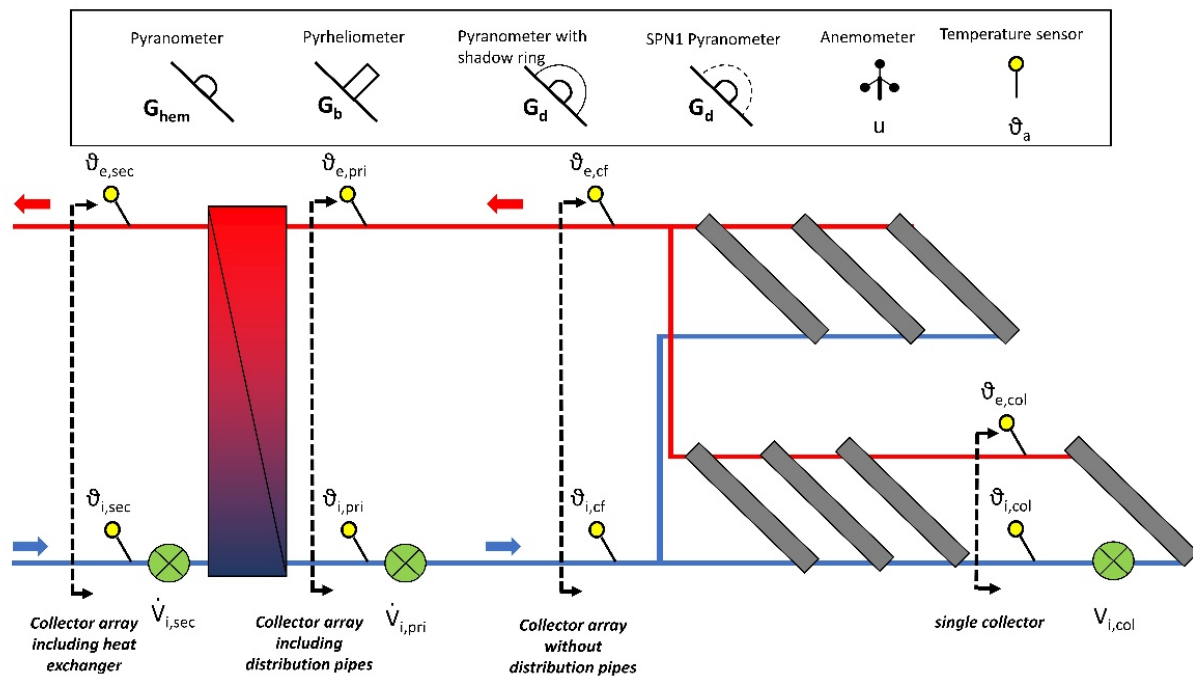


Figure 2: System boundaries for test methods. The D-CAT method has the system boundaries “Collector array without distribution pipes”.

manufacturers’ specifications. The collector is tested over the whole operating range with at least four fluid inlet temperature levels which shall be spaced evenly over the operating range of the collector. During a test sequence, the inlet temperature must be kept within ± 1 K. A test period consists of 4-5 sequences (days) where all important operating conditions should occur. Days are categorized in “day types” with mostly clear sky conditions and partly cloudy conditions. A test sequence has a length of at least 3h. With these different test sequences, the aim is to reach decoupled collector parameters [10].

The method is not directly applicable to in-situ testing of collector arrays for the following reasons. First, the method is designed for collectors and not collector arrays:

- For collector arrays, the installation conditions cannot be modified and might diverge (different row spacings, tilt angles and orientations).
- External and internal beam shading and reduction of the diffuse irradiance due to view obstructions occur.
- Flow- and temperature distribution and pipe losses affect the thermal performance.
- The traveling time of the fluid through the collector array and time constant are different.

Second, the requirements regarding measurement equipment are rarely met regarding sensor accuracy and measurement points:

- Oftentimes, low precision sensors are used which require an uncertainty assessment. For collector arrays, only the total tilted irradiance is typically measured.
- The measurement of wind speed as prescribed in the standard at different locations of a collector is not possible in the field. Furthermore, the representativity of the measurements is much more

problematic, when a value like wind speed or radiation is measured in one spot in large collector arrays.

Third, the standard prescribes test sequences which cannot be observed in normal plant operation:

- The inlet temperature is influenced by the heat sink, e.g. the return temperature of a district heating network, and is typically neither stable nor does it cover the whole operating range.
- The volume flow varies if speed control pumps are used, which is common for large collector arrays.

The **New Dynamic Method (NDM)** by Amer and Nayak [33] was developed for flat plate collector testing. The model used in the test method splits the collector in segments of length Δx in the flow direction of the collector. The width w of a segment is equal to the distance between the axes of two adjacent riser tubes. The thermal capacity is lumped in one node referenced to the mean temperature of the fluid. Radiation gains are proportional to the optical efficiency of the incident hemispherical radiation and heat losses are captured with a constant heat loss coefficient. The modeling is based on the energy balance for the segment

$$\dot{m} c_f(T_f) [T_f(x + \Delta x, t) - T_f(x, t)] = F'(\tau\alpha) G(t) w\Delta x - F'U_L [T_f(x, t) - T_a(t)] w\Delta x - (Mc)_{\Delta x} \frac{dT_f(x, t)}{dt} \quad (1)$$

Under the assumption that the thermal capacity is uniformly distributed along the collector array we have

$$\frac{(Mc)_{\Delta x}}{w\Delta x} = \frac{(Mc)_{fin}}{wL} = \frac{(Mc)}{A_{P,col}} = (mc) \quad (2)$$

Dividing by $w\Delta x$ and normalizing the length L to one, assuming homogeneous flow distribution and taking limits leads to a partial differential equation

$$\frac{\dot{m} c_f(T_f)}{A_{P,col}} \frac{\partial T_f(x, t)}{\partial x} = F'(\tau\alpha) G(t) - F'U_L [T_f(x, t) - T_a(t)] - (mc) \frac{\partial T_f(x, t)}{\partial t} \quad (3)$$

This first-order PDE can be solved with the Laplace transform technique for the outlet temperature and has an explicit solution. The thermal performance test according to NDM can be conducted under normal weather conditions or with shielding the collector within an opaque or semi-transparent shield for 5 min. and then exposing the collector to the sun for 15 – 30 min. An advantage of the NDM method is, that a constant inlet temperature is not required. As shown in the paper, the method gives reliable results under different weather conditions ranging from almost steady to highly variable. A disadvantage of the procedure is, that it only yields three collector parameter and it thus not able to comprehensively describe the collector by differentiating between beam and diffuse irradiance and quadratic heat losses. A newer method inspired by the NDM is the L-QDT method [34]. The NDM method shares some similarities with D-CAT method as the thermal model is also based on the energy balance of segments in the flow direction. The D-CAT 1-N model (see chapter 6.4) is an extension of the model in equation (3).

2.3 In-situ testing for collectors and collector arrays

Collector test methods like the NDM method which do not have restrictions on operating conditions could in principle be applied in-situ. An **early version of the QDT method** was applied to a large scale flat plate collector module of 11 m², installed at a test array in Sweden. The system was running for 24 h a day. Hourly mean values were used with good results [29]. Another interesting application was at the Södertörn SDH test plant, also located in Sweden, which had 9 sub-arrays with different collector types (7 with flat plate collectors, 2 with evacuated tube collectors) [35]. The evaluation showed the importance of using an incidence angle correction term for beam radiation modeling. Optical parameters could be determined accurately, but there were difficulties with the estimation of the quadratic heat loss coefficient and heat capacity.

The **Dynamic Solar Collector (DSC)** test method has also been applied in-situ [36]. It combines filtering theory and the least square method. The method has no restrictions regarding solar irradiance, inlet temperature and volume flow. The model predicts the collector area rather than optical parameters. Evaluations of the test procedure show that the method can accurately predict the fluid outlet temperature, but the collector parameters are not reproducible [27] [37], and systems with different characteristics may not be well characterized by it [38].

The **In-situ Collector Certification (ICC)** is an adaption of the QDT method to test single collectors in a field installation [5]. Research work in connection with the development of the method laid the basis for the new “Annex P5.5 In-Situ Collector Certification” of the Solar Keymark Scheme Rules, which now allow in-situ certification of collectors with the following use case: “In-situ certification is targeting but not limited to collectors which because of their size, power output, weight, operating conditions or on-site production can hardly be tested in a laboratory” [32]. The method is applicable to all collector types and delivers the same collector parameter as the QDT method for outdoor testing. In comparison to the QDT method, the required boundary conditions regarding volume flow and inlet temperature are relaxed to have less interference with the control system. With sufficiently long averaging intervals, fluctuations of the inlet temperature of up to 5 K and 15% of the mass flow are acceptable [39]. Deviating from ISO 9806 [10], a Sunshine Pyranometer SPN1 [40] can be used to measure the diffuse radiation. A bootstrapping procedure to assess the quality of the parameters has been implemented in addition to the QDT method [39]. Details of the method have not been published yet. Similar to the QDT method, ICC is not directly applicable to collector arrays.

For collector arrays, Bosanac and Nielsen [41] proposed a method called **In-situ Check of Collector Array Performance (ICCP)**. The method is applicable to collector arrays with flat plate collectors with liquid as heat transfer medium. The model is similar to the QDT model. The method was applied to a collector array of 60 m² with measurement data resampled to one minute. Repeated applications to fourteen 5-day sequences within a measurement season showed a high repeatability of the optical efficiency ($\pm 2\%$) and heat losses coefficient ($\pm 15\%$), but a lower repeatability of the incident angle modifier ($\pm 25\%$). The method only considers data with a total irradiance $> 400 \text{ W/m}^2$ and recommends a minimum variation of the temperature difference between collector mean and ambient temperature between 10 - 60 K and incidence angle between 10° and 70° for accurate results. The obtained results are interesting, although the application to a small collector array does not allow deviations for larger arrays, as collector array specific challenges are not discussed in the paper.

A new **In-situ Solar Collector Field Test (ICFT)** has been developed recently by Kong, Furbo

and Peres [42]. The test method models the solar collector array (or one or multiple collector rows of the array) as a large collector similar to the QDT model

$$\begin{aligned} \dot{Q}_{sp} = & F'(\tau\alpha) K_b S_b G_b + F'(\tau\alpha) K_d S_d G_d - a_1(\bar{T} - T_a) - a_2(\bar{T} - T_a)^2 \\ & - a_3 u(\bar{T} - T_a) + a_4 (E_L - \sigma_{SB} T_a^4) - a_5 \frac{d\bar{T}}{dt} - a_6 uG \end{aligned} \quad (4)$$

Pipe losses are not modeled. The slope and orientation of all collectors are the same. The parameters a_7 (wind speed dependence of infrared radiation exchange) and a_8 (radiation losses) of the QDT model are not included (see equation (13) of ISO 9806 [10]), but they are usually not relevant for flat plate collectors. The notable difference to the QDT model is the use of the shading coefficients S_b and S_d for the beam and diffuse radiation. The paper gives formulas to calculate the shading share for collectors with identical and different slopes, one fixed and one tracking collector and two tracking collectors. The parameters are estimated with multiple linear regression. The method has been applied to two flat plate collector arrays in Denmark with aperture collector areas of 11.866 m²_{ap} and 5.960 m²_{ap} using a simplified version of equation (4) not including parameter a_3 , a_4 and a_6 . Even though the thermal power output and solar yield prediction improves significantly by using the estimated parameters, they differ substantially from the data sheet, especially the incidence angle modifier b_0 (+100 % and +140% respectively) and heat capacity a_5 (-49.5% for the second field). These deviations are not explained in the report. The drawbacks of the method are the same as for the application of the QDT method to collector arrays (see chapter 2.2).

The **Performance Check (PC)** is the most widespread in-situ test method for collector arrays. It has been used in Denmark for approximately 10 years and was described in a fact sheet of IEA SHC Task 45 [43]. Recently, it has been proposed as an input to a new ISO standard and a working group under ISO/TC 180 is elaborating the standard right now. The description below refers to the current working document. The overall principle of the PC method is to check the measured power against the estimated power when the collector array is running close to full power. It can be used in connection with commissioning of the collector array and/or for continuous on-line surveillance. Flat plate and concentrating collector arrays can be tested. The estimated power is calculated based on the collector parameters from the ISO 9806 [10] test plus some safety factors. The equation used to estimate the collector array power is chosen depending on the collector type and targeted uncertainty level. For non-concentrating collectors, two equations are available

$$\dot{Q}_{est} = n_{col} \cdot A_{G,col} \cdot \left[\eta_{0,hem} G - a_1(\bar{T} - T_a) - a_2(\bar{T} - T_a)^2 - a_5 \frac{d\bar{T}}{dt} \right] \cdot f_{safe} \quad (5)$$

$$\begin{aligned} \dot{Q}_{est} = & n_{col} \cdot A_{G,col} \cdot \left[\eta_{0,b} K_b G_b + \eta_{0,b} K_d G_d - \dots \right. \\ & \left. - a_1(\bar{T} - T_a) - a_2(\bar{T} - T_a)^2 - a_5 \frac{d\bar{T}}{dt} \right] \cdot f_{safe} \end{aligned} \quad (6)$$

where the temperature \bar{T} is the average of inlet and outlet temperature of the collector array over the evaluation period, usually one hour.

Table 2: Restrictions on operating conditions according to the PC method.

<i>Operating condition</i>	<i>Limits (eq. 5)</i>	<i>Limits (eq. 6)</i>
Shadows	No shadows	No shadows
Incidence angle	$\leq 30^\circ$	—
Change in collector mean temperature	$\leq 5 \text{ K/h}$	$\leq 5 \text{ K/h}$
Ambient temperature	$\geq 5 \text{ }^\circ\text{C}$	$\geq 5 \text{ }^\circ\text{C}$
Wind velocity	$\leq 10 \text{ m/s}$	$\leq 10 \text{ m/s}$
Hemispheric radiation G	$\geq 800 \text{ W/m}^2$	—
Beam radiation G_b	—	$\geq 600 \text{ W/m}^2$

Equation (6) is used when the direct and diffuse radiation on the collector plane is available. It will normally have lower uncertainties than equation (5). The safety factor f_{safe} is taking pipe and other heat losses, measurement uncertainty and other uncertainties into account. To limit uncertainties, restrictions on the operations conditions are used as described in table 2.

Only measurement points which satisfy these restrictions are considered. Measurement data are logged (at least) each minute. Averaged data are recorded (at least) each hour. These averaged data are then used for the PC method to compare the measured and estimated power according to equations (5) or (6). For checking the collector performance, the measurement period shall have at least 20 data records.

A major advantage of the PC method is its easy applicability (spread sheet tools suffice) and a straightforward and unambiguous implementation of the method based on the description. The PC method is therefore well suited as a guarantee procedure at commissioning. Note that the method does not estimate collector parameter based on measurement data, but uses the parameter values from the laboratory test. Therefore, the method does not allow a yield simulation based on in-situ parameter as the ICCP, ICFT and D-CAT methods do. The used operating conditions do not account for the dynamic behavior of the collectors or short-term fluctuations. Nevertheless, the method is very helpful for a quick assessment. It oftentimes can make sense to use the PC and D-CAT method in combination.

A method for an **annual solar yield guarantee** was also elaborated in IEA SHC Task 45 [20]. It defines a reference annual specific solar yield and uses linear correction functions for the annual solar radiation level, ambient temperature level and operation temperature level. The theoretical background for this method is the analytical model for the daily energy input/output relationship for solar collector systems [7]. The guaranteed output is the corrected annual specific solar yield multiplied by a safety factor for other influences and uncertainties. As the calculation of the corrected specific solar yield varies a lot between plants and operating years, guarantees are only given with high safety margins in practice. Therefore, the procedure is seldomly applied as a guarantee procedure.

An exception for the seldom use of annual solar yield guarantees are projects of the German collector producer, turn key supplier and plant operator Ritter XL Solar, which gives yield based performance guarantees as a fixed solar annual solar yield. For a SDH project with 1,422 m² collector area in Germany, they guaranteed an annual solar yield 10% below the expected yield [44]. The prerequisite for this is, that Ritter XL Solar unifies all roles of collector manufacturer, designer and plant operator and does not have to deal with the conflicting interests of these parties (see chapter 1.4).

Another method for quality assessment of the solar yield is the **In-situ Short Term Testing (ISTT)** method for large scale solar thermal systems [16] [45]. The basic idea of the ISTT method

is a target/actual comparison with two simulations of the yearly solar yield. The first simulation uses the data sheet values of the components, whereas the second simulation uses parameters that were estimated by fitting the simulation model to measurement data that were acquired during a 4-6 week long measurement campaign. The parameters to be estimated are chosen according to a sensitivity analysis of the yearly energy output of the simulation model. The parameters which have a strong influence on the energy output should be included in the parameter estimation procedure. After the parameter estimation, the model of the system/plant with the estimated parameters has to be validated before the simulation of the yearly reference solar yield. Measurements are done with temporary clamp-on sensors. For the simulation of the collector array, the method recommends the use of a dynamic model with discretization in the flow direction of the fluid, like the MFC (Matched Flow Collector) model implemented in TRNSYS Type 101 [46]. The basic idea of a target/actual comparison of the solar yield with two simulations (data sheet and estimated parameters) is also present in the D-CAT method (see chapter 9.4). The ISTT method is very flexible and can be applied to any collector array if there are simulation models available. But the application of the method is very complicated, needs a special simulation model for each plant with a potentially different set of parameters, which makes results difficult to compare and trace. Furthermore, the method does not specify data processing techniques. No applications of the method outside scientific research projects are known to the authors.

2.4 In-situ performance evaluations from operators' perspective

An important perspective for the development of in-situ test procedures is the existing common practices of plant operators in evaluating their plants. The following is a description of the monitoring practice of the project partner SOLID, a turnkey supplier and operator of large scale solar thermal plants, as an example. Many plants are operated with an ESCo (Energy Service Company) business model (also known as Solar Contracting). The ESCo takes responsibility for the investment, design and operation of the plant. The heat is sold to housing facility owners and/or utilities. For SOLID as the plant operator, performance monitoring is essentially the basis for billing the delivered energy on the one hand and for plant optimization and fault detection on the other.

Typically, calibrated heat meters are used for all systems, which are positioned at the main system boundaries (often the primary or secondary side of the heat exchanger for SDH applications). Within the collector array, inlet and outlet temperature, additional temperatures at the exit of collector rows, ambient temperature, total irradiance in the collector plane, pump speeds and valve positions are typically measured. For larger collector arrays, additional heat meters are placed in subarrays. Some plants have wind sensors. Beam radiation is only measured for plants with on-going scientific research projects. Operational data are typically recorded in 1 min. or 10 s sampling. The most common evaluations are:

- Specific solar yield (yield per m² collector area) comparison for a specific plant for different periods: monthly yield, annual yield, accumulated yield over the year
- Specific solar yield comparison with other plants: annual yield, monthly yield
- Comparison of measured and calculated thermal power output when the plant is running close to full power
- Measured and simulated solar yield over any time interval
- Direct graphical comparison: see figure 3 for an example based on monthly energy yields, and figure 4 for an example based on power output plots.

For selected measurement points, e.g. pressure measurement in the solar circuit, there is an automatic alarm if the values are below or above a defined threshold. All plants have a visualization (line plots of the most important measurement points) which is accessible by remote access.

Automated evaluations of plant performance are also provided by the So1arHeatData.eu platform, owned by the Danish District Heating Association [47]. The platform provides absolute and specific solar yields and solar radiation data on times scales down to an hour as well as input-output, production and efficiency and solar fraction plots. An example is shown in figure 5. To make in-situ test procedure valuable for the plant operator, it must have additional benefits to these evaluations.

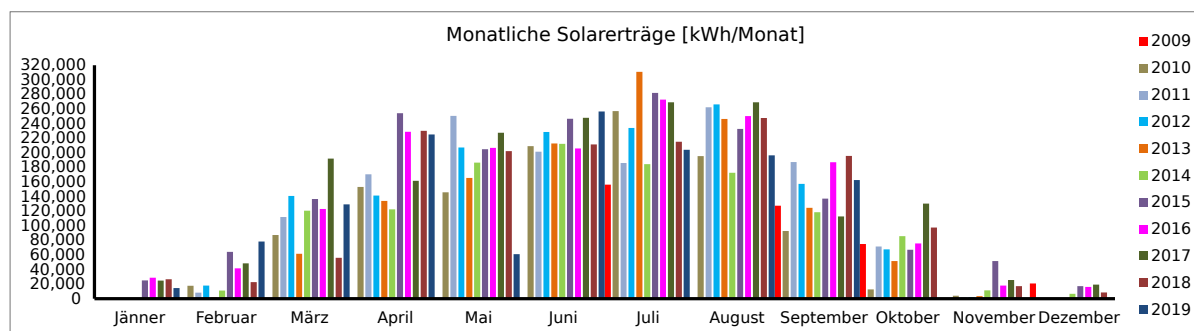


Figure 3: Comparison of monthly solar yield over 10 years. For one installation, the monthly solar yields are plotted over 10 years of operation. Grouping by month reveals outliers (e.g. May 2019) which need to be systematically analysed. Source: SOLID.

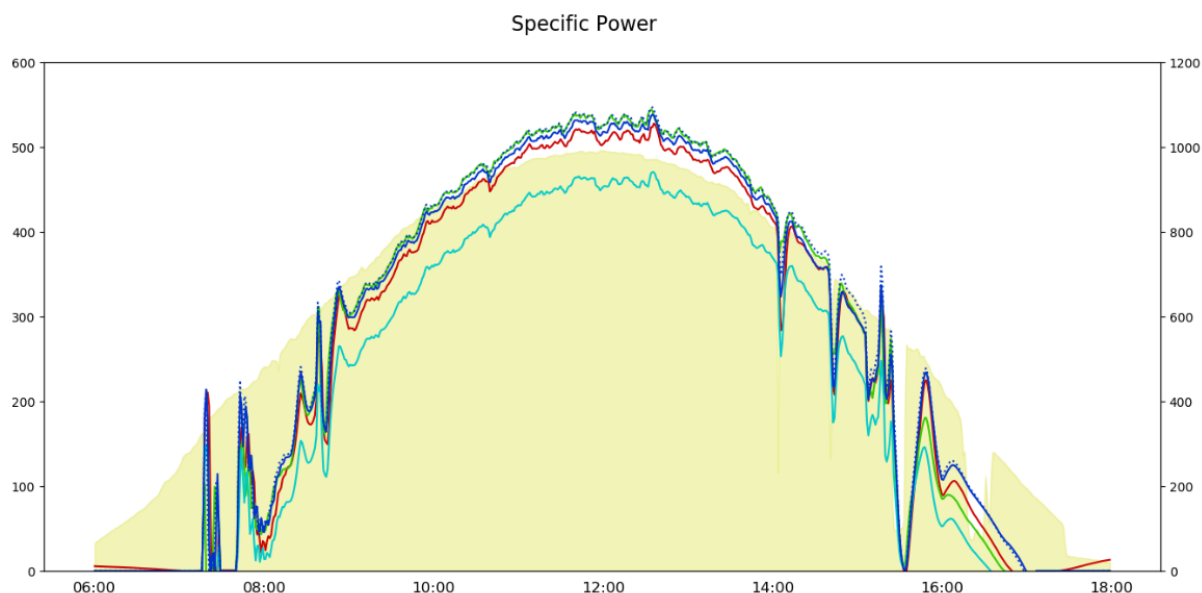


Figure 4: Thermal power output of a solar collector array vs. incoming radiation: The specific power output $[W/m^2]$ (left axis) is plotted over one day and compared with the radiation on the collector array $[W/m^2]$ (right axis). Source: SOLID.

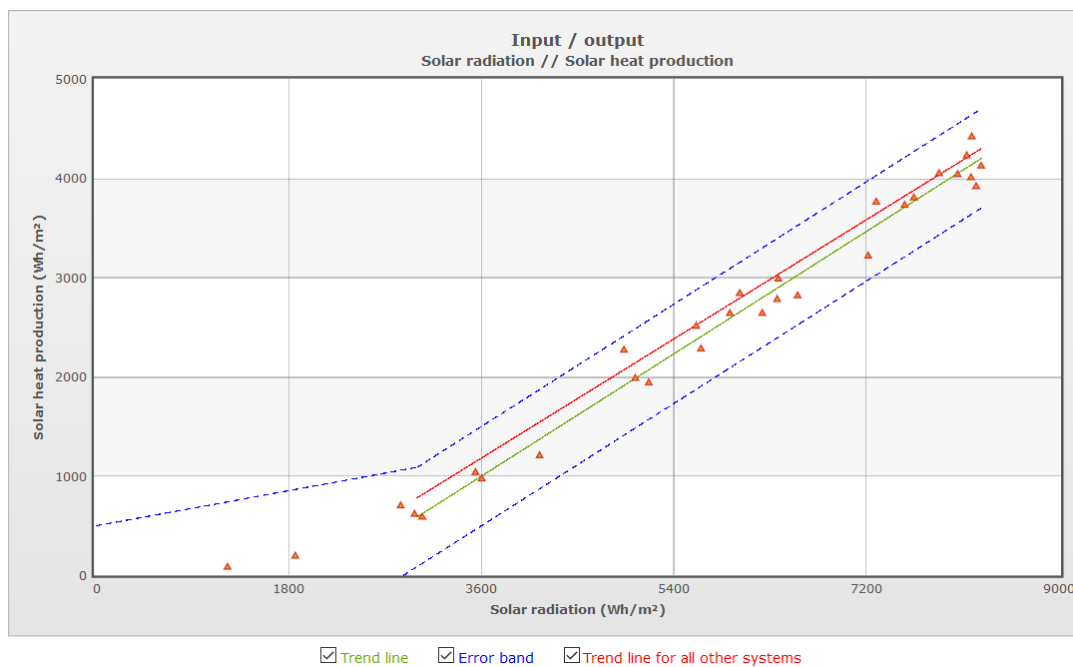


Figure 5: Input-Output diagram [47] evaluation of the large scale solar thermal installation at Silkeborg.

2.5 Research need and challenges

Overall, the available test procedures are not sufficient to characterize collectors within a field installation with characteristic, reproducible parameters that capture their thermal performance under “real-world” conditions. The D-CAT method addresses the following challenges:

- **Collector array model:** Existing approaches either use an over-simplified model for the collector array dynamics (e.g. direct application of the QDT model) which are not suitable for large collector arrays (when using data from the normal plant operation under fully dynamic conditions) or require a complex representation of the collector array in a dynamic simulation tool.
- **Radiation model:** None of the available methods is able to bridge the gap between the typical radiation measurement setup for large collector arrays (total tilted irradiance in the collector plane) and collector arrays model which need beam and diffuse tilted irradiance as inputs, which is crucial for dynamic modeling [15]. The reduction of the diffuse irradiance due to view obstructions is not considered.
- **Data selection and parameterization:** Existing approaches either have very restrictive conditions for the data selection (e.g. PC method with quasi-stationary intervals) or do not contain any restrictions (e.g. ISTT). In the first case, a model parameterization might not be possible at all, in the latter case parameters might be unreliable. Other methods (e.g. ICCP) recommend variations in the data which are rarely present. Data selection is an underrepresented topic for most methods and advanced statistical methods for parameter estimation are seldomly used.
- **Clear interpretation of parameters for different measurement setups:** Existing approaches do not elaborate how comparable parameters can be obtained for different measurement setups

or missing measurement points to allow a meaningful comparison between different plants and with the data sheet. For example, different collector array models might be used conditional on the fact if beam radiation is measured or not, which makes a comparison difficult. A clear interpretation of the parameters (e.g. if they include or do not include pipe losses, etc.) and definition of system boundaries is often missing.

- **Missing procedures for solar yield guarantees:** The existing procedures are not suitable for a solar yield assessment, either because they do not provide reproducible parameters, have high methodological uncertainties due to oversimplification (e.g. guarantee with fixed annual yield) or are too complicated (e.g. ISTT method). Yield based evaluations by plant operators are not able to systematically differentiate possible reasons for yield differences which accrue to the collector as a component.
- **Measurement uncertainty:** The effects of measurement uncertainties on the estimated parameters is not addressed for collector array test methods or dealt with by so-called safety factors (e.g. PC method), although the QDT method contains recommendations in the informative Annex D of ISO 9806 [10].
- **Automation and low cost:** Many test procedures are difficult to automate or do not provide a description of how they can be automated for easy applicability and low cost. A short measurement period to reduce costs is desirable, but is less of an issue if no additional measurement equipment needs to be installed.

The D-CAT method aims to contribute to the solution of these challenges.

3 Measurement of test plant “Fernheizwerk” (FHW)

A cornerstone to develop and validate the D-CAT method is the availability of high-precision measurement data of large solar thermal plants. To this aim, a large solar thermal plant in Graz (Austria) was equipped with high-precision measurement equipment. The plant feeds into the district heating network of Graz. It is located in close proximity to the gas-fired district heating plant FHW (Fernheizwerk), where the plant takes its name from. It is one of best-measured large scale solar thermal plant in the world and offers a unique opportunity to study the performance of large solar thermal plants.

3.1 Plant description

The FHW plant has a total gross collector area of 8,249 m_{gr}² (5,774 kW nominal thermal power). The first collector array with 5,000 m_{gr}² (3,500 kW) was put in operation in 2008 and is located on the roof-top of a waste recycling facility. The second collector array with 3,249 m_{gr}² (2,274 kW) was built in three stages in 2014/2015, 2016 and 2018 and is located on a grass field. Figure 6 depicts the collector array on the grass field in direct vicinity of the central district heating plant of Graz as viewed from the south-west. The plant was designed by the MeQuSo project partner S.O.L.I.D. Gesellschaft für Solarinstallation und Design GmbH² and is operated by solar.nahwaerme.at Energy Contracting GmbH.

A unique feature of the plant is the deployment of ten different collector types from six manufacturers, including flat plate, parabolic trough and heat pipe collectors. Table 3 gives an overview of used collector types.

Within the project, six collector arrays which together represent the installation as depicted in figure 6, consisting of high-efficiency flat plate collectors of five manufacturers were equipped with high-precision measurement equipment (as indicated in the last row of table 3). An array consists of multiple collector rows with a common return and supply connection. Five arrays with a total gross collector area of 2,165 m_{gr}² (1,515 kW) are in the same circuit (2a), whereas one array with a total gross collector area of 255 m_{gr}² (178 kW) is separated by a heat exchanger (2b) because the collector has an aluminium absorber which requires a special anti-freezing liquid. Two arrays of circuit (2a) were not included as they deploy different collector types. Collectors in subarray (2c) were excluded, as that part was built after the measurement setup was already specified. Collector array (1) was excluded from the beginning due to financial restrictions. The mounting of the collectors on the grass field was done with rammed steel profiles and drilled-in steel screws, see figure 7.

Collectors face south direction (180°). The design of the array aimed at tilt angles of the collectors of 30° and row spacings of 3 m. As collectors are aligned at their bottom edges and the size differs slightly between collector types, the height of the upper edges of the collectors above the ground varies a bit. Additionally, the ground is slightly uneven and tilt angles and row spacing show minor differences due to the mounting technique. Tilt, row spacing and height above ground were measured separately at the beginning, middle and end for each collector row. The results are displayed in table 4.

²now SOLID Solar Energy Systems GmbH



Figure 6: Collector array of FHW plant with ground-mounted collectors. Source: SOLID, Picfly.at Thomas Eberhard.



Figure 7: Collector mountings at the FHW plant.

Table 3: Overview of all collector types installed at the FHW plant.

Manufacturer	Collector type ^a	Model	Gross area	Total area	Measured in MeQuSo
(1) Collectors on roof-top (inauguration 2008), A_G = 5,000 m²					
ökoTech	FPC (harp, single-glazed & foil)	HT 12.5 Export	12.5 m ²	5,000 m ²	no
(2a) Collectors on grass field (inauguration 2014/2015), south to north, A_G = 2,745 m²					
ökoTech	FPC (harp, single-glazed & foil, double-glazed)	HT	12.7 - 16.7 m ²	200 m ²	no
KBB	FPC (harp, single-glazed & foil)	K5Giga+ (harp)	12.4 m ²	522 m ²	yes
ökoTech	FPC (harp, double-glazed)	HT 12.5 Export	12.5 m ²	400 m ²	yes
ökoTech	FPC (harp, single-glazed & foil, double-glazed)	HT 2009	12.5 m ²	125 m ²	no
Arcon south	FPC (harp, single-glazed & foil)	HT-HEATstore 35/10	13.6 m ²	516 m ²	yes
Arcon north	FPC (harp, single-glazed & foil)	HT-HEATstore 35/10	13.6 m ²	516 m ²	yes
GREENoneTEC	FPC (meander, double-glazed)	GK 3133	13.2 m ²	211 m ²	yes
(2b) Collectors on grass field (inauguration 2016), A_G = 255 m²					
Savosolar	FPC (direct flow, single-glazed)	SF500-15	16.0 m ²	255 m ²	yes
(2c) Collectors on grass field (inauguration 2018), south to north, A_G = 504 m²					
Absolicon	parabolic trough (W-E tracking)	T160	22 m ²	88 m ²	no
Akotec	heat pipe	MEGA	12.99 m ²	208 m ²	no
Arcon	FPC (harp, single-glazed & foil)	HT-HEATstore 35/10	13.6 m ²	109 m ²	no
KBB	FPC (meander, single-glazed & foil)	K5Giga+ (meander)	12.4 m ²	99 m ²	no

^aFPC = flat plate collector

Table 4: Tilt, row spacing and height above ground for the measured collector arrays.

<i>Array</i>	<i>Tilt [degree]</i>			<i>Row spacing [m]</i>			<i>Height above ground [m]</i>		
KBB	29.1	30.9	29.9	3.01	3.25	3.11	1.59	1.59	1.59
ökoTech	29.2	31.1	29.9	2.99	3.19	3.09	1.53	1.57	1.54
Arcon (south)	30.8	31.6	31.2	3.10	3.12	3.11	1.67	1.79	1.72
Arcon (north)	30.4	31.4	31.0	3.08	3.56	3.23	1.61	1.69	1.67
GREENoneTEC	29.1	30.2	29.7	3.27	3.27	3.27	1.49	1.51	1.50
Savosolar	29.5	30.9	30.0	3.11	3.79	3.25	1.64	1.78	1.73

Towards the east of the collector array, the main transport pipe of the district heating network of Graz, a 19 km long connection between the town of Mellach and Graz, passes the plant. The temperatures in the transport pipe are typically around 130/65 °C in the main heating period in winter and around 95/55 °C in summer. The maximum capacity of the transport pipe is 320 MW (with a 65 K spread between supply and return temperature). The solar thermal plant is feeding into the return flow of the district heating network and is separated from the grid by two heat exchangers. There is no storage, the plant directly feeds into the grid. Feed-in temperatures below the flow temperature of the network are technically feasible, as the decrease in flow temperature in the transport pipe is not significant due to the low share of the solar thermal power output in comparison with the transported heat in the pipes. The plant uses speed-controlled pumps, scalable between 30% and 100% of the maximum pressure head.

3.2 Measurement setup

3.2.1 Measurement points and sensors

Figure 8 shows the position of the measurement sensors: All five arrays in solar circuit (2a) are equipped with volume flow, return and flow temperature sensors, which allows to calculate the thermal power output for each array separately. Additionally, the inlet and outlet temperature for each array and the flow temperatures for each row are measured. For one specific row, additional measurements of the inlet and outlet temperatures of single collectors are put in place. Pressure measurement are done for two arrays. For the solar circuit (2b), the measurement setup is the same with the exception that the volume flow is measured on the secondary side of the heat exchanger. Additionally, the inlet and outlet temperature of each array and the flow temperatures for each row are measured. For a precise evaluation of the collector performance, high-precision measurement of solar radiation, both total tilted radiation and beam/diffuse radiation is important. For this purpose, a pyranometer in the collector plane and a pyranometer, mounted on a sun-tracker are used. Ambient temperatures are measured in three spots, wind speed is measured on the horizontal. Complementary measurements include global and diffuse horizontal radiation measurements by pyranometers mounted near the pyrhelimeter. A webcam is used to gain a visual impression on the situation of the site. Sensors and data logger specifications are listed in table 5.

Table 5: Sensors and data logging.

<i>Sensors</i>	
Volume flow	Electromagnetic flow sensor OPTIFLUX 4000 DN32 IFC 100
Fluid temperature	Resistance Thermometer Pt100 (EN 60751 F.01), placed directly in fluid (without thermowell)
Ambient temperature	Resistance Thermometer Pt100 (EN 60751 F.01), with ventilation unit
Total radiation in collector plane	Pyranometer Kipp&Zonen SMP 21
Beam radiation (DNI)	Pyrhelimeter Kipp&Zonen SHP1 (mounted on Kipp&Zonen SOLSYS 2 suntracker, sun sensor for active tracking)
Global radiation	Pyranometer Kipp&Zonen SMP 11
Diffuse radiation	Pyranometer Kipp&Zonen CMP 11 with shadow ball
Wind speed (horizontal)	Ultrasonic Wind Sensor Lufft V200A-UMB
Pressure	Pressure transmitter Huba Control Typ 520
<i>Data logging</i>	
Data logger	PLC B&R Industrial Automation X20CP1483, four wire (4 L) connection totemperature sensors
Sampling rate	1 second

3.2.2 On-site installation

The volume flow is measured with electromagnetic flow sensors. To meet the installation requirements regarding inlet and outlet pipe lengths, it was necessary to increase the length of the return pipe for four collector arrays, as depicted in figure 9.

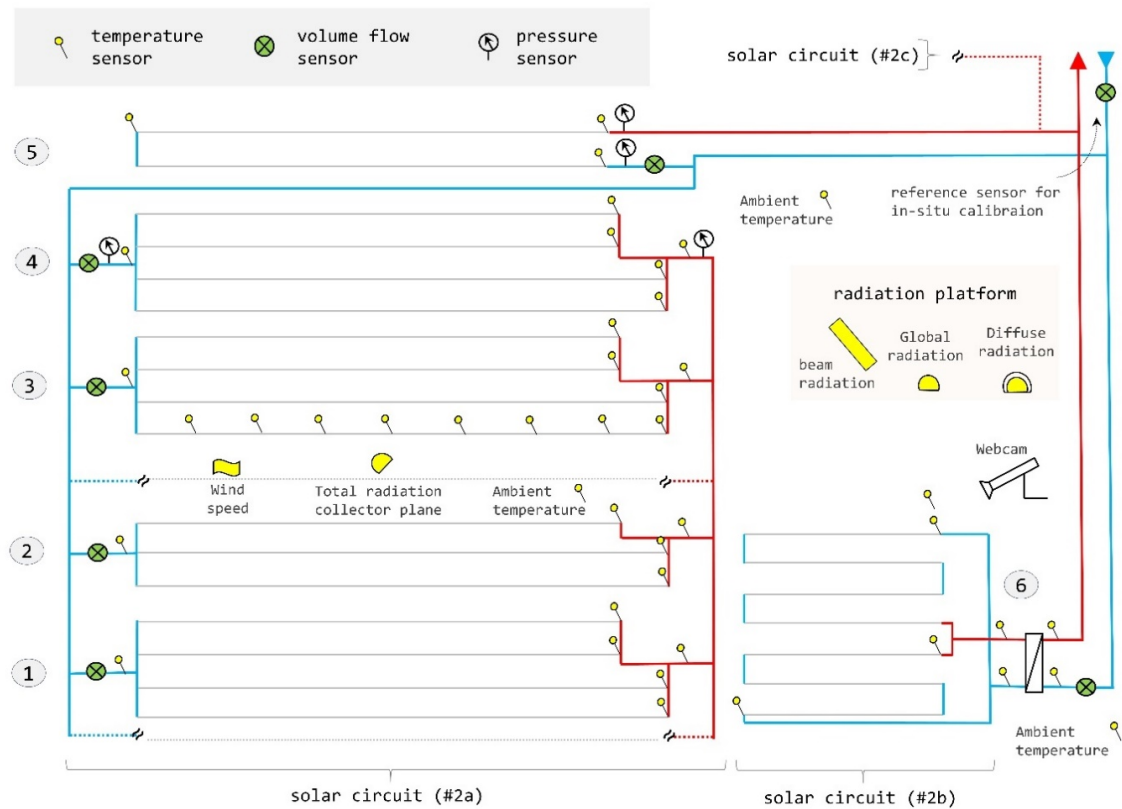
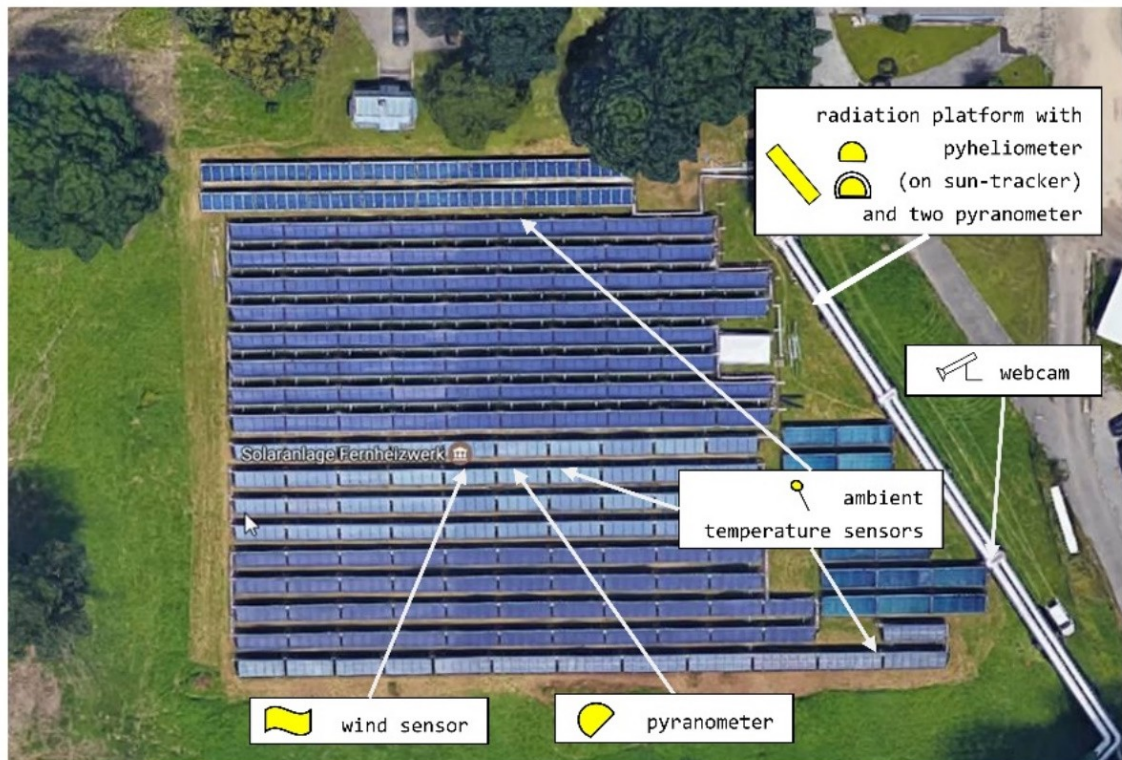


Figure 8: Measurement setup of the FHW plant, with sensor positions, position of solar tracker and webcam (adapted from *Google Maps*).



Figure 9: The volume flow sensors require settling sections upstream and downstream of the sensor.

Temperature measurements are placed directly in the fluid. Additional bends were installed at outlet pipes of four arrays to improve the approaching flow conditions (figure 10, left). For the measurements of the inlet and outlet temperatures of single collectors, a device developed by the collector manufacturer was used, depicted in figure 10, right. It consists of two bends, where one bend has a socket to mount a temperature sensor in counter flow to the flow direction.



Figure 10: Temperature measurement at the mixed outlet of all rows of one collector array (left). Temperature measurement between collectors (right).



Figure 11: Pyranometer (top left), ambient temperature sensor with ventilation unit (middle left), wind sensor (bottom left) and radiation platform including pyrheliometer and unshaded and shaded pyranometer (right).

The positions of the radiation, ambient temperature and wind sensors and webcam are shown in figure 8 (page 30). Pictures of the installation can be found in figure 11. The sun-tracker with the pyrheliometer and additional global and diffuse horizontal sensors is mounted on a platform above the district heating transport lines 3 m above ground to diminish view obstructions.

A webcam is placed in the south-east corner of the collector array (see figure 12). Pictures are taken every 5 min. The purpose of the webcam is to get a visual impression on shading, detect major defaults (e.g. broken collector glasses) and to document the vegetation and additional relevant events (e.g. maintenance work). A sample screen shot can be seen in figure 12, where a bird can be seen in the foreground and a tent used for maintenance in the background. Webcam pictures helped to manually exclude time periods, which were not representative for array operation, e.g. shading of the collectors due to the tent used for maintenance.

3.2.3 Calibration and fluid test

All volume flow sensors were calibrated in the field on 2016-11-25. A high-precision reference sensor, which was calibrated by the manufacturer at 5 points (15%, 40%, 60%, 80% and 100% of the nominal volume flow), was placed on the joint return pipe (top left corner in figure 8, page 30). One collector



Figure 12: Mounting of webcam at FHW plant (left) and sample picture (right).

array was left open at a time, while all the other arrays were closed off with ball valves on both sides. Each sensor was calibrated at 4 or 5 different flow rates, encompassing the whole operation range. For each flow rate, the speed-controlled pumps were operated with the same speed for at least 5 minutes, while the flow rate was measured by the reference sensor and the sensor in the field. These data were then averaged for each sensor and calibration point separately and a linear calibration correction (between the calibration points) was implemented.

Temperature sensors were calibrated in the laboratory of AEE INTEC. Pyranometer in the collector plane (SMP 21) and the pyrhelimeter (SHP 1) were calibrated by the manufacturer at the start of the measurement campaign. Additional radiation sensors mounted on the sun-tracker were calibrated on-site at FHW plant with the pyranometer SMP 21 who was mounted temporarily on the sun-tracker and the pyrhelimeter.

To determine the density and heat capacity of the fluid in the solar loop (propylene glycol), a laboratory test was conducted at ILK Dresden [48] as the filling/re-filling of the anti-freezing liquid before the start of the measurement campaign was only partially documented and due to fluid degeneration. Furthermore, fluid properties in data sheets can be unreliable and measurements of the concentration with a refractometer can have large uncertainties [49]. The sample was taken on 2018-11-15. Laboratory measurements for the density were interpolated with a second order polynomial, with ρ_f in [kg/m³] and T in [°C]

$$\rho_f = 1049.951 - 0.431 \cdot T - 0.00187 \cdot T^2$$

For the heat capacity, a third order polynomial was used; c_f is in [kJ/kg] and T in [°C]

$$c_f = 3.624 - 0.00639 \cdot T - 0.0000590 \cdot T^2 - 0.000000269 \cdot T^3$$

Figure 13 shows the values for the density and heat capacity in reference to the propylene-glycol Tyfocor L[®] with different concentrations. Measurements with a customary refractometer showed a concentration of 43.5%, which is in line with the retrieved values for the density. The heat capacity values vary between different concentrations according to the data sheet and using a concentration of 43.5% would have led to a substantial error.

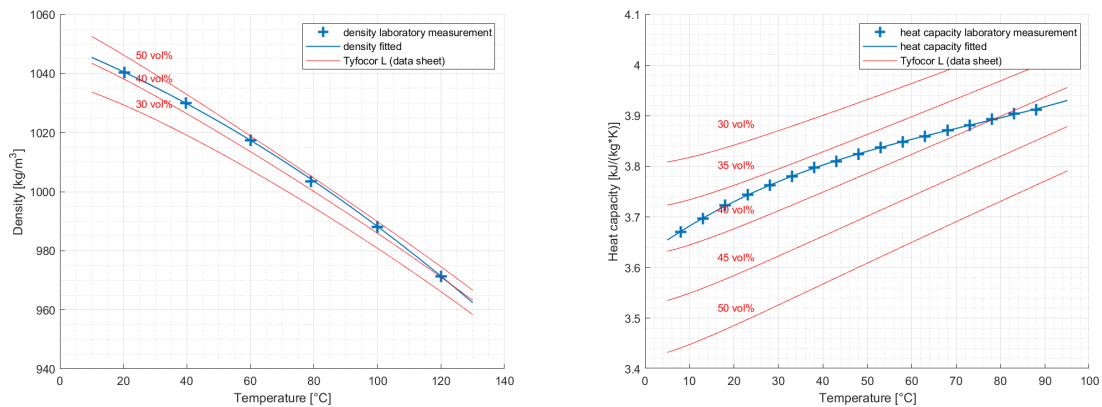


Figure 13: Thermodynamic properties of the FHW heat transfer fluid, compared to Tyfocor L[®]: density (left) and heat capacity (right).

3.3 External Shading

For a fair assessment of the collector array performance, environmental conditions (beam and diffuse radiation, ambient temperature) need to be determined with reasonable accuracy. Conditions with external shading are excluded from the analysis in the D-CAT method, as it is difficult to determine the radiation on the collectors for these conditions, which could lead to a bias in the analysis.

For the FHW plant, external shading is a major issue. Towards west, the transport pipe of the district heating grid with a height of approx. 3 m passes the collector array in close distance (see figure 14, left) and casts shadows in the morning. Towards south, there are buildings and trees (approx. 20 to 50 m distance) which cause shading for low sun altitude angles. Towards west, there are trees (approx. 20 to 50 m distance) which cause shadow in the afternoon (see figure 14, right).



(a) towards south



(b) towards west

Figure 14: View towards south with transport distribution pipe (left) and view towards west (right) of FHW plant.

Shading objects (buildings and trees) close to the collector array and the large area occupied by the six measured arrays of around 60 m x 90 m lead to inhomogeneous external shading among and within the six measured arrays. This made the consideration of the 3D topography necessary. A 3D model was set up in *SketchUp* as part of a master thesis at AEE INTEC [50]. A screenshot of the model is shown in figure 15.

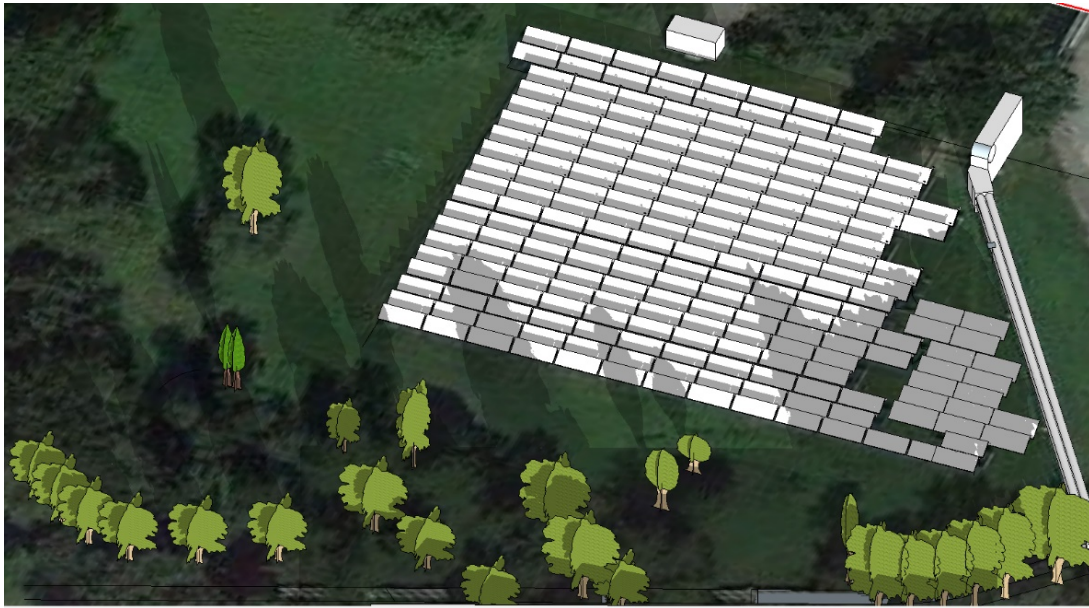


Figure 15: Screenshot of the SketchUp 3D model for the FHW plant.

The basic 2D aerial picture to build the model was imported from Google Earth and complemented with building heights from a local GIS provider [51]. Collector dimensions, space between collectors, row spacings, height of the collectors above ground and tilt were measured at the beginning, middle and end of each row. The dimensions of district heating transport line were measured on-site as well. The height of the trees was calculated based on measurements of the position relative to reference points and the view angle measured by an angle measurement device. Based on the SketchUp model, for each day the first time point where external shading stops in the morning for all six arrays and the last time point where external shading begins in the afternoon for at least one array was determined with the built-in shadow function of the program, which visually displays shadows for the model for manually selectable times. The external shading pattern was regular in the sense that between these two time points, there were no intermittent periods with no shading, thus the whole period where all six arrays were captured with this methodology. These start and end time points were then visually validated with webcam pictures, which showed a very good agreement.

The results of the external shading calculations are shown in figure 16. Days with plant operation where no external shading occurs is between the 2nd of February and 10th of November. Total hours without external shading amount to 1,693 h per year. As can be seen in this example, excluding periods with external shading can substantially reduce the dataset to be used for performance checks. Internal shading is treated in chapter 7.1.2.

3.4 Continuous quality assurance

After the installation of the measurement equipment in June and August 2016, data were recorded from 2016-08-22 until 2019-10-15. For the validation of the D-CAT method, only data from 2017 and 2018 were used, as special care for the maintenance of the measurement equipment and surveillance of the plant performance was limited to these two years. During these two years, the following quality assurance measures were undertaken to ensure the quality of measurement data:

- Regular on-site inspection of the measurement equipment (typically two-week intervals) regarding

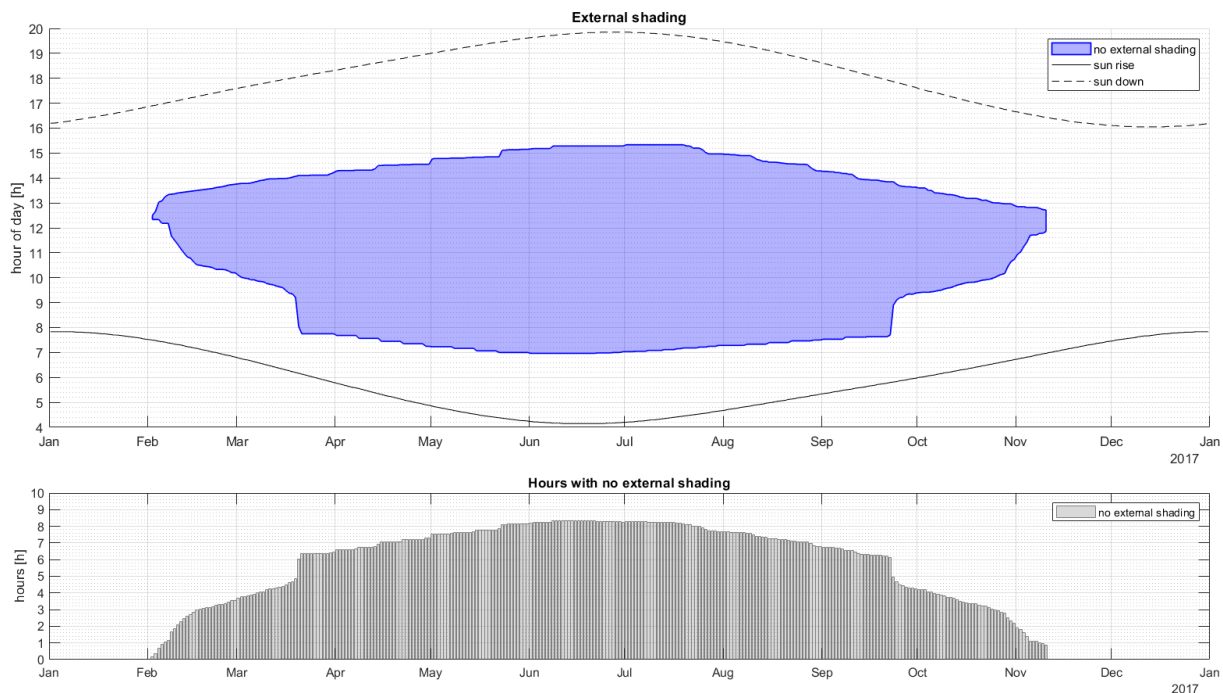


Figure 16: Periods with no external shading (top) and daily hours with shading-free periods (bottom) for the FHW plant.

sensor condition, cables, time drift of data logger, etc.

- Regular cleaning of radiation sensors (typically once a week)
- Regular inspection of the plant (e.g. broken foil or glass of the collector, thermal insulation, soiling, etc.) on-site and with webcam pictures (typically once a month)
- Regular check with plant visualization (typically once a month)
- Automated check for data transmission (run once a day)
- Automated check for missing data, physically implausible values, etc. (run typically once a week)
- Documentation of all plant events (e.g. power supply interruption, maintenance work, grass cutting, etc.) in log book and with photographs

Sample pictures of the on-site quality assurance are displayed in figure 17. Experience showed that especially the pyranometer was affected by soiling and needed regular cleaning. Major plant events during the measurement campaign was an operation interruption due to extension of collector array and a power supply interruption which lead to stagnation in the middle of 2018.

3.5 Measurement uncertainty

Measurement uncertainties for the deployed sensors were determined based on the specifications on the data sheets of the manufacturer (see table 6) and the calibration procedure. The maximum error for the fluid density was stated as $\pm 0.5\%$ and for the heat capacity $\pm 1\%$ by the test laboratory [48].



Figure 17: Soiling of pyrheliometer in winter (top left), broken glass of collector shortly after inauguration (top right), soiled collector (bottom).

Different uncertainty sources for a particular sensor (e.g. zero off-set, long term stability, non-linearity, temperature dependence) were combined to a sensor uncertainty expressed as the standard deviation of a normal distribution according the Guide to the expression of uncertainty in measurement (GUM) [52]. For calculated values, which are function of measured values (e.g. mass flow as a product of volume flow and fluid density) the GUM procedure can be used as well or Unscented Transform (UT) for an improved uncertainty propagation for non-linear functions (see chapter 8.3). Table 6 shows the uncertainty for four different operating conditions of one collector array with high/low volume flow and high/low ΔT between flow and return side respectively, which can occur when plant is running close to full power (operating point 1), heating up (operating point 2 and 4) or days with intermittent operation (operating point 3). The uncertainty is expressed as $\pm 2\sigma$ (standard deviation), which is a 95.45% confidence interval for the normal distribution, i.e. 95.45% of the measured values are expected to lie in this interval. As can be clearly seen, the relative uncertainty ($\pm 2\sigma/\text{value}$) of the volume flow, density and heat capacity is very similar for the four operating points. The uncertainty expressed as $\pm 2\sigma$ for the temperature measurements is also similar. The uncertainty for the calculated thermal power output is below $\pm 1\%$ for operation point 1 and reaches 2.4% for operating point 3.

These values indicate a high measurement accuracy. Note that the overall uncertainty of the thermal power output is reduced for higher ΔT , as the temperature measurements have a large influence on the thermal power output and the uncertainty of the temperature measurement is small compared to the other uncertainties. The evaluation of a single collector with this measurement setup would have a large uncertainty as the ΔT is very small for collectors connected in series.

Table 6: Measurement uncertainties for selected operating conditions.

	<i>Measurement</i>		<i>Calculation</i>	
	<i>Value</i>	$\pm 2\sigma$	<i>Value</i>	$\pm 2\sigma$
Operating point 1				
Full power: high volume flow, large ΔT				
\dot{V}	8.09 m ³ /h	± 0.034 m ³ /h ($\pm 0.42\%$)		
T_{in}	71.3 °C	± 0.24 K		
T_{out}	102.4 °C	± 0.26 K	274 kW	± 4.86 kW
ρ_f	1010 kg/m ³	± 5.83 kg/m ³ ($\pm 0.58\%$)		($\pm 0.887\%$)
c_f	3.88 kJ/kg·K	± 0.045 kJ/kg·K ($\pm 1.15\%$)		
Operating point 2				
Heating up: low volume flow, middle ΔT				
\dot{V}	3.64 m ³ /h	± 0.017 m ³ /h ($\pm 0.47\%$)		
T_{in}	58.0 °C	± 0.22 K		
T_{out}	70.4 °C	± 0.24 K	49 kW	± 1.47 kW
ρ_f	1018 kg/m ³	± 5.88 kg/m ³ ($\pm 0.58\%$)		($\pm 1.499\%$)
c_f	3.85 kJ/kg·K	± 0.044 kJ/kg·K ($\pm 1.15\%$)		
Operating point 3				
Intermittent operation: high volume flow, small ΔT				
\dot{V}	8.20 m ³ /h	± 0.035 m ³ /h ($\pm 0.425\%$)		
T_{in}	70.1 °C	± 0.24 K		
T_{out}	78.3 °C	± 0.26 K	67 kW	± 3.19 kW
ρ_f	1010 kg/m ³	± 5.83 kg/m ³ ($\pm 0.58\%$)		($\pm 2.381\%$)
c_f	3.88 kJ/kg·K	± 0.045 kJ/kg·K ($\pm 1.15\%$)		
Operating point 4				
Heating up: low volume flow, small ΔT				
\dot{V}	3.43 m ³ /h	± 0.016 m ³ /h ($\pm 0.425\%$)		
T_{in}	60.4 °C	± 0.23 K		
T_{out}	68.9 °C	± 0.24 K	32 kW	± 1.31 kW
ρ_f	1017 kg/m ³	± 5.87 kg/m ³ ($\pm 0.585\%$)		($\pm 2.04\%$)
c_f	3.85 kJ/kg·K	± 0.045 kJ/kg·K ($\pm 1.15\%$)		

σ = standard deviation

value $\pm 2\sigma$ is equal to a 95.45% confidence interval for a normal distribution

4 Overview of the Dynamic Collector Array Test (D-CAT) method

4.1 Aim and scope

The aim of the project MeQuSo was to increase the planning reliability and quality assessment for large solar thermal (LST) plants by developing an in-situ test procedure able to assess the thermal performance of collector arrays under “real-world” conditions. The main achievement of the project is the development of a proof of concept for a new collector array test method called **D-CAT (Dynamic Collector Array Test)**. The aim of the method is to characterize collector arrays in operation in a quantitative way, with parameters describing the real collectors’ behavior in the field. These parameters are the parameters of a physical model describing collector array operation, and are learned (estimated) based on measurement data. D-CAT is performed in-situ, i.e. it is based on measurements taken directly at the plant and not in the laboratory. Having in-situ collector parameter as the outcome of the in-situ testing is the most general way to perform an in-situ test.

The D-CAT method addresses the challenge that the solar yield and collector array performance in particular are affected by multiple influencing factors like design, components, operation, load and environmental conditions (as explained in chapter 1.4). These factors have a combined effect on system behavior; it is hard to disentangle them and to attribute observed system behavior to one particular factor. The D-CAT method helps to disentangle the influencing factors by deriving in-situ collector parameters which capture the current condition of the collectors and their actual, “real-world” performance characteristics. Performance reductions that concern the collectors on a component level (such as soiling, broken insulation, faulty foil tension etc.) are reflected in the estimated parameters.

For instance, heavily soiled collectors will have worse values for the optical parameters than clean collectors. Collectors with broken insulation or faulty foil tension will have higher heat loss coefficients. Great care is taken in order not to distort the collector characterization: This is approached by factoring out those performance relevant factors which do not accrue to the collectors on a component level (e.g. weather conditions, collector array geometry, hydraulic setup, etc.). D-CAT tries to clearly distinguish between the performance of the deployed collectors (that the collectors were in the appropriate condition when installed on-site and remain so after some time in operation) and the overall plant performance (influenced by weather conditions, demand, control strategy, row spacing etc.). This is an important step towards successful risk sharing in LST projects (see chapter 1.4 and figure 1, page 11).

4.2 Main features and characteristics

This is a summary of the main features and characteristics of the D-CAT method:

- 1) D-CAT can be run as a fully automated system test that returns an in-situ characterization of collector arrays. The characterization is based on parameters that quantify the main physical phenomena in collector arrays; the parameters describe a collector array as an “average”/typical collector (not a selected single collector).
- 2) The method is applicable to collector array configurations and measurement setups typically found in LST plants. The D-CAT method is based on a differential equation model for collector arrays, applicable to typical configurations of LST plants. This model is used as in a grey box approach, i.e. the model structure is combined with measured operating data of LST plants to estimate the model parameters, numbers that characterize the collector array behavior in terms of the “typical” collector. The D-CAT method has a similar physical modeling approach

as the QDT procedure of ISO 9806 [10] for single collectors, but it extends the ISO model to the specific conditions found in long collector rows and collector arrays.

- 3) The method is applicable to fully dynamic conditions that occur in normal plant operation. There are no requirements to run special test sequences or heavily filter out data to only consider “quasi-dynamic” system states as done in the QDT test (see chapter 2) since the D-CAT model is capable of describing fully dynamic operating conditions, The plant control needs not be adapted for the test, and no special test sequences need to be run. The experimental data used for D-CAT are simply the operating data recorded during normal system operation
- 4) In the current state of development, the D-CAT method is limited to arrays with flat plate collectors, which are the most common collector technology in LST plants; extensions to other collector types are possible within the existing framework of the method.
- 5) The system boundaries of the collector array model are the entrance and exit to the collector array. Collector array modeling puts emphasis on the most important influencing factors for thermal performance, but avoids an over-detailed representation to facilitate the application of the procedure.
- 6) D-CAT provides a standardized and traceable framework for data acquisition, data processing and parameter estimation.

4.3 Use cases

The authors see the following use cases for the D-CAT method:

- **Commissioning:** Target/actual comparison with guaranteed thermal power output/yield. A commissioning test for the collectors checks if their performance at the start of operation of the plant meets the target values of the guaranteed thermal power output or yield based on data sheet parameters or contracted specifications. The involved parties are the collector manufacturer (as warrantor) and the plant designer or operator (as warrantee). An example is the “Guaranteed power output method” [53] and “Guarantee of annual output” [43]. The D-CAT method can both be used for thermal power output and yield guarantees.
- **Surveillance (comparison over time):** Detecting trends with repeated testing and building systematic knowledge on collector performance over time. On-going surveillance is important to detect faults, assure long-term performance, schedule maintenance measures and improve operation. A comparison with the simulated performance helps to assess simulation models and risks for future projects.
- **Control:** Parameterization of collector array models for improved control. Improved control can lead to higher solar yield. Using in-situ parameterization of the collectors with the D-CAT method instead of data sheet values allows a better modeling of the outlet temperature for model-based/model-based predictive control.
- **Testing at a different location (comparison for different locations):** Transparent comparison of collector arrays, building systematic knowledge on collector performance across different collector types and arrays. Systematic evaluations can provide transparency on solar yields at different locations, as evaluations for Denmark show [54]. Plant operators and designers get a good insight into collector performance at different locations, array designs, or control strategies. The reliability of the technology can be proven to decision makers and investors.

4.4 System boundaries and measurement setup

The performance boundaries of the D-CAT method is the collector array without pipes as depicted in figure 18. This part of the collector array is modeled with the parameterized collector array model (core model), whose parameters are estimated by the procedure.

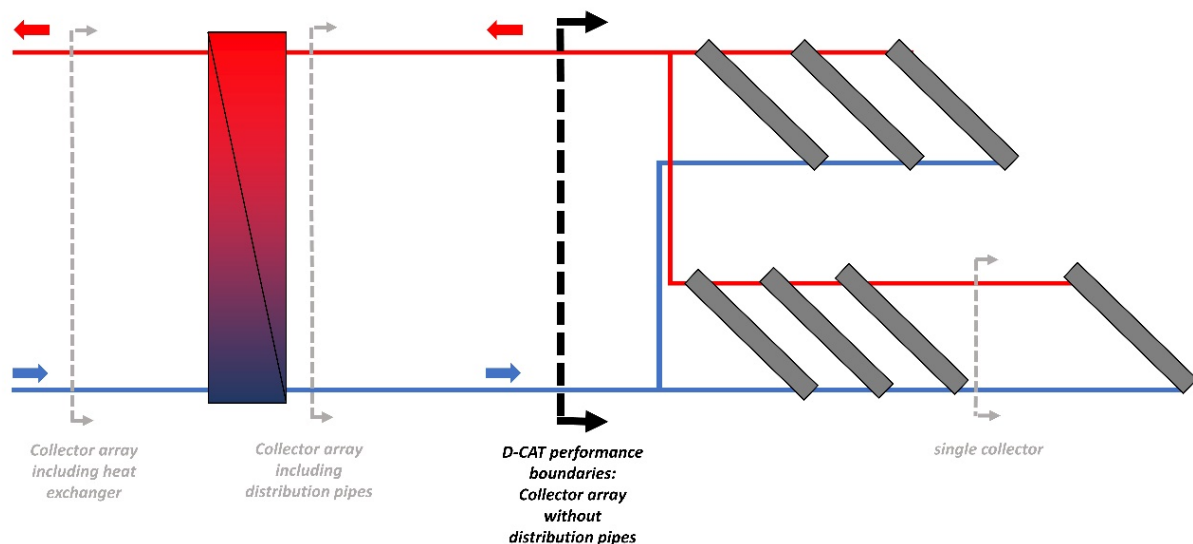


Figure 18: Performance boundaries.

The inputs of the core model are listed in table 7. Typically, not all of these inputs are actually available as measurement data, i.e. captured by sensors at the respective location of the plant. To overcome this difficulty, the D-CAT method uses a pre-simulation step to calculate these inputs based on the available measurement data with auxiliary models for radiation, heat exchanger and pipes; figure 19 explains this in a conceptual sketch. All combinations of measurement setups that allow calculating the core model inputs (see table 7) are measurement setups to which the D-CAT method can be applied. The typical measurement setup for commercial installations is marked in orange.

Table 7: Inputs for collector array model (core model).

<i>Input</i>	<i>Description</i>
G_b	Beam radiation in collector plane
G_d	Diffuse radiation in collector plane
\dot{C}_f	Capacity flow in solar collectors circuit; calculated from volume flow, fluid density and fluid heat capacity
T_{in}	Collector array inlet temperature (after distribution pipes)
T_{out}	Collector array outlet temperature (before distribution pipes)
T_a	Ambient air temperature

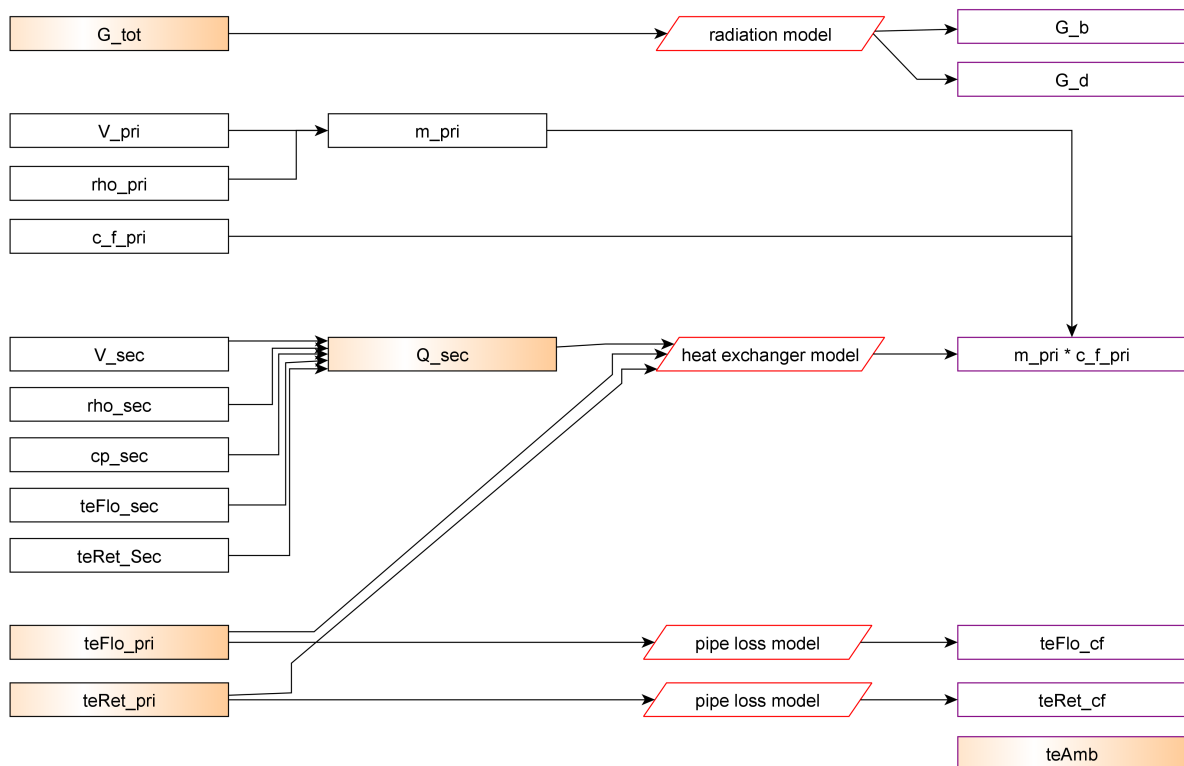


Figure 19: Calculation of model inputs for different measurement points.

4.5 Building blocks

An overview of the method is given in figure 20. The main building blocks will be explained below.

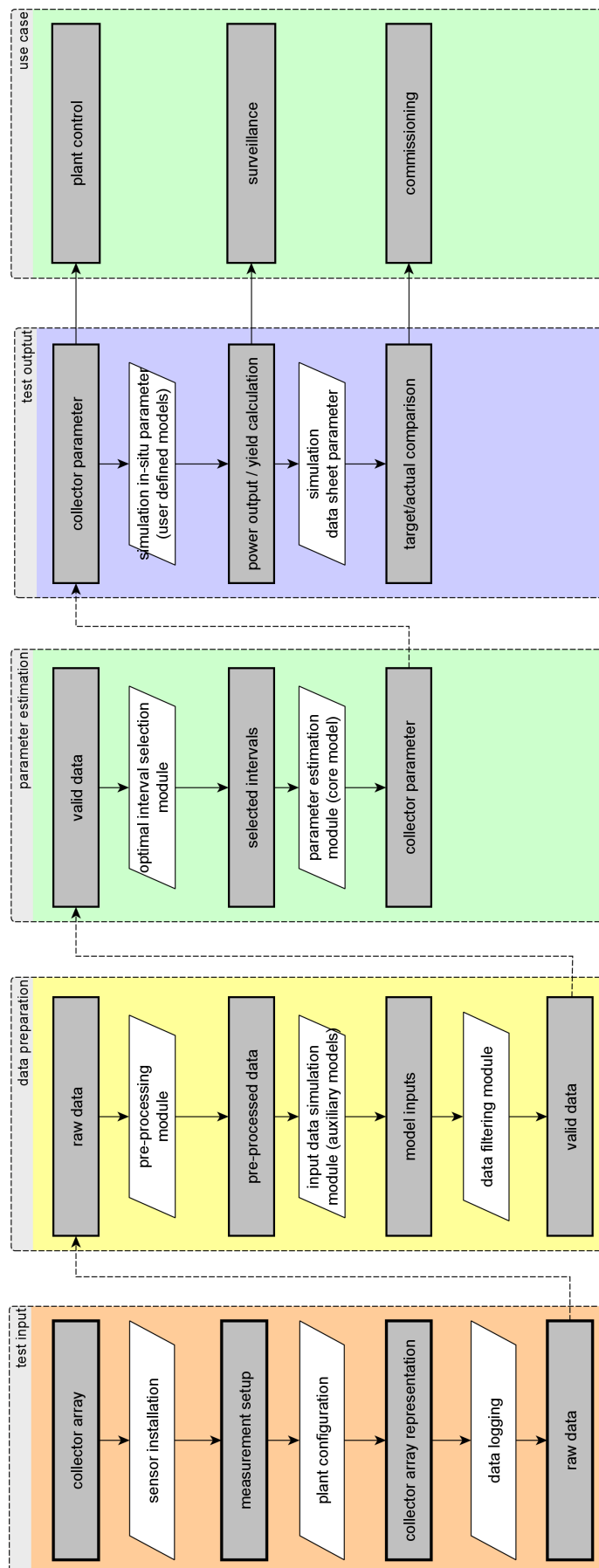


Figure 20: Overview of the D-CAT method.

Configuration and data acquisition

The starting point of the test procedure is the *collector array*, which is to be evaluated. Possible *measurement setups* are described in chapter 5.1. Apart from the measurement data, collector array parameters are needed. After the *collector array representation* of the plant in the evaluation tool (see chapter 5.2), the manual configuration is done and the D-CAT test procedure runs fully automatically with the recorded *raw data*.

Data preparation

Data pre-processing to assure the data quality is described in chapter 5.3. Auxiliary models (see chapter 7) are used to calculate the model inputs if they are not directly measured (e.g. beam and diffuse irradiance if only the total tilted irradiance is measured) or if the measurement data needs to be corrected (e.g. modeled average diffuse irradiance on the collectors if view obstructions are significant instead of measured diffuse irradiance). The most elaborate transformation is the radiation processor (see chapter 7.1)). Data filtering is applied to select *valid data*, i.e. periods where the model is applicable (see chapter 6.6).

Parameter estimation

The core of the method is the parameter estimation procedure. In the first step, a set of optimal intervals is selected automatically, where each interval makes a substantial contribution to determine the model parameters (see chapter 8.2). These *selected intervals* are then used to estimate the model parameters of the core model (D-CAT 2-N model, see chapter 6.5; D-CAT 1-N model, see chapter 6.4) as described in chapters 8.3 and 8.4.

Test outcome

The outcome of the test are *collector parameter*, which can be used for *power output / yield calculation* or *target/actual comparison* for different use cases, as explained in chapter 9.

5 Plant configuration and data preparation

The first steps in performing the test procedure is the measurement data acquisition, plant configuration and data pre-processing.

5.1 Data acquisition

The D-CAT methods works with different measurement setups. The main characteristics of a measurement setup are the measurands, position of the sensors and installation conditions, sensors and their specifications, sampling rate and measurement period. Figure 21 shows the sensors and their positions for the low precision (minimum) measurement setup; figure 22 shows the high precision (ideal) measurement setup.

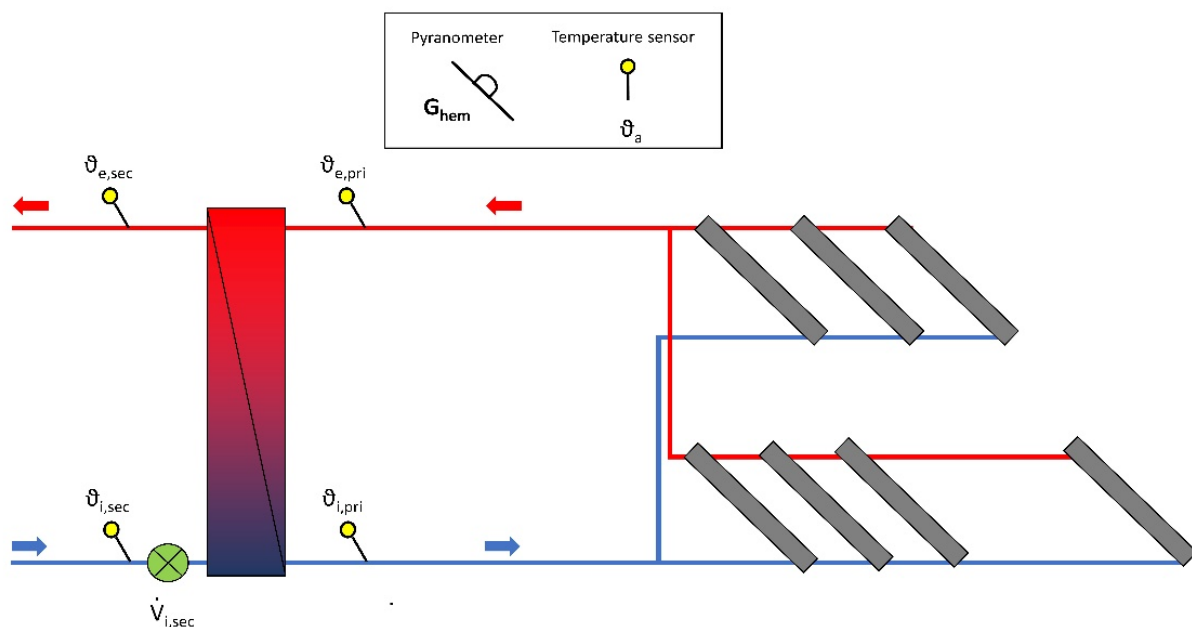


Figure 21: Low precision measurement setup.

Table 8 lists the characteristics for both setups. The FHW plant (see chapter 3) fulfills the criteria for the high (ideal) measurement setup. Measurement setups can lie between these two extremes.

Solar thermal plants (and large scale plants in particular) meet apart from few exceptions the minimum requirements regarding measurands, location and installation conditions of sensors, as these are necessary for basic plant monitoring and control. If the heat is sold to a third party (e.g. a district heating grid operator), the heat delivered by the collector array is oftentimes measured on the secondary side. If the concentration or fluid properties of the solar circuit are not known with reasonable accuracy, it might be better to measure on the secondary side. Refractometer measurements of the concentration can have considerable uncertainty and data sheets indications of fluid properties might be misleading. The most critical part is often the radiation measurement. Silicon cell sensors have issues with temperature and spectral responses and soiling [55]. Clamp-on metering of the volume flow and temperature is not advised in general, as this can lead to a strong bias [11]. For a new plant,

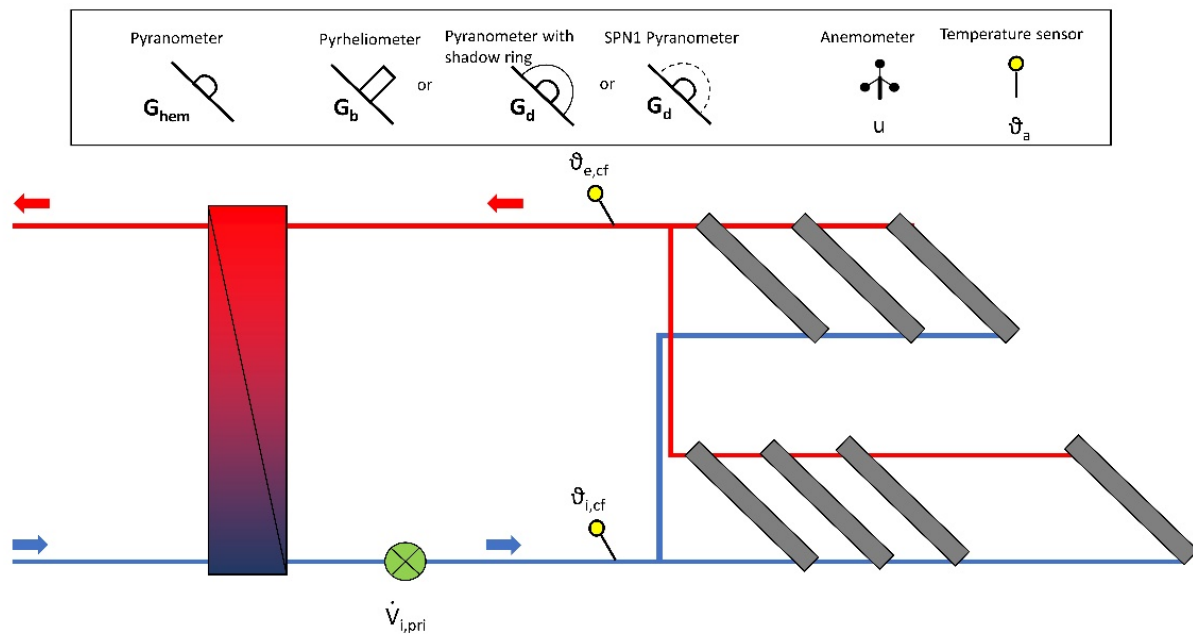


Figure 22: High precision measurement setup.

Table 8: Description of measurement setups.

Category	Low setup (minimum)	High setup (ideal)
Measurand, position and installation condition	<i>total radiation</i> in collector plane, <i>volume flow</i> in secondary circuit (with return and flow temperature), <i>fluid properties</i> (density & heat capacity) from data sheet, <i>return/flow temperature</i> with thermowell at heat exchanger, <i>ambient temperature</i> with ventilation unit	<i>total radiation</i> in collector plane, <i>beam radiation</i> (DNI) or <i>diffuse radiation</i> , <i>volume flow/mass flow</i> in solar circuit, laboratory test for <i>fluid properties</i> (density & heat capacity), <i>return/flow temperature</i> directly at entrance of the array, <i>ambient temperature</i> with ventilation unit, horizontal <i>wind speed</i>
Sensors	typical sensors for routine measurements in LST	comparable to ISO 9806 [10] recommendations
Sampling rate	1 minute	1 second (averaged to 10 seconds)
Measurement period	4-5 days (depending on plant operation)	6 months (depending on plant operation)

a pipe segment for the volume flow meter with a shut-off valve is easy to install if high-precision measurements might be needed at a later stage. Some plants have sampling rates of 5 min., 15 min. or even 1 h timesteps of data logging, but with modern data loggers and transmission technology, higher sampling rate are becoming the standard.

Better measurement setups require radiation measurements with a pyranometer. Most important is the measurement of the total radiation, but additional beam or diffuse measurements can significantly increase the precision. Existing plants can easily be equipped with better radiation sensors, as this does not interfere with the plant operation. Volume flow meters need to be compatible with the heat transfer fluid. Ideally, the temperatures are measured directly in the fluid instead of using thermowells, which reduces the response time. Averaging 1 s data to 10 s data is typically recommended because of the time constant of sensors and random errors and better results for the parameter estimation. A good guideline regarding installation conditions is provided by [15]. Checking the inclination of radiation sensors, regular cleaning of the pyranometer domes and regular inspection of the sensors and data logging is essential. It is also recommended to have a log book with relevant plant events (e.g. fluid re-filling, replacement of collectors, stagnation events, etc.). A webcam can help to track relevant plant events in hindsight.

The required measurement period depends on the variability of the operation conditions. For a good estimation and distinction of the model parameter, a variation of the influencing factors for the thermal power output is important. For the parameter estimation, 20 intervals with 1.5 h length were the plant is operation are generally used (see chapter 8.2). For highly variable operating conditions (return temperature, beam and diffuse radiation, etc.), these could be available in a 4-5 days measurement period. For some plant it might require up to 6 months from spring to autumn. In most cases, the average measurement period will be within these two extremes.

Every measurement setup, even for high precision measurements, has to deal with the problem, that the conditions can vary within an array and measurements at one location in the collector array may not be representative for another location. For the tilted radiation measurement, additional sensors in other spots of the collector array can be helpful, but this must be decided on a case-by-case basis. For the collector array model, the averages of the measured values could be used. Shading models (see chapter 7.1) are used to determine when internal shading occurs. Wind speed is not used as an explanatory variable in the collector array model, as it varies too much within the array and between a measurement in the collector plane and horizontally above the collectors. Wind speed measurement are only needed to exclude operation conditions with too high wind speed for a better estimation of the collector parameters. Ambient temperature measurements are less problematic, as the ambient temperature changes slowly and varies little within an array (sensors should be ventilated and not placed in the sun). Sensors should be placed at the location which is deemed to be most representative of the plant. For example, radiation measurement should be done within the array and not in the front row where there are additional reflections from the ground.

5.2 Plant configuration

With the plant configuration a “representation” of the plant in an evaluation tool is created. The representation entails the measurement as times series of numeric values, their unit and additional information relevant for data pre-processing and handling (e.g. sensor precision, allowed maximum gap for data interpolation, etc.). It entails additional information of the plant which are not given by the measurement data (e.g. size of the collector array, measurement setup, etc.) in a standardized way. The plant configuration must be such that the D-CAT method runs automatically where the user just chooses the characteristics of the evaluation, e.g. the measurement period. The plant configuration

Table 9: Plant parameters.

	<i>Abbreviation</i>	<i>Description</i>
Geographical information	λ	latitude
	ϕ	longitude
	ϕ_{st}	longitude of standard meridian
	ASL	sea level
Collector array	A_G	gross area
	D_{row}	row spacing
	H_{ground}	height of collectors above ground
	L_{row}	row length
	V_f	fluid volume
	n_{front}	number of front rows in collector array(s)
	n_{back}	number of back rows in collector array(s)
	β	tilt angle of collectors
	ζ	ground tilt angle
γ	azimuth	
	$\rho_f(T), c_f(T)$	fluid formulae for density and heat capacity
Single collector	$A_{G,col}$	gross area of collector
	H_{col}	height
	L_{col}	length
	W_{col}	thickness
Radiation model	d_{sens}	distance of radiation sensor from collector plane
	h_{sens}	position of sensor relative to top of collector
	κ_{sens}	external shadow angle
Heat exchanger model		depending on model, see chapter 7
Pipe model		depending on model, see chapter 7

method needs to be applicable to the typical hydraulic layouts and measurement setups.

Different valid measurement setups with their measured quantities are shown in chapter 5.1. Additionally, information on external shading needs to be provided (see chapter 7.1). The necessary parameters are listed in table 9. Note that only standard parameter are needed. Additional settings for initial conditions for the parameter estimation are explained in chapter 6.8, for the radiation model in chapter 7.1.

The D-CAT method was implemented in the software tool **ADA (Advanced Data Analysis)** [56], which has been developed by AEE INTEC since around 3 years. The tool is based on MATLAB[®] and uses object-oriented programming. It contains modules for data import, data pre-processing, calculations/algorithms, plots and data export. The method to represent plants was initially developed in the project METHODIQA [57] [58] and was later extended. The representation of a plant is based on a directed graph. A directed graph (or digraph) is a graph that is made up of a set of vertices connected by edges, where the edges have a direction associated with them. The main vertices are so-called blocks. Blocks contain structured information about a part of the plant or the measurement setup, e.g. collector array, heat meter, radiation measurement, etc. A representation of the FHW plant in the ADA tool is shown in figure 23.

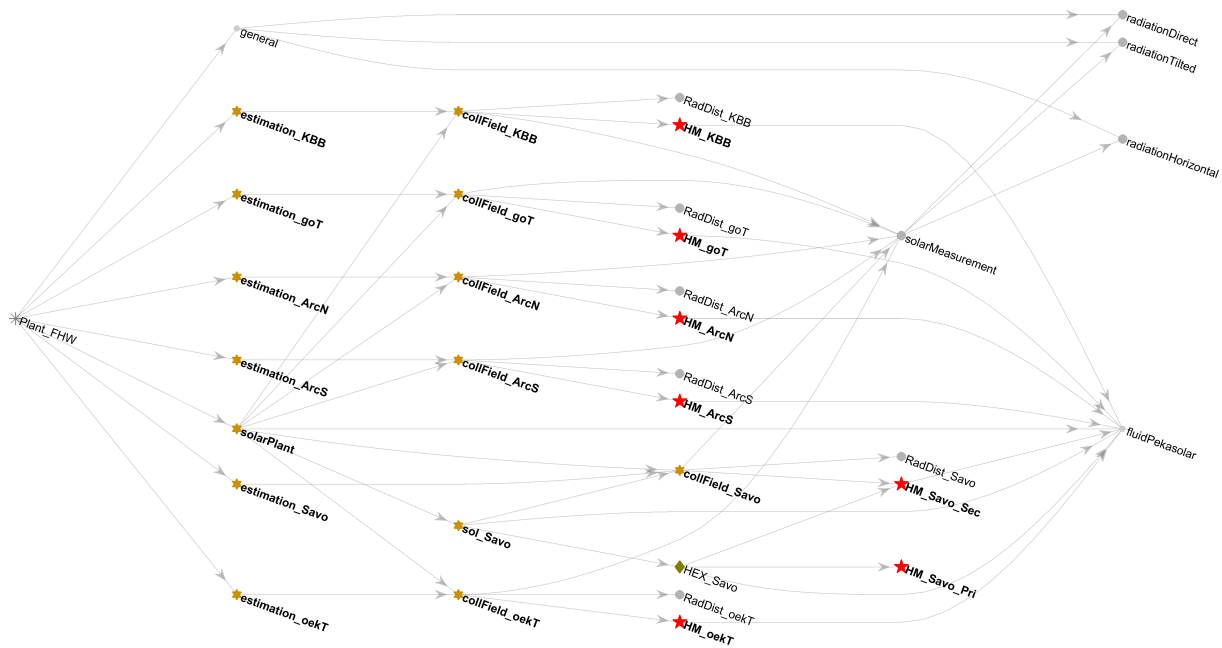


Figure 23: Representation of FHW plant (with main vertices) as a graph in ADA.

Blocks consist of *raw datapoints*, *regularized datapoints*, *virtual datapoints*, *parameter* and *virtual parameters*:

- *Raw datapoints* represent a specific measured quantity (e.g. ambient temperature) with the corresponding timestamps as recorded by the data logger or external sources. Raw datapoints are objects (in the software sense) and contain additional information on the measured quantity, e.g. its uncertainties, plausibility checks, maximal gap for interpolation, ignored ranges for the data, etc.. A screenshot of the properties of is given in figure 24.
- *Datapoints* are similar to raw datapoints, but contain regularized values after automated checks. These values are used for the algorithm calculations (together with virtual datapoints, parameter and virtual parameter)
- *Virtual datapoints* represent a calculated quantity with the same time grid as datapoints (e.g. fluid density)
- *Parameters*: represent a quantity which remain constant over the evaluation interval (e.g. gross collector area)
- *Virtual parameters*: represent a calculated quantity which remains constant over the evaluation interval (e.g. view factor of a pyranometer towards the sky)

Raw datapoints, regularized datapoints, virtual datapoints, parameter and virtual parameter are also on the directed graph, connected to the blocks. Algorithms are assigned to blocks (e.g. Block_CollectorField). For the calculation, an algorithm and a concrete block (e.g. collField_KBB, see figure 23) are chosen. The algorithm searches the graph for all the (virtual) datapoints and (virtual) parameters it requires for the calculation; it calculates them and stores the results in a cache. Virtual datapoints and virtual parameters are ways to implement physical models in ADA. The following steps are done to configure a plant in ADA, templates are available for all steps:

```

'pr.nb.general.DPs.teAmb'
RawDatapoint with properties:
    keep_in_memory: 0
    import_function: [1x1 ImportFunction]
    raw_data_info: [1x1 struct]
    raw_data_not_readable_ratio: 9.4394e-04
    ts1_raw_as_imported: [1x1 DatapointTimeSeries]
    ts2_raw_notignored: [1x1 DatapointTimeSeries]
    ts3_calibrated: [1x1 DatapointTimeSeries]
    ts4_checked: [1x1 DatapointTimeSeries]
    stored_values_: []
    calibration: []
    regularization_obj: []
    max_gap: 30 min
    datapoint_type: [1x1 DT_Temperature_Ambient]
    resampling_method: 'nanmean'
    ignored_ranges: [1x1 IgnoredRanges]
    ts: [1x1 DatapointTimeSeries]
    plausibility_checks_: [1x2 PlausibilityCheck]
    sensor_checks_: [1x1 SC_sensorHangs]
    time_data_start: 2016-08-21 23:59:00
    time_data_end: 2019-10-15 02:17:13
    compatible_unit: [1x1 CombineableExponentsClass]
    name: ''
    notes: 'T_Aussen_ws_PT100'
    display_name: 'teAmb'
    FQN: 'Plant_FHW.nb.general.rawDPs.teAmb'
    fingerprint: '36030ccf3ea94ae1b9b625afe3b7f997'
    uncertainty: [1x1 Uncnty.Chain]
    allow_uncertainty: 1

[1x1 RawDatapoint] teAmb
=====
notes: 'T_Aussen_ws_PT100'
FQN: 'pr.nb.general.DPs.teAmb'
block: 'parent_blocks'

[ Details ] -----
type: 'DT_Temperature_Ambient'
PC_1: 'PC_minViolated'
PC_2: 'PC_maxViolated'
SC_1: 'SC_sensorHangs'
data_start: '2017-09-17 00:00:00'
data_end: '2017-09-17 23:57:00'

[ Actions ] -----
(values)  values  std dev  uncertainty
(plot)    plot    plotCI
(parents) Plant    Project
    
```

Figure 24: Ambient temperature as an example of how RawDatapoints are implemented in ADA. Left: command window view with clickable links. Right: properties of the RawDatapoint object.

- 1) Create new plant
- 2) Add blocks (e.g. Block_CollectorField) and link them to represent the plant's hydraulics
- 3) Define datapoints by assigning data sources/raw data files using automated, pre-defined import functions
- 4) Define block parameters (e.g. collector area)
- 5) (optional) Share parameters and datapoints among blocks
- 6) (optional) Define calibration corrections and sensors/measurement uncertainty for the datapoints
- 7) Define project regularization method and sampling interval

5.3 Data pre-processing

Once the plant configuration is done, the next step is the data pre-processing. Data pre-processing is essential when working with data from real plants to assure plausible data. The following steps are performed automatically

- Merge data from different sources for each raw datapoint. Data are ignored if they have an invalid timestamp or there are multiple timestamps with different values
- Import data raw data and assign them to raw datapoints. Data must contain numeric values or be classified as NaN (not a number)
- Exclude data with timestamps who are outside the evaluation interval or are ignored by manually set ignored ranges (e.g. maintenance work)
- Apply calibration correction

- Apply plausibility checks to raw data. Plausibility checks determine if measured quantities are within physically plausible bounds (e.g. ambient temperature smaller than 50 °C). Unplausible values are set to NaN.
- Apply plausibility check to parameter values (e.g. gross collector area must be larger than 0 m²)
- Regularization of data. Use a time grid with a defined sampling rate (e.g. 1 second), i.e. t_1, t_2, t_3, \dots of values, where $t_{i+1} - t_i$ is equal to the sampling rate for all i and interpolate or take averages of data according to interpolation function, maximal allowed gap, etc.
- Unit conversion to the preferred unit of the datapoint
- Apply sensor checks (which operate on regularized values rather than raw data values), e.g. check if the total radiation is close to zero during night time
- Average / concatenate data to the desired sampling for the parameter estimation (e.g. 10 seconds)
- Calculation of virtual parameter and virtual datapoints. Virtual datapoints also contain calculations by auxiliary models, e.g. the decomposition of the total irradiance in its beam and diffuse part and calculation of the average irradiance on the collectors. After the calculation of the virtual datapoints, the data inputs for the parameter estimation procedure are available.
- Calculate standard uncertainty for each datapoint and virtual datapoint. The standard uncertainties depend on the datapoint values or calculation procedure and change over time. They have the same time grid as datapoints and virtual data points.
- Store calculation of virtual parameter, virtual datapoints and standard uncertainties to avoid potentially time-intensive recalculation

Although the procedure runs automatically, plots summarizing plant operation (e.g. daily yield, efficiencies, input-output diagrams as described in chapter 2.4) can be helpful for intuitive assessment of the data quality. After pre-processing, data are regularized and checked for basic plausibility. Following this procedure, all used data are either valid numeric values or invalid for some reason and stored as NaN.

6 Collector array modeling

6.1 Grey box modeling approach

One of the central goals of the D-CAT collector array test is to assess the operation of large collector arrays in a physically correct way. MeQuSo addressed this challenge by basing its analysis on a dynamic collector array model that is deployed in a grey-box approach: The model combines engineering and physical knowledge of collector arrays with the information contained in measurement data. The physical knowledge is introduced in the form of differential equation terms that describe energy transport and energy balances, and it can be formulated as a state-space model with given structure, but unknown parameters (see chapter 8.3 for a formal problem statement of the parameter estimation process).

In short, what we want is a dynamic physical model capable of describing the observed behavior of collector arrays. The model parameters will then be learned or calibrated in an optimization procedure in order to achieve a good fit between the modeled and the measured data such as the data collected at the FHW plant.

Chapter 6 is structured as follows:

- Chapter 6.2 lists the orienting guidelines used for the MeQuSo model.
- The model development process is briefly explained in chapter 6.3 and 6.4.
- The final 2-N model is explained in chapter 6.5, its validity is discussed in chapter 6.6.
- The numerical mathematics used for model solution are in chapter 6.7.
- Chapter 6.8 explains how the model is initialized (prior to numerical model solution) and how the parameters are initialized (prior to optimization).

Note: This chapter describes the collector array core model; it assumes the model predictor quantities to be known and ready to use as model inputs. Some of these model predictors require previous calculation using auxiliary models (refer to figure 19, page 42 for an overview): For instance, it might be necessary to split measurements of total radiation into beam and diffuse radiation. In the case of the FHW plant, beam and diffuse radiation were already measured separately; if only total tilted radiation is available, a radiation decomposition model has to be applied first. Additionally, the diffuse radiation to be used as model input may be used “as-is”, or again corrected by a physical model described in chapter 7. Refer to chapter 7 for details about radiation modeling for the dynamic collector array model.

6.2 Guidelines in model development

One of the core tasks for the in-situ collector array test is the development of a suitable data-based model. To do so, a data-based physical modeling approach is chosen. Following the modeling-for-a-goal principle, we will explain the guidelines that led us to the development of the D-CAT collector array model.

- **Model goal:** Explicitly, the main goal of the D-CAT collector array model is to get precise model parameter estimations. The parameters must have a straightforward physical interpretation,

comparable to the parameters of the ISO 9806 [10] standard on which Solar Keymark and single collector tests are based. The proposed method therefore follows a physical modeling approach based on the quasi-dynamic test procedure of ISO 9806 [10], but extends and adapts the ISO model to the boundary conditions and measurement setup of collector arrays. This mainly affects the dynamic behavior of collector arrays, and solar radiation on collector arrays as model input; both topics are addressed by suitable physical models.

- **Dynamic system behavior:** The D-CAT test should run passively, that is, it should make use of measurement data taken from normal system operation, and not require running extra test sequences in the tested collector array. This means that the model used for D-CAT must be capable of explaining the collector array behavior under fully dynamic conditions. This includes a sufficiently good fit under all relevant physical effects of collector arrays, as they were measured in the FHW collector arrays. Also in terms of model calibration, it is crucial to include the full system dynamics and not limit the evaluation to stationary or quasi-stationary system operation, as that would result in a loss of information leading to reduced precision, bias and correlation in the model parameters.
- **Collector array as technical component:** The desired test result is a characterization of the collector array as a technical system component. This means that the characterization should be as independent from weather conditions as possible, as independent from operating conditions as possible and as independent from different measurement setups as long as the operation is within the normal operating limits. The estimated model parameters should allow for straightforward interpretation of the current condition of the collector array, that is: the parameters should have physical interpretation. Black box models (e.g. [59]) are rejected for this reason. The ISO 9806 [10] fulfills this prerequisite to some extent for single collectors. The extension to collector arrays developed in MeQuSo will be discussed in this chapter. The D-CAT model is required to be applicable to flat-plate collectors only, although extensions are possible, and the D-CAT test procedure could be applied to other collector types just as well.
- **Simplicity and easy applicability:** The collector array model should be applicable with as little extra parameterization effort as possible to typical plant configurations. This distinguishes D-CAT method as a grey-box approach from white-box modeling used in many simulation software, where system behavior is described without taking measurement data of system operation into account. In order to produce accurate results, white box models require considerable effort to thoroughly define model input parameters, usually not available in practice. A parameterization with typically available measurement data must be possible. Effects which improve the accuracy of the outlet temperature or thermal power output only marginally, but require substantial additional modeling effort are not considered. For this reason, the temperature- and flow distribution within collectors among different collector rows and the hydraulic arrangement is not considered [49]. Wind speed is not included in the model, as it is not possible to measure it representatively for collector arrays.
- **Shading:** modeling external shading of beam radiation on large collector arrays requires considerable effort in parameterization and system description and leads to unreliable results. For regularly shaped arrays, the reduced irradiance for conditions where internal shading occurs could be calculated according to auxiliary models (see chapter 7.1.2). Using conditions with internal shading for the parameter estimation is possible, but not recommended as a general rule, as it could add more uncertainty to the parameter estimation.

Summary: Following these guidelines, the model development process in MeQuSo lead to a dynamic system model named 2-N model. This model is based on models already proposed in literature, e.g. [60] and [61]. In the MeQuSo project, the model was adapted to explain collector array effects until no clear model deficiencies were left. Finally, in a validation process based on the FHW measurement data, the 2-N model proved able to reproduce all relevant physical effects in good fit. From the model’s perspective, this is important in order to obtain unbiased model parameters in model calibration.

The 2-N model has good predictive power, being able to explain the system dynamics with a small number of model parameters (9). One central goal of the D-CAT test is to learn these model parameters in a data-driven approach. The model parameters are learned from measurement data in a parameter estimation process based on a training process; this process is described in chapter 8.

6.3 QDT model

The model used in the current version of the ISO 9806 standard [10] actually is a dynamic solar thermal collector grey-box model. It provides the following formula to model the specific power output of a solar thermal collector (“QDT model”)

$$\dot{Q}_{sp} = F' (\tau\alpha) (K_b G_b + K_d G_d) - a_1 (\bar{T} - T_a) - a_2 (\bar{T} - T_a)^2 - (mc) \frac{d\bar{T}}{dt} \quad (7)$$

The specific power output \dot{Q}_{sp} is calculated using the following simple formula; the fluid density needs to be evaluated at the temperature of the location where the volume flow is measured, not at the mean fluid temperature \bar{T}

$$\dot{Q}_{sp} = \dot{V}_{sp} \cdot \rho_f(T) \cdot c_f(\bar{T}) \cdot (T_{out} - T_{in}) \quad (8)$$

The term “quasi-dynamic” refers to the fact the test method based on the QDT model requires measurement data with reduced dynamics in the input data (see ISO 9806 standard for details). This is an important difference in methodology compared to the D-CAT collector array model, which has to accept fully dynamic data and does not require quasi-dynamic conditions. There are a number of reasons why this model cannot readily be used for the D-CAT purposes of large collector arrays; these reasons will be explained below.

Problems with QDT model for collector arrays

Thermal Power: In principle, the QDT model could be applied to collector arrays as well. Besides being “quasi-dynamic” (reduced input dynamics), the model is unsuitable for collector arrays for another important reason: The QDT model chooses the *thermal power output* as the explained variable. The thermal power formulation implicitly assumes that the power output can be calculated instantaneously, based on the difference between collector outlet and inlet temperatures with the current volume flow.

This, however, cannot be applied to collector arrays: The main reason is the *travel time* of the heat transfer fluid in its transport between inlet and outlet of an array. For nominal volume flows, the travel time of the FHW plant is in the range of 3 to 5 minutes, at nominal flow rate, more at reduced pump rotation. The same is true for many large solar thermal arrays making use of flat-plate and also other collector technologies. The fluid travel time results in a “time shift” between inlet and outlet, and this is the reason why it does not make sense to compare inlet and outlet temperatures on an instantaneous basis, which is implicitly done when thermal power output is calculated.

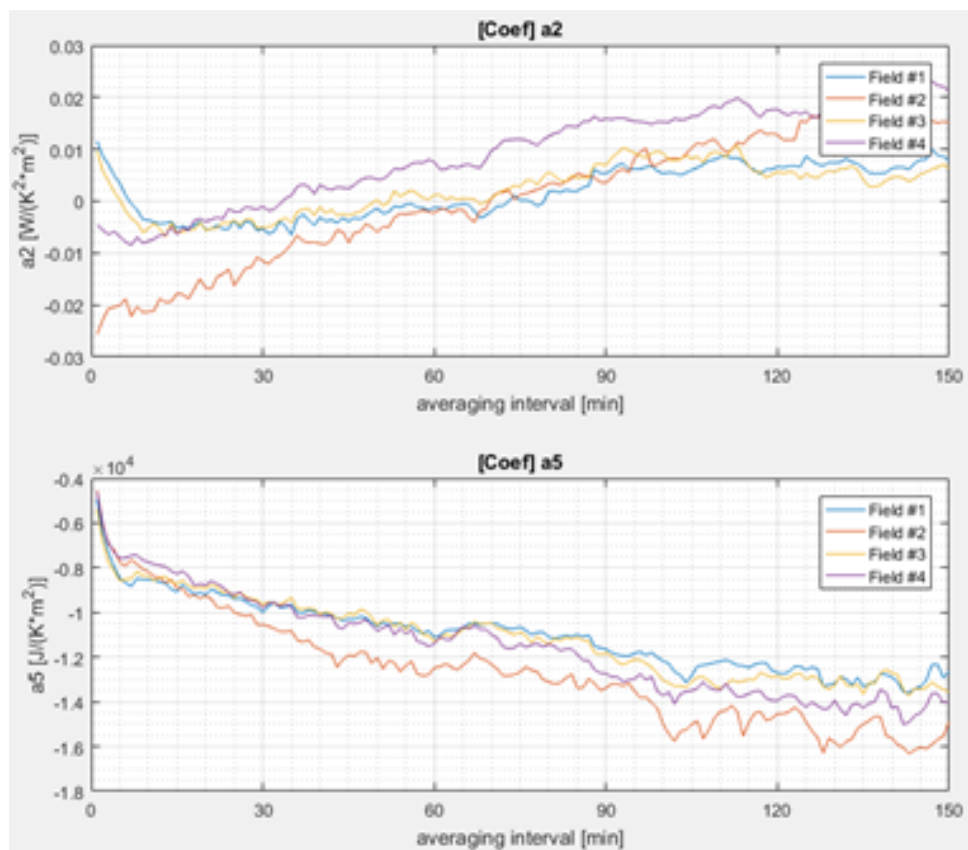


Figure 25: Model parameters of the QDT model depend on the chosen averaging time: Quadratic heat loss coefficient (a2, top) and heat capacity coefficient (a5, bottom) resulting from MLR regression are plotted over the chosen averaging time (x axis).

Heat capacity: Using the QDT model, the measurement data are averaged over some time period, typically around 5 minutes. Multiple linear regression (MLR) is then applied to estimate the model parameters, providing a fast and simple estimation method. However, the averaging makes the heat capacity, the (mc) term in the equation, hard to estimate because the heat capacity parameter depends on the chosen averaging time (see figure 25). This, again, introduces a bias not only on the heat capacity, but also on the other model parameters. The D-CAT model allows for a stable and physically meaningful estimation of the heat capacity coefficient.

6.4 D-CAT 1-N model

In order to overcome the described deficiencies of the QDT model, an extension model has been developed. This “1-node model” or **1-N model** explicitly models the *fluid transport* along the main flow direction of a collector array, resulting in a partial differential equation (PDE). Such models are oftentimes used for control purposes [62]. The model involves one spatial variable, namely the main flow direction, thus the short name 1-N model. This model does not involve calculation of a thermal power output. Rather, the model explains the temperature along the flow direction of a collector array, so the temperature depends on time t and flow position x .

$$(mc) \frac{\partial T(x, t)}{\partial t} = F'(\tau\alpha)(K_b G_b + K_d G_d) - a_1(T(x, t) - T_a) - a_2(T(x, t) - T_a)^2 - \dot{C}_f \frac{\partial T(x, t)}{\partial x} \quad (9)$$

The transport term $\partial T(x, t)/\partial x$ is driven by the capacity flow which is given by the following equation³

$$\dot{C}_f = \dot{V}_{sp} \cdot \rho_f(T) \cdot c_f(T) \quad (10)$$

An interesting property of this 1-N model is the fact that it uses the same physical parameters as the QDT model. This means that the estimated parameters of this model are comparable to the data sheet parameters of solar collectors from e.g. Solar Keymark tests based on ISO 9806 [10]. Most dynamic test procedures are based on comparable 1-node models [27].

For simplicity of nomenclature, the treatment of beam radiation in equation (9) is represented by the parameter K_b . Actually, the beam radiation parameter is treated in the same way as in the ISO 9806 [10]; that is, the beam radiation enters the model as

$$K_b = 1 - b_0 \left(\frac{1}{\cos(\theta_{col})} - 1 \right) \quad (11)$$

with $F'(\tau\alpha)$ and b_0 being the unknown model parameters that have to be estimated from measurement data.

The 1-N model accepts a wider range of input data, compared to the QDT model: The model involves no thermal power calculation and thus does not require quasi-stationary input data. The 1-N model describes how dynamic changes in the volume flow and inlet temperature are transported along the collector array, using the transport term $\dot{C}_f \cdot \partial T(x, t)/\partial x$.

However, the 1-N model is not capable of accurately describing the collector array output temperature under fully dynamic conditions, see figure 26. Unphysical behavior of the modeled temperature course reveals structural deficiencies that need to be overcome. The structural deficiencies would lead to a bias in the estimated model parameters, and although the 1-N model is simpler than the 2-N model (chapter 6.5 below) we do not recommend using the 1-N model for collector array evaluations of fully dynamic operating conditions.

³Note that the fluid properties (density and heat capacity) need to be evaluated at the temperature T where the volume flow is measured, not at the mean fluid temperature \bar{T}

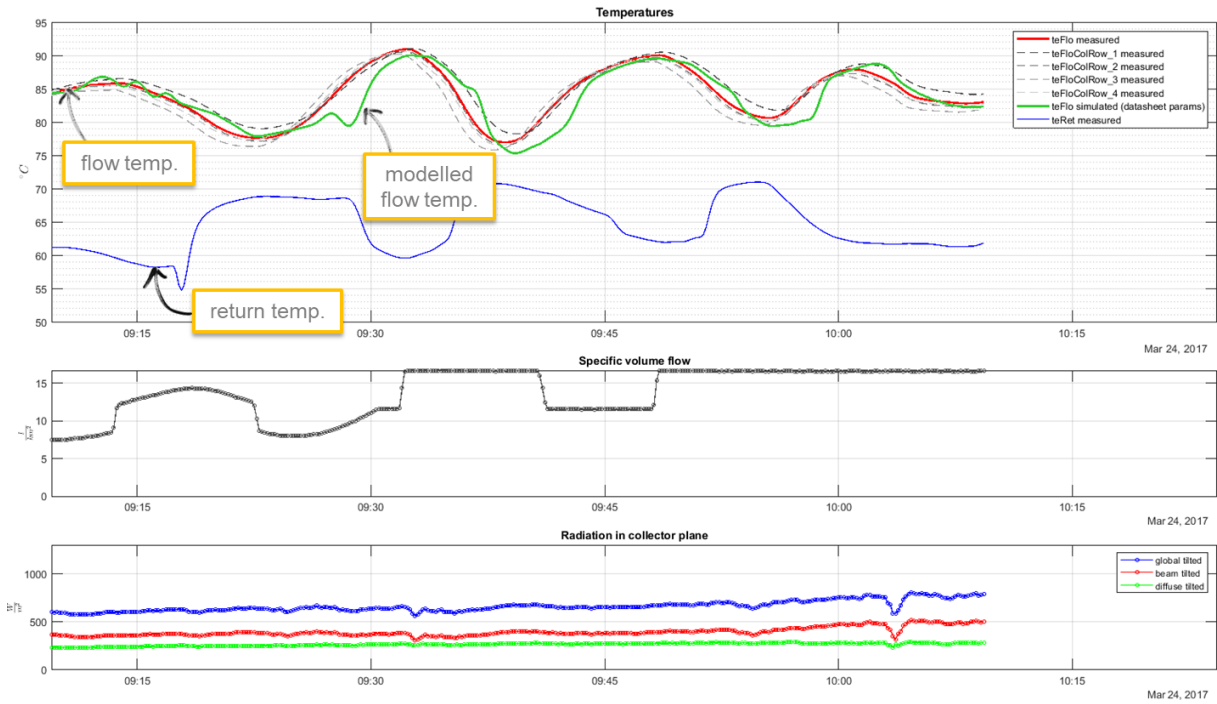


Figure 26: Exemplary application of the 1-N model to a 1-hour interval of data from one of the FHW collector arrays. While the modeled flow temperature roughly follows the measured temperature (upmost subplot), the model output shows some clear structural deficiencies (e.g. around 9:30).

6.5 D-CAT 2-N model

The “2-node model” or **2-N model** tries to overcome the structural deficiencies mentioned above for the 1-N model. It describes the temperature of the solid or metal part of the collector array. Fluid temperature $T_f(x, t)$ and metal temperature $T_m(x, t)$ are modeled as separate states, resulting in two coupled equations

$$(mc)_m \frac{\partial T_m(x, t)}{\partial t} = (\tau\alpha) (K_b G_b + K_d G_d) - a_1 (T_m(x, t) - T_a) - a_2 (T_m(x, t) - T_a)^2 - (\alpha - \alpha' \dot{V}_{sp}) (T_m(x, t) - T_f(x, t)) \quad (12)$$

$$(mc)_f \frac{\partial T_f(x, t)}{\partial t} = (\alpha - \alpha' \dot{V}_{sp}) (T_m(x, t) - T_f(x, t)) - \dot{C}_f \frac{\partial T_f(x, t)}{\partial x} \quad (13)$$

The fluid temperature $T_f(x, t)$ depends directly on volume/capacity flow; the metal temperature $T_m(x, t)$ depends directly on weather conditions (radiation, ambient temperature) and only indirectly on fluid flow. The 2-N model equations (12) and (13) are two separate partial differential equations, linked by a term that describes the energy exchange between fluid and solid part, due to convection and conduction, the term $(\alpha - \alpha' \dot{V}_{sp}) (T_m(x, t) - T_f(x, t))$.

The convective heat transfer between solid and fluid is described in the 2-N model by the parameters α and α' . α can be interpreted as the lumped convective-conductive heat transfer between fluid and metal, at nominal volume flow. This heat transfer is volume-flow dependent, and the parameter α'

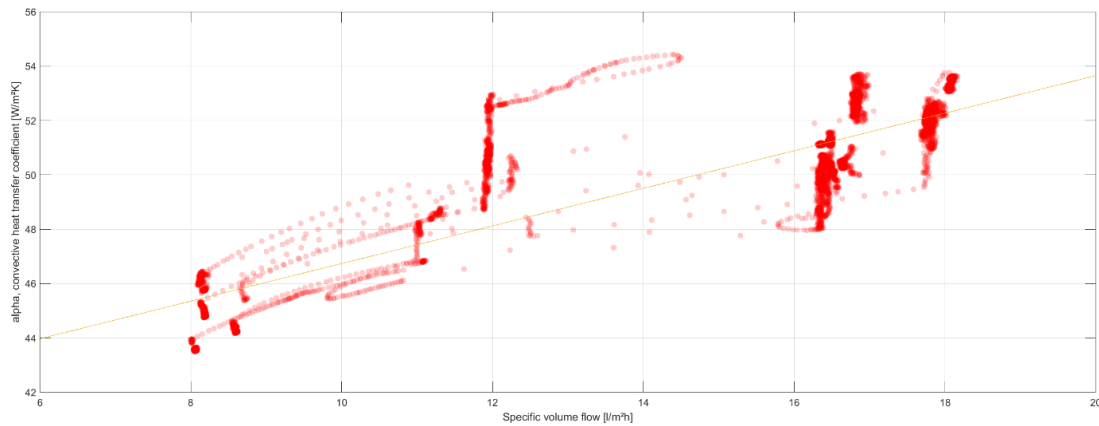


Figure 27: Volume flow dependence of the convective heat transfer coefficient α on volume flow through a collector array. A simple linear correction model has been used in the present D-CAT 2-N model.

takes into account that heat transfer is lower at lower volume flows, as shown in figure 27. The convective heat transfer depends on the Reynolds number in the collectors' absorber pipes. To keep things simple, the Reynolds number is approximated by volume flow, in the 2-N model equations 12 and 13. A simple linear correction model is used to incorporate the volume flow dependence. The volume flow correction term \dot{V}_{sp} is the specific volume flow in the collector array, not in the absorber pipe. While it's the absorber pipe volume flow which is responsible for the local heat transfer from metal to fluid, local and total collector array volume flow are essentially linked by a constant, and this constant is included in the estimated parameter α' . The heat transfer coefficient α is also temperature-dependent; implementing a temperature correction of α might also improve the model fit, but would come at the expense of one more model parameter, and we found that the volume flow dependence dominates the temperature dependence. This is why the metal-to-fluid heat transfer is corrected for volume flow dependence, but not for temperature dependence.

The same simplification in nomenclature already used in the 1-N model, equation (9), is used here in equation (12). In verbose notation, K_b , the IAM for beam radiation, is modeled by parameter b_0

$$K_b = 1 - b_0 \left(\frac{1}{\cos(\theta)} - 1 \right) \quad (14)$$

This means that the beam radiation G_b is modeled by the two unknown parameters ($\tau\alpha$) and b_0 which need to be estimated from measurement data. More complex IAM models, using an exponent different from 1 for the incidence angle dependent term in the parenthesis are available, see e.g. [63], but these models have not been used mainly for two reasons: (1) They introduce another parameter to the model, and the model would not be linear in the parameters anymore. (2) The incidence angle modeling approach used here is the same as the one used in the ISO 9806 [10]. Two node and multi-node models have been used in test procedures (e.g [64] [65] [66] [67]).

The beam radiation G_b and diffuse radiation G_d used in equation (12) can either be measured or modeled. Note that testing according to ISO 9806 [10] requires that no shadow is to cast on the collector and no significant view obstructions or reflections from surrounding buildings and surfaces shall affect the collector. The beam radiation G_b and diffuse radiation G_d used in equation (7) are therefore the same along the collector height and measurements at the top of the collector are

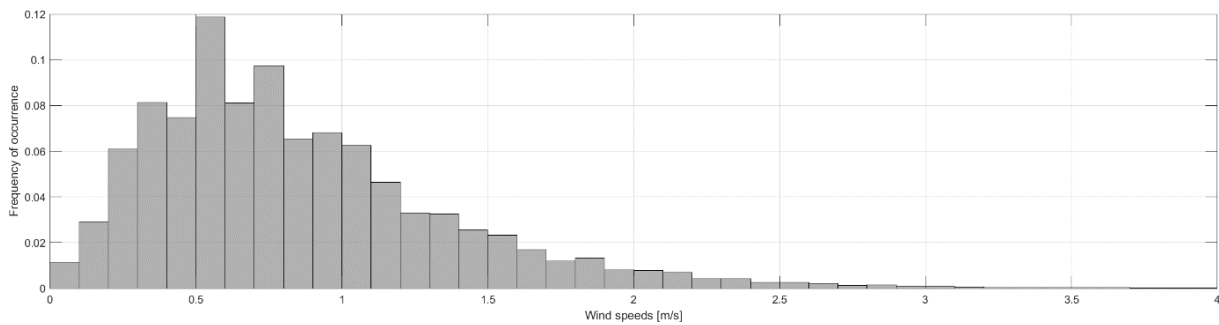


Figure 28: Histogram of wind speeds at the site of the FHW plant in Graz for the year 2018. Wind speeds are consistently in a very low range with practically no high wind speed data available at the FHW site; the same is true for the other two measured years, 2017 and 2019.

representative for the average irradiance on the collector. If view obstructions and reflections are significant, the diffuse radiation G_d in equation (12) might be corrected with radiation modeling that accounts for these effects (see chapter 7.1). The same applies to equation (9) for the 1-N model.

More complex models might include terms such as energy losses due to wind or radiative energy losses to the sky. Both terms have been neglected in the present study for the following reasons: Wind speeds were consistently low at the site of the FHW plant in Graz, where the measurement data have been collected. Practically no wind speeds > 3 m/s were available in the measurement data, as becomes apparent from figure 28. Together with the fact that all tested collectors are double-glazed flat plate collectors known to have low wind-dependence, we decided not to take the wind term into account. Radiative energy losses are known to be small for double-glazed collectors and have thus also not been taken into account for the D-CAT 2-N collector array model.

Model parameter description

Table 10 gives an overview of the parameters used in the D-CAT 2-N model⁴. These parameters shall be estimated by measurement data as will be described in chapter 8. Table 10 also holds a short description on how each parameter is typically affected by long term field operation of a collector array.

The authors would like to stress that the D-CAT based on the 2-N model allows characterization of collector arrays as a technical component, clearly separating collector parameters from the weather conditions in the test data. To a large extent, the results are also independent from the fact that operating conditions deviate from design conditions (such as temporarily higher system operating temperatures).

In simple terms, if the operating temperatures changes (e.g. due to some external boundary condition outside the scope of the collector manufacturer) or irradiance levels change (“year with bad weather”), the collector array parameters do not change: The parameters keep being a good representation of the collector array as a technical component. On the other hand, if the collectors (as a component) change (e.g. soiling, wet insulation, degraded heat transfer inside the collector etc.), this change will be reflected in the model parameters. In this way, the D-CAT collector array test represents a neutral and detailed characterization of a collector array as a technical component, largely independent from external conditions.

⁴For the sake of simplicity, the model equations are re-written here in simplified syntax, omitting the explicit space and time dependence, i.e.: T_m is equivalent to $T_m(x, t)$.

Table 10: Overview of the parameters used in the D-CAT 2-N model, equations (12) and (13).

Parameter	Parameter description	Notes	Typical value	Physical unit
$(mc)_m$	Heat capacity of the solid part of the collector array	Estimation is not degraded by taking time averages. Total heat capacity includes $(mc)_m$ and $(mc)_f$	2500	$\frac{J}{m^2K}$
$(mc)_f$	Heat capacity of the collector heat transfer fluid	Known by measurement of heat transfer fluid, or estimated by data	4000	$\frac{J}{m^2K}$
$(\tau\alpha)$	Zero loss coefficient	May decrease over time due to material degradation. Not the same as $F'(\tau\alpha)$ in ISO 9806 [10]; here, F' is modeled by α and α'	0.8	—
b_0	Incidence angle modifier	Degrades with dirt depositing on collector cover in field operation	0.15	—
K_d	Incidence angle correction for diffuse radiation	May degrade in the same way as b_0	0.93	—
a_1	Heat transmission coefficient	Refer to solid temperature, not fluid temperature (like in ISO 9806 [10])	2.5	$\frac{W}{m^2K}$
a_2	Temperature dependence of heat transmission coefficient	Same note as for a_1	0.01	$\frac{W}{m^2K^2}$
α	Convective heat transfer coefficient between T_m and T_f	Described in a lumped way as F' in the 1-N model	60	$\frac{W}{m^2K}$
α'	Volume flow dependence of the convective heat transfer	Just like α , does not degrade with dirt deposits on the collector cover	4	$\frac{Ws}{m^3K}$

6.6 Model validity

The 2-N model models the temperature in fluid and metal part of a collector row as a one-dimensional transport phenomenon; in other words, fluid and metal temperatures are modeled as a set of distributed states along the main fluid direction. $x = 0$ is the point where the heat transfer fluid enters the collector array and where T_{in} is assumed to be known. At $x = 1$, the fluid exits the collector array, and T_{out} is assumed to be known. In case these temperatures are not directly available, the 2-N model can be combined with a standard heat exchanger model (see chapter 7.3) and/or pipe model (see chapter 7.2) to model the piping between collector array and heating central.

All more detailed effects that take place *within collectors* are not modeled; this is a model simplification. Due to the hydraulic construction of large-scale harp or meander collectors (see figure 29), the fluid travel time through a solar collector is not a deterministic number. For instance, the travel time is different for each absorber pipe of a harp collector, so there is no such thing as a deterministic travel time. In the model, equation (13), the fluid transport in a collector row is assumed to be deterministic and is approximated by the mean volume flow in all absorber pipes, the total volume flow.

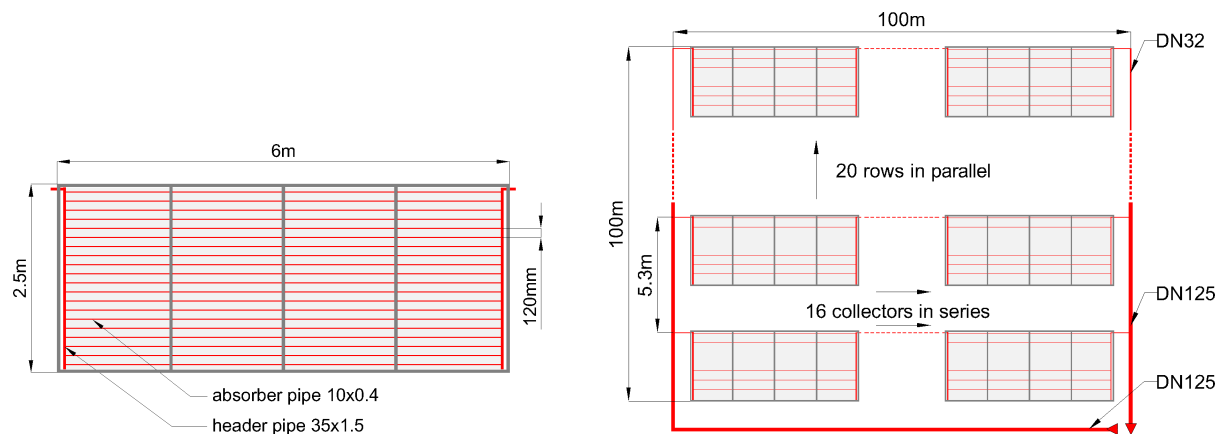


Figure 29: Schematic drawings of hydraulic setup of large-area harp collector (left) and exemplary collector array using harp collectors (right) [49]. The exact dimensions are not important here and are just exemplary values.

Also higher-level hydraulic effects are not taken into account by the 2-N model. In fact, the object modeled by equations 12 and 13 is a collector row. Applying it as a collector array model is equivalent to assuming that all collector rows of the array get exactly the same volume flow, and that the travel times through the collector rows are not necessarily the same. In other words, the model ignores the internal piping in collector arrays, and the model assumes that the volume flow distribution in the array is homogeneous. This is usually a valid assumption for LST plants, either because balancing valves are used or because the hydraulic setup is favorable. The exact conditions under which it is reasonable to assume homogeneous flow distribution in collector arrays are described in detail in [68].

The hydraulic effects described here are illustrated in figure 30 under dynamic volume flow and temperature conditions. The collector row outlet temperatures reveal that the travel times through the rows differ slightly, and that the volume flows are not perfectly homogeneous (different outlet temperature levels).

On one hand, this design is a model simplification. On the other hand, explicitly modeling the collector array piping would considerably increase the burden associated with using the model. Ignoring collector array piping makes the model easier and more straightforward to be used in the framework of a general collector array test like the D-CAT test.

As becomes clear from looking at figure 31, the 2-N better describes the measured flow temperature, compared to the 1-N model. A fundamental version of the 2-N model has been proposed in [60] and [61] and has been further extended in the MeQuSo project. This D-CAT 2-N model is capable of explaining the dynamic behavior of large collector arrays over a very wide range of operation modes. As will be explained in subsequent chapters, the 2-N model can be solved numerically in an efficient way, and we recommend using this model for the purposes of dynamic collector array evaluation, optimization and testing.

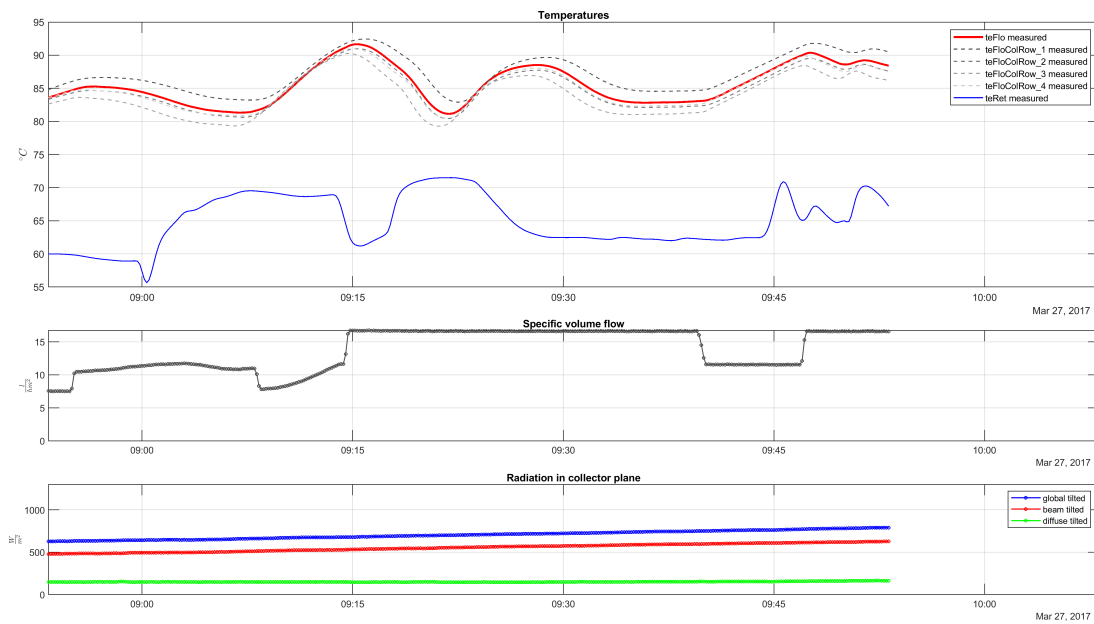


Figure 30: Comparison of collector row outlet temperatures and the mixed collector array outlet temperature. For one of the FHW collector arrays consisting of four collector rows, the four collector row outlet temperatures are plotted in the top subplot (dotted lines). The solid line is the array outlet temperature, measured after the four collector row mass flows are mixed; this is the temperature modeled by the D-CAT 2-N model. The subplot in the middle depicts the total collector array volume flow that results in fluctuating return temperatures. For less dynamic operating conditions, the travel time differences among the collector rows are much less significant.

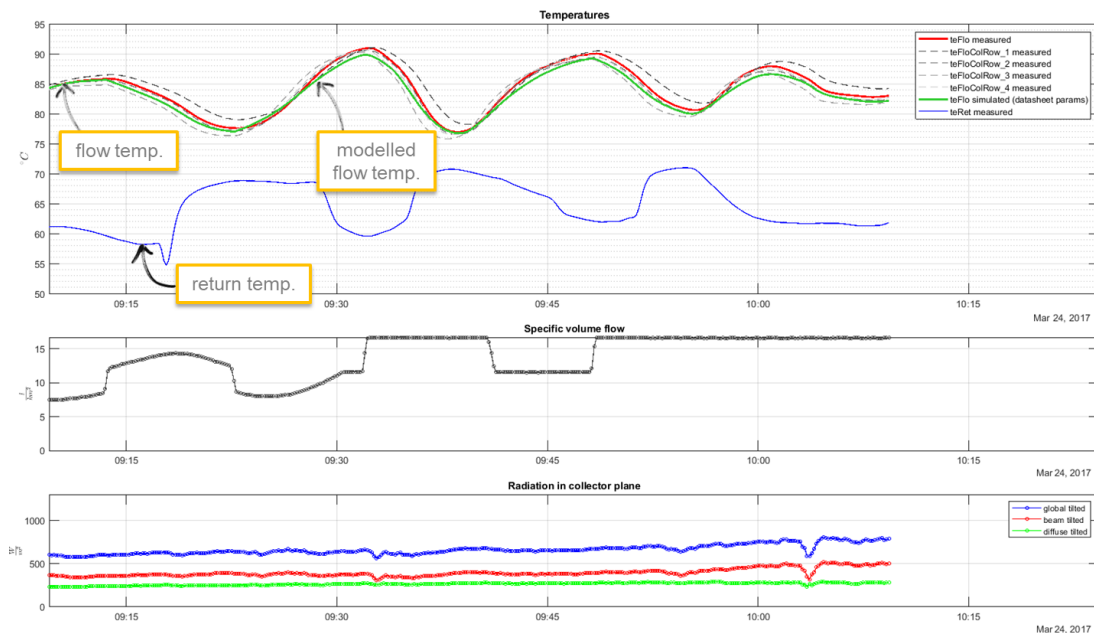


Figure 31: Exemplary application of the 2-N model to the same collector array and the same 1-hour interval as in figure 26. Apparently, the 2-N model (with 100 numeric discretization compartments in flow direction) does not show the same structural deficiencies as the 1-N model and is capable of an accurate enough description of the flow temperature.

The 2-N model used for the D-CAT test describes the temperature of a collector array during operation (collector array pump on, volume flow > 0), that is, the output temperature and the temperatures within the collector array as so-called “hidden states”.

- During **operation**, the outlet temperature sensor measures the mixed fluid temperature of several rows of collectors.
- During **night time** with no volume flow, however, the same temperature sensor measures the temperature in the pipe itself and does not represent the collector array temperature. In other words, due to practical measurement restrictions, the collector array model cannot be used at night time or at all times with zero volume flow.

The described scope of model validity naturally separates the measurement data into **chunks of usable and not usable data**. Figure 32 shows a graphical representation of the domain of validity for the D-CAT 2-N model.

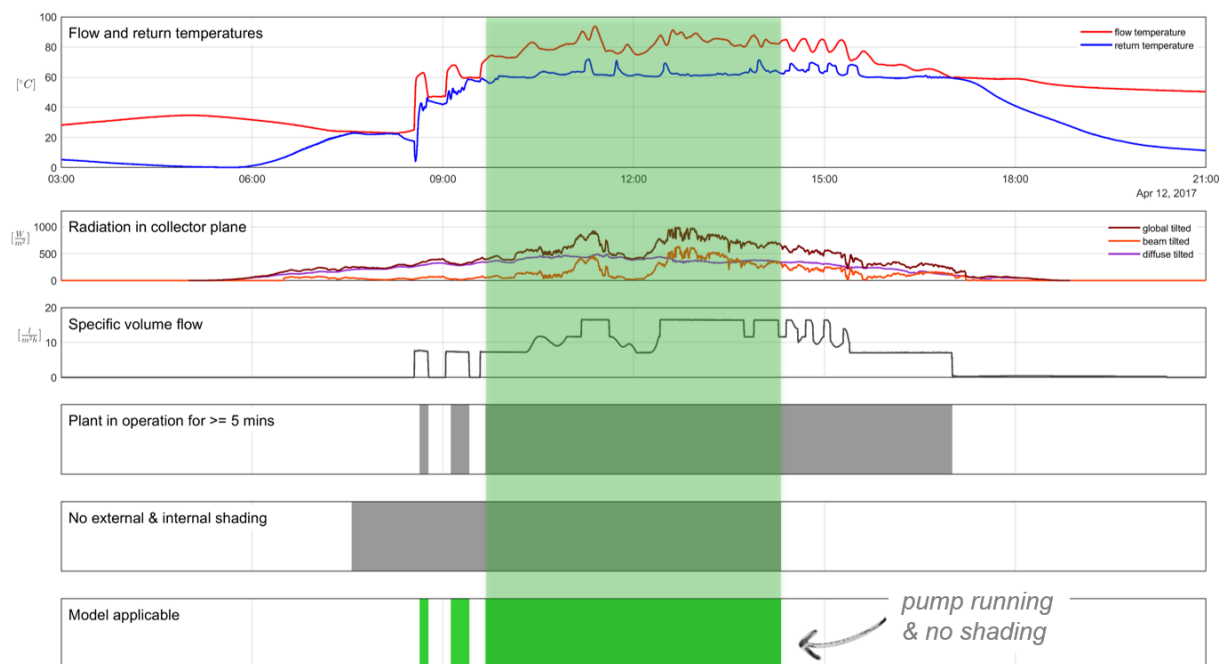


Figure 32: Domain of model validity for the D-CAT 2-N model: The requirements are that there is no shading on the tested collector array, and that the pump has been in operation for at least 5 min. All other dynamics (in radiation, volume flow and inlet temperature) are accepted.

Apart from the condition that the collector array volume flow be > 0, collector arrays are required to be **unshaded**, be it external shading (e.g. from trees or buildings) or internal shading (from other collector rows).

- **Internal shading** could be handled easily by a geometric radiation model, but this would introduce significant uncertainty due to practical accuracy limitations (e.g. row distances in the field).

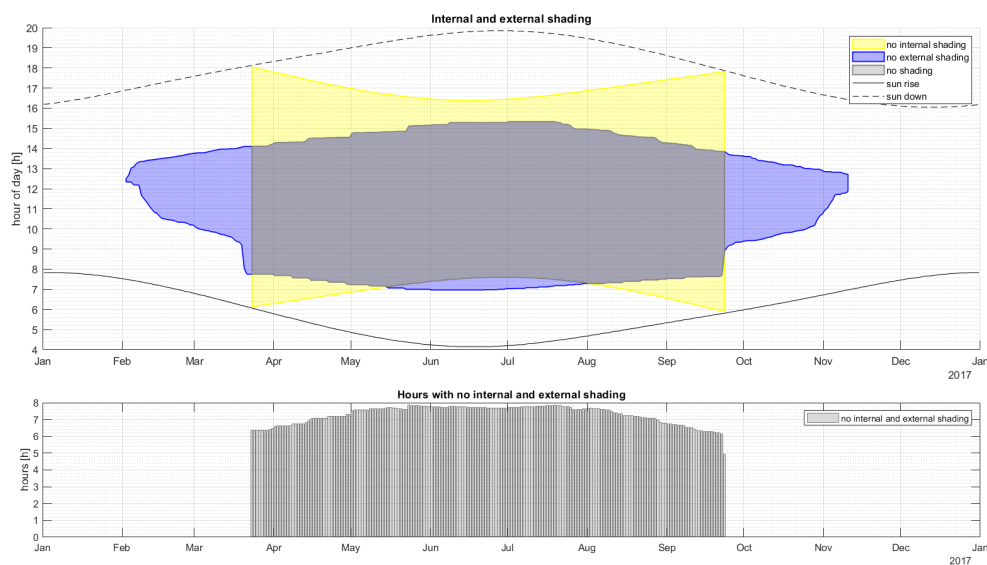


Figure 33: Internal and external shading of FHW plant. The core area labelled “no shading” marks the data intervals that can be used with the D-CAT method for data selection and parameter estimation of the FHW collector arrays.

- **External shading** is very hard to model exactly and would introduce a non-negligible bias into the parameters.

The combination of external shading and internal shading is shown in figure 33. For the whole year, there are 1,348 hours without internal and external shading. As can be seen, potential hours for the evaluation can be substantially reduced by shading, especially for collector arrays with narrow row spacing as is the case for the FHW plant. Using conditions with internal shading for the parameter estimation is possible (as in the ICFT method, see chapter 2.3, page 18), but it is not recommended as a general rule: While the effect of partial shading on collector outlet temperature is small up to approx. 30% of shading, the amount of shading is hard to determine exactly in practical collector fields, due to variations in row spacing, tilt angle etc. The uncertainty that would be introduced into the collector array parameters by taking into account partially shaded operating hours is deemed to be more severe than the advantage of having more data. Additional investigations would be necessary to achieve a final answer to the question if partially shaded data should be taken into account for parameter estimation, up to some limit of e.g. 20% or 30%.

Based on this reasoning, we defined the **model validity** to include only conditions where there is no shading, and the pump has been running for at least 5 min. The collector array output temperature is measured in a collecting pipe, carrying the mixed heat transfer fluid from several collector rows. Heat losses along the collecting pipes are negligibly small, but capacitive effects are not. Therefore, the goal of the **minimum pump operation time** constraint is to reduce thermal capacitance effects in the collecting pipes.

- Another goal is to make sure all collector rows reached stable volume flows after the pump switches on, and that the heat transfer fluid, coming from several collector rows, has enough time to mix before it reaches the temperature sensor. In this way, the measured outlet temperature

measured in the collecting pipe is a reliable representation of the true collector array outlet temperature.

- Following our experiences with the D-CAT method, this 5-minutes minimum operation time constraint could possibly be relaxed to 1 or 2 minutes, but the results shown in this report all use a 5-minutes constraint.

All other features in the measurement data are accepted in an unrestricted way. In particular, the **full dynamic behavior** of radiation, volume flow and flow and return temperatures is accepted for the D-CAT collector array test.

With the D-CAT 2-N model, we have at hand a nonlinear coupled PDE model. In the authors' opinion, this is a parsimonious model in that it describes the dynamic behavior of a collector array accurately enough for our purposes, allowing for a wide range of data, and it still comes with a relatively small number of model parameters (9 instead of 6 for the 1-N model). These 9 parameters are lumped, that is: Each model parameter has 1 value that represents the whole collector array. This can be interpreted as the "typical" collector that best represents the collector array.

6.7 Numerical model solution

The D-CAT 2-N model consists of two coupled partial differential equations, nonlinear in states (linear in T_f , nonlinear in T_m), linear in the parameters. The model requires beam and diffuse radiation to be given as separate inputs. In the common case that only total tilted radiation is available from measurement, a radiation model has to be applied to calculate beam and diffuse radiation as separate model inputs. This issue is with in chapter 7.1 about radiation modeling.

The numerical model solution procedure has been implemented in MATLAB[®]. The basic approach to the numeric solution is the *method of lines*; for reference, see [69] for instance. Following the method of lines, the spatial derivatives of model equation (13) are discretized, giving rise to a system of ordinary differential equations (ODEs), so the model can be formulated as a *state-space model* (see chapter 8.3).

The *spatial discretization* has to take the modeled transport effect into account, thus a backward finite difference scheme for the first derivative $\partial T_f(x, t)/\partial x$ has to be used – central difference schemes would be numerically unstable for this 1-dimensional transport problem. We used a second order accuracy backward difference scheme which performed well.

The spatial grid is uniform along the flow direction, except for a small uniform part near the inlet of the collector array, where the measured return temperature is available as spatial boundary condition at $x = 0$ (see figure 34). Here, an auxiliary node is added in order to account for the fact that the inlet temperature is constant until entering the collector array. A similar reasoning is used at the collector outlet: The measurement equation of the state-space formulation consists of a linear extrapolation of the modeled fluid temperature to the point where the temperature was measured in the collector array.

The number of equations in the state-space model depends on the chosen number of numeric discretization compartments. For the FHW collector arrays, model results depended on the number of compartments up to a number of 50 to 100. Since the model solution time only very slightly depends on the number of compartments, 100 compartments have been used throughout the analysis in the MeQuSo project.

The 2-N model, formulated as a nonlinear state-space model, was solved using a traditional MATLAB[®] *stiff solver* (we tried *ode23s* and *ode23tb*, finding that the latter is faster and good enough). The numeric solution process benefits from the fact that the D-CAT 2-N model has an

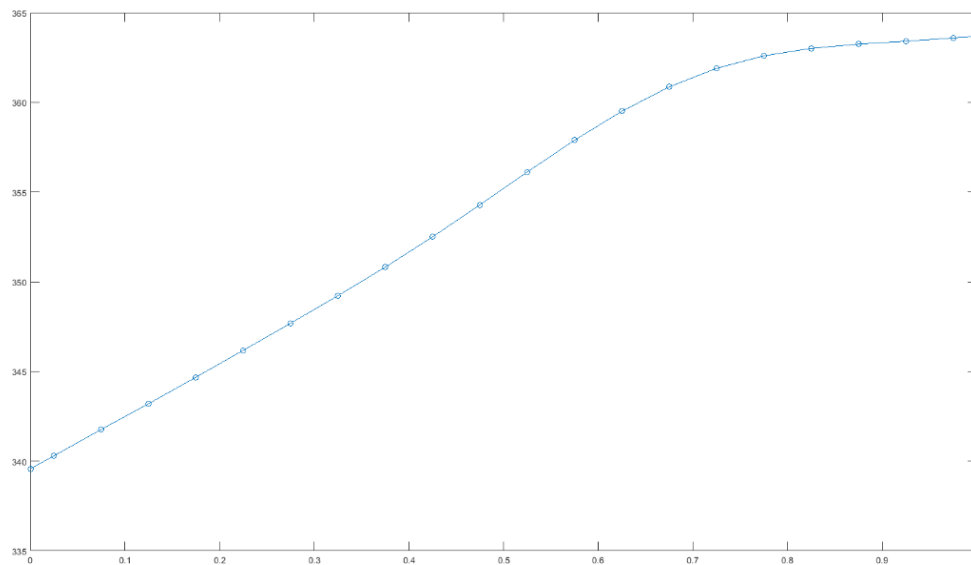


Figure 34: Uniform spatial grid along the collector array main flow direction, represented by the x axis (0 = collector array inlet, 1 = collector array outlet). Note the non-uniform grid at inlet and outlet of collector array.

analytic Jacobian. The Jacobian depends on both the states (the metal temperatures only) and the model parameters, so it has to be updated in each optimization run and during iterative ODE solution. The stiff behavior is due to the different time scales of the involved physical effects, with fast-changing dynamics being present mainly in radiation, volume flow and inlet temperature. Gradients within the collector array (represented by the hidden fluid temperature states) are depicted in figure 35.

6.8 Model and parameter initialization

Model Initialization

At time $t = 0$ of a simulated time interval, only measured inlet and outlet temperatures are known, but the hidden states are unknown and thus need to be initialized to some value. Initialization becomes necessary since we do not require measurement data to be quasi-dynamic. The model states are initialized assuming steady-state conditions (temporal derivatives assumed to be zero). This results in an initialization error which decreases over time, as other model effects dominate. Following [70], the time constant of water-driven solar thermal collectors at a specific mass flow range of approx. $10 \text{ kg/m}^2\text{h}$ (typical range for FHW) is in the range of 15 minutes. Based on this, a “pre-simulation” time of 30 minutes (twice the time constant) has been chosen for the MeQuSo approach. This approach should ensure a small model initialization error.

Parameter Initialization

For all flat-plate collector types evaluated during the MeQuSo project, data sheets based on the ISO 9806 standard [10] / Solar Keymark were available. These data sheet values for single collectors were used to calculate a-priori estimations of the model parameters. Table 11 describes, for each parameter of the D-CAT 2-N model, the procedure used to calculate initial parameter values used in the parameter estimation process. This parameter estimation process and the optimization are

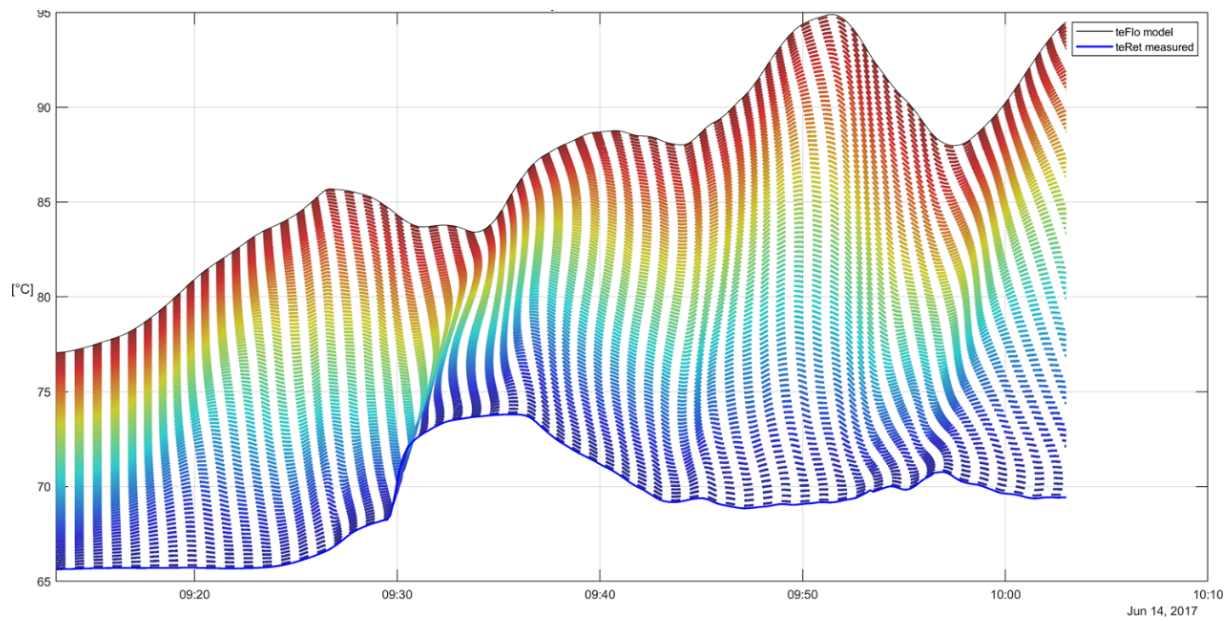


Figure 35: Visual representation of the fluid temperatures (hidden states) along the main flow direction of a collector array, from inlet temperature (bottom) to outlet temperature (top)

described in chapter 8.

What follows is an outline to estimate an initial value for parameter α based on the collector array measurements inlet and outlet temperatures T_{in} , T_{out} and capacity flow \dot{C}_f (needed anyway for parameter estimation) and the collector efficiency factor F' . The calculation is based on the collector heat removal factor F_R (see chapter 6 in [14]).

$$\begin{aligned}
 T_f &= 0.5 (T_{out} + T_{in}) \\
 U_L &= a_1 + a_2 (T_f - T_a) \\
 c &= \frac{\dot{C}_f}{U_L} \\
 F_R &= c \cdot \left[1 - \exp\left(-\frac{F'}{c}\right) \right] \\
 \dot{Q}_{sp} &= \dot{C}_f (T_{out} - T_{in}) \\
 T_m &= T_{in} + \dot{Q} \cdot \frac{1 - F_R}{U_L \cdot F_R} \\
 \alpha &= \frac{\dot{Q}_{sp}}{T_m - T_f}
 \end{aligned} \tag{15}$$

This final value for alpha can be used as an estimate for the model parameter α . The calculation can be done on an instantaneous calculation basis, that is, for each single measurement. Figure 36 shows the distribution of all α values calculated in this way for one of the FHW collector arrays for the year 2018.

Table 11: Model parameter initialization approaches for the D-CAT 2-N model.

<i>Parameter</i>	<i>Initialization</i>
$(mc)_m$	The data sheet has an estimate of the total collector heat capacity. Subtracting the fluid heat capacity yields a simple estimate for the solid part heat capacity.
$(mc)_f$	For the FHW plant, the fluid properties density and heat capacity were determined in the lab, see chapter 3.2.3. At least a good estimate of these fluid properties is usually available. The collector array fluid volume V_f can be estimated based on the fluid volume of a single collector which is usually known from the data sheet.
$(\tau\alpha)$	The collector data sheet has a value for the parameter $F'(\tau\alpha)$. To calculate $(\tau\alpha)$ from this data sheet value, divide $F'(\tau\alpha)$ by the collector efficiency factor. The collector efficiency factor F' is either available from the collector manufacturer, or it can be estimated based on collector geometry using well-known collector formulae in Duffie & Beckman [14]. Typical F' values for the collectors under consideration in MeQuSo are around 0.95.
b_0	Data sheet value can be used directly.
K_d	Data sheet value can be used directly.
a_1	Can be calculated from data sheet value in much the same way is estimated from taking into account see above.
a_2	Same as a_1
α	See detailed description below this table.
α'	Can be estimated directly by plotting data, see figure 27.

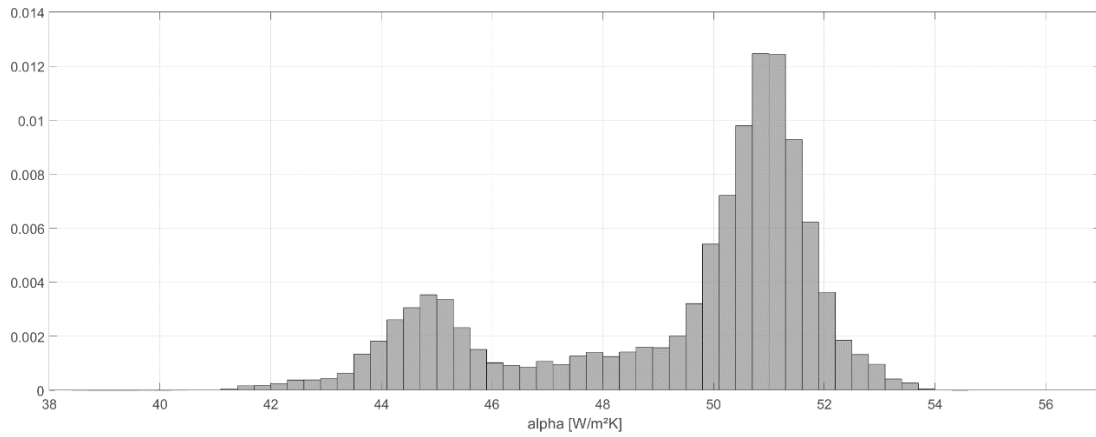


Figure 36: Histogram of α , the convective heat transfer coefficient between metal and fluid part in the D-CAT 2-N model, calculated using the calculation drafted above.

The distribution is basically a consequence of volume flow and temperature of the heat transfer fluid. The bimodal nature of the distribution is a consequence of the fact that the collector array is typically either used at full volume flow (α values around 51) or with the pump running at lowest rotation speed (α values around 45). This distribution is accounted for in the D-CAT 2-N model by a volume flow dependent correction of α .

7 Auxiliary models

The D-CAT method uses a defined set of input variables and parameters to model the collector array outlet temperature (see chapter 6.5). Depending on the measurement setup of the plant, input variables may not be given directly as measurement data from sensors, but may only be derived from measurement data by additional modeling. This can be case if the measurands do not exist (e.g. only the total tilted radiation is measured, but not the beam and diffuse parts separately) or measured are located elsewhere (e.g. temperature measurements before long transmission lines, not at the entrance of the array, volume flow measurement on secondary side instead of primary side). Another problem is the measurement representativity problem. A measure might be available, e.g. beam and diffuse irradiance in the collector array, but this might not be representative for irradiance the collectors actually get, as lower parts of the collectors receive less irradiance than the spot where the radiation is measured (see chapter 2.1).

Models which transform measurement data to input variables are called “auxiliary models”. These models are then used for a pre-simulation step, which transforms a time series of measurement data to a time series of input variables. Figure 20 (page 43) gives an overview how different measured variables are transformed to model input variables. The use of auxiliary models makes the D-CAT method applicable to broad range of measurement setups. In this chapter, the basic equations to calculate the capacity flow, radiation modeling, heat exchanger modeling and pipe heat loss modeling are explained. The modeling in the MeQuSo project was focused on the collector array and for heat exchanger and pipe heat loss modeling, no additional models were developed. An innovative radiation model, which was the developed in the project CollFieldEff⁺ (FFG project no.: 854735) was used, which will be described briefly in this chapter and in more detail in a forthcoming publication. Note that the D-CAT method is compatible with different radiation, heat exchanger and pipe loss models. In general, modeling approaches should depend their suitability of a particular plant and the trade-off between modeling accuracy and effort.

7.1 Radiation models

7.1.1 Overview

The D-CAT model for the collector outlet temperature as described in chapter 6.5 requires the beam and diffuse tilted irradiance as input variables. External shading by surrounding buildings or trees and internal shading by modules placed in anterior rows, can lead to a non-uniform distribution of the beam irradiance in the array (see figure 37, left). Due to view obstructions and reflections, the diffuse irradiance distribution can also be non-uniform. For modules within an array, lower parts typically receive less irradiance, as the sky view is obstructed by modules placed in anterior rows. A pyranometer placed on top of the collector typically overestimates the irradiance on the collectors, because it is not affected by internal shading and the sky view is not obstructed (see figure 37, right). If these effects are significant, radiation modeling should be used to calculate the **average beam and diffuse irradiance on the collectors**. More detailed models and the average beam and diffuse irradiance are not recommend as explained in chapter 2.5.

The procedure to model the average beam and diffuse irradiance depends on the measurement setup. Figure 38 shows which models is applied for which setup. The measurement of the total tilted irradiance (case A) is the typical measurement setup for commercial applications. Case B is the measurement setup at FHW plant (with case D das additional redundant measurements). For measurement setups B and D, the beam radiation is available. It does not matter whether the beam

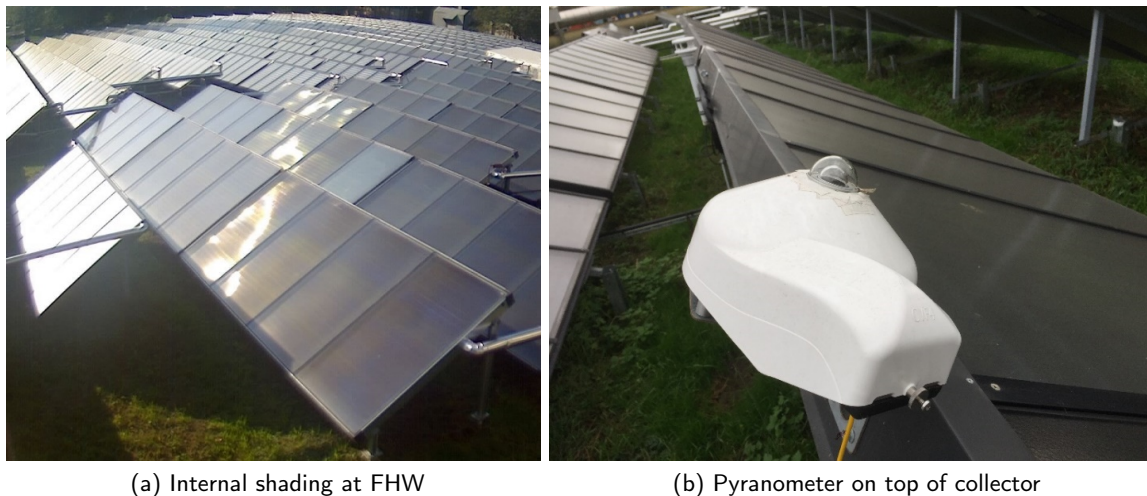


Figure 37: Example of internal shading at the FHW plant and irradiance reductions (left) compared to a pyranometer placed on top of a collector row (right) lead to non-uniform irradiance distribution.

radiation is measured on the horizontal or titled surface (with two pyranometer as the difference of total radiation minus diffuse) or at normal incidence with a pyrheliometer as it is the case with the FHW plant, as conversion of these measurements are only a matter of geometry. All measurement setups use a **tilted collector model (TCM)** to calculate the average beam and diffuse irradiance on the collectors based on the horizontal beam and diffuse values (see 7.2.5). If these radiations are not measured (case A, B, C), additional models are applied to calculate them. The **radiation decomposition model (RDM)** splits global horizontal radiation in its beam and diffuse part (see 7.2.5). The **tilted sensor model (TSM)** is a sub-model of the titled collector model and calculates beam and diffuse titled radiation for a defined spot (where the sensor is located) in the collector array (see 7.2.5). An innovative approach of the D-CAT method is to use RDM + TSM (case A) and TSM (case B) and inversely by solving the model for the horizontal beam and diffuse irradiance which matches the tilted measurement.

7.1.2 Internal and external shading of beam irradiance

Data where external shading occurs is excluded from the analysis. For each timestamp of the measurement data a logical mask (external shading true/false) is needed. Such logical masks can be calculated from shading diagram calculations, radiation modeling tools or rules of thumb depending on the geometry and surroundings of the collector array and the trade-off between modeling effort and accuracy. An example is the determination of external shading conditions for the FHW plant described in chapter 3.3. The D-CAT method does not prescribe a certain method per se to retrieve the logical mask.

Internal shading calculations for regularly shaped arrays, i.e. collector rows with the same length and collector sizes, tilt, row spacing and azimuth as depicted in figure 39, is a matter of geometry. Formulas to calculate the shading height H_s and length of the shadow L_s for collector arrays conditional on collector height H_{col} , row length L_{row} , collector tilt β , row spacing D_{row} and azimuth γ can be found in [71]. Extension for rows with different slopes and tracked collectors can be found in [42].

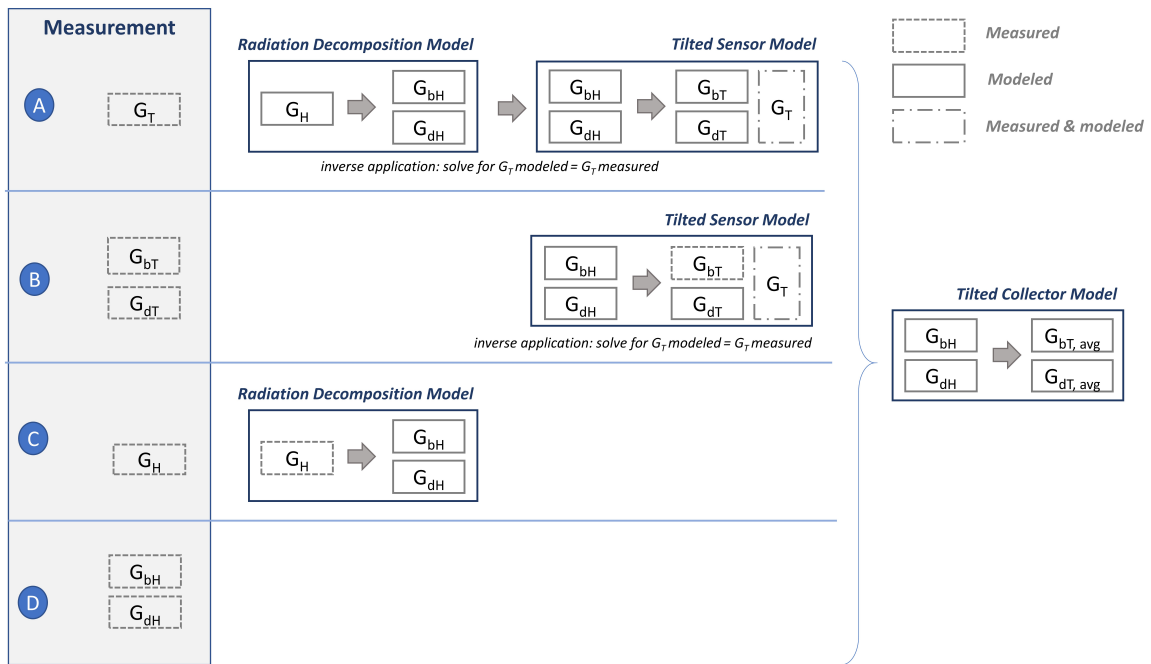


Figure 38: Overview radiation modeling.

The shaded share for a row is then

$$S = \frac{L_s}{L_{row}} \cdot \frac{H_s}{H_{col}} \quad (16)$$

This formula can be applied to multiple collector arrays where each array is regularly shaped. For n collector arrays with a total collector area of A , where array i has a tilted beam irradiance of $G_{bT,i}$, k_i rows (one front row and $k_i - 1$ back rows), shaded share S_i and total collector area A_i , the average beam irradiance can be calculated as follows

$$G_{bT,avg} = \sum_{i=1}^n \frac{A_i}{A} \left[\frac{1}{k_i} \cdot G_{bT,i} + \frac{k_i - 1}{k_i} \cdot (1 - S_i) \cdot G_{bT,i} \right] \quad (17)$$

Results for the FHW plant are displayed in figure 40. Days with no internal shading are between 23rd of March and 23rd of September, exactly six months in total. Total hours without external shading amount to 1,693 h h per year.

7.1.3 Radiation Decomposition Model (RDM)

The aim of radiation decomposition models is to split the total horizontal (global) irradiance in its beam and diffuse part. Most models calculate the diffuse share as function of the clearness index k_T , the ratio between the horizontal irradiance G and extraterrestrial irradiance G_o . With increasing atmospheric clearness, this index approaches unity. Formulas to calculate the and extraterrestrial irradiance with $\pm 0.01\%$ accuracy by Spencer (1971) can be found in [14] (equation 1.4.1 b).

$$k_T = \frac{G_H}{G_0} \quad (18)$$

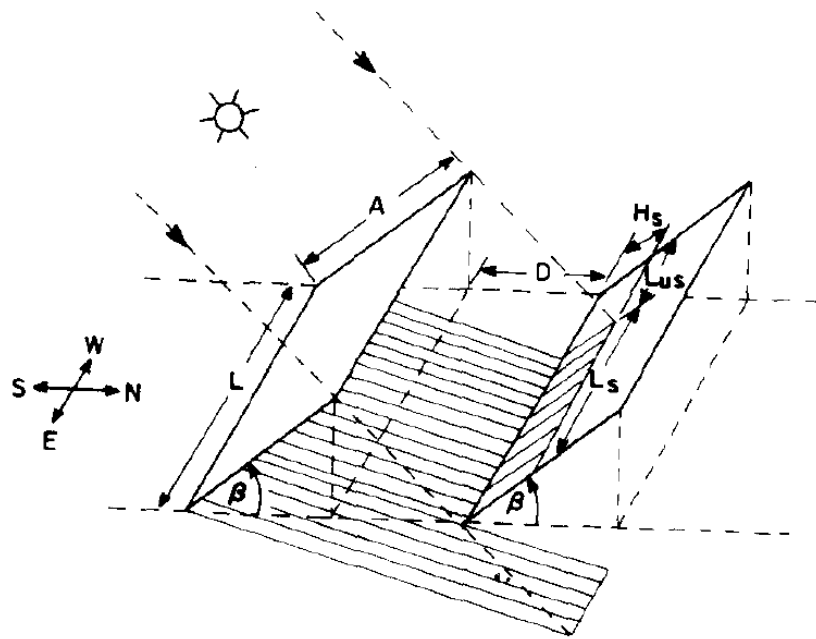


Figure 39: Internal shading calculation [71].

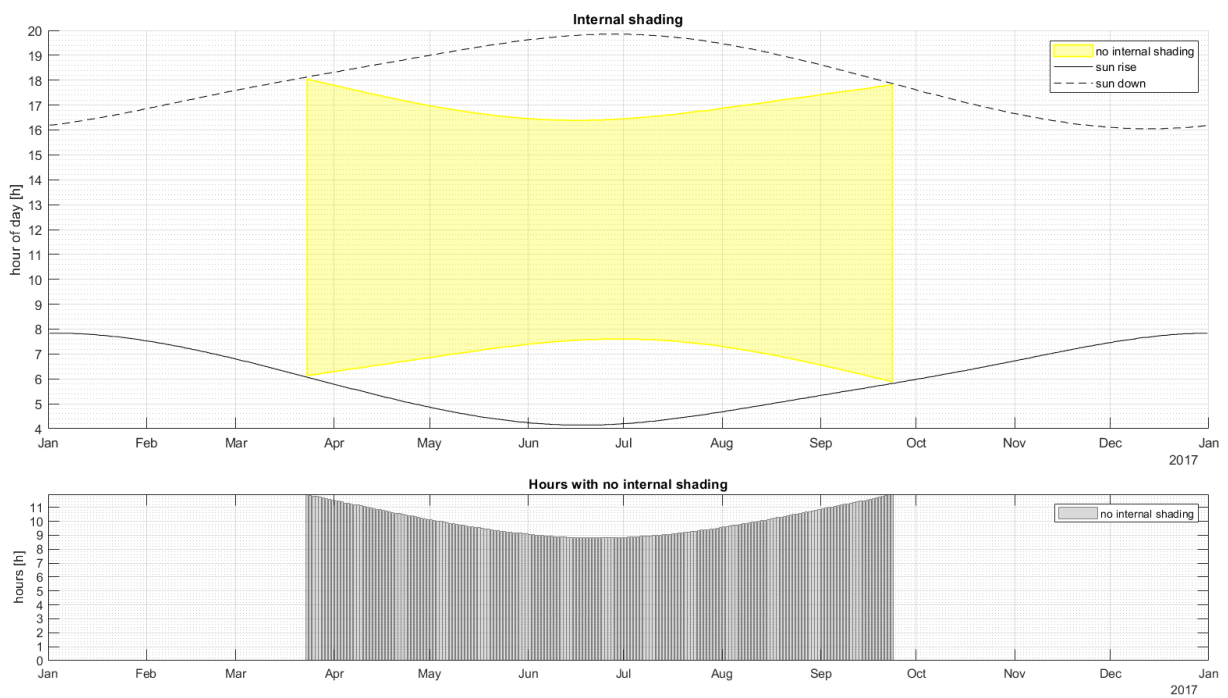


Figure 40: Internal shading of the FHW plant.

A popular model to calculate the diffuse share is the Erbs correlation [72]

$$E(G_H) = \frac{G_{dH}}{G_H} = \begin{cases} 1.0 - 0.09 k_T & k_T \leq 0.22 \\ 0.9511 - 0.1604 k_T + 4.388 k_T^2 & 0.22 < k_T \leq 0.8 \\ -16.638 k_T^3 + 12.336 k_T^4 & \\ 0.165 & k_T > 0.8 \end{cases} \quad (19)$$

A plot of the Erbs correlation is shown in figure 41. Other models are from Orgill and Hollands [73], Reindl et al. [74] and Skartveit et al. [75]. An comprehensive model comparison can be found in [76]. More advanced models like Skartveit et al. which take into account drifting clouds by using values of following and preceding time steps can be difficult to solve backward (case A in figure 38).

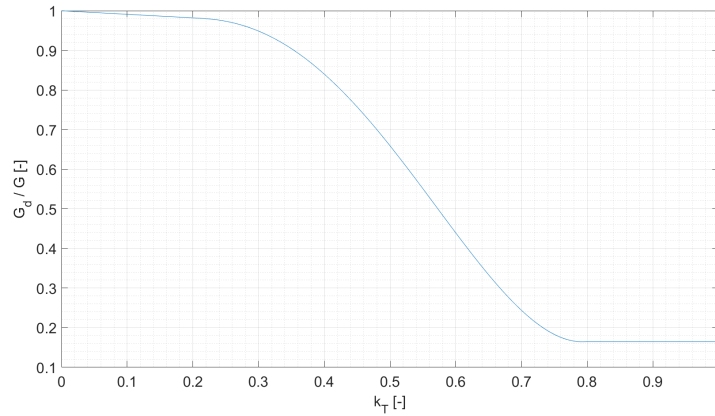


Figure 41: Erbs correlation.

7.1.4 Horizontal plane to tilted surface irradiance models

The calculation of the total irradiation on tilted surfaces is a common topic in radiation modeling, as climate stations typically only measure global radiation. Models differ on how they treat the distribution of the diffuse radiation over the sky dome, which is a function of cloudiness conditions and atmospheric clarity. The distribution over the sky dome consists of an isotropic part which is uniformly distributed over the entire sky dome. The second part is the circumsolar diffuse, which is concentrated around the sun disk, resulting from forward scattering of solar radiation. The third part is referred to as horizon brightening, which is most pronounced in clear skies. It is concentrated near the horizon. Models considering circumsolar diffuse and/or horizon brightening are called anisotropic models [14]. A popular anisotropic model is by Hay-and-Davies [77]

$$G_T = (G_{bH} + G_{dH} \cdot A_i) R_b + G_{dH} \cdot (1 - A_i) \cdot F_{c-s} + G_H \cdot \rho_g \cdot F_{c-g} \quad (20)$$

The anisotropy index A_i determines the fraction of the horizontal diffuse which is to be treated as forward scattered (circumsolar diffuse). The Hay-and-Davies model considers this radiation part to be incident at the same angle as the beam radiation. The factor R_b is the ratio between the beam radiation on the horizontal and the tilted surface. It is function of the sun position, leading to incidence angle θ_z on the horizontal surface and the tilt and azimuth of the tilted surface, leading to incidence

angle θ_{col}

$$R_b = \frac{G_{bT}}{G_{bH}} = \frac{\cos(\theta_{col})}{\cos(\theta_z)} \quad (21)$$

The view factor of the collector towards the sky F_{c-s} discounts part of the sky dome which cannot be seen from the tilted surface

$$F_{c-s} = \frac{1 + \cos(\beta)}{2} \quad (22)$$

The radiation from the ground is calculated by the radiation received from ground with view factor F_{c-g} where the incident radiation on the ground G is assumed to be reflected equally in for every solid angle with reflectance coefficient ρ_g

$$F_{c-g} = \frac{1 - \cos(\beta)}{2} \quad (23)$$

If we set $A_i = 0$, we have the isotropic model. The Hay-and-Davies does not account for horizon brightening. Models which include horizon brightening were developed by Perez et al. [78], [79] and [80]. Anisotropic models typically have lower prediction errors and the isotropic models [81]. As the Hay-and-Davies model and Perez model often have similar results [82], the D-CAT method uses the Hay-and-Davies model as its standard model, as it is computationally easier, especially for the backward application.

7.1.5 Tilted sensor model (TSM) and tilted collector model (TCM)

The models described in chapter 7.1.4 are useful to calculate the irradiance on the front row of a collector array, where the view factor of the collector towards the sky and towards the ground is the same for each segment along the collector height. For collectors within an array the situation is different:

- Collectors receive less diffuse radiation from the sky, because the sky view is obstructed. Lower parts are more affected than upper parts.
- Collectors receive less diffuse radiation from the ground, because the ground b factor is smaller.
- The ground receives less radiation from the sky, due to ground shading and a smaller sky view factor diminishing the diffuse radiation.
- The collector receives additional radiation from the backside of the collector placed in front. This effect is typically very small and is neglected

A simplified version is used in the D-CAT method and presented below. The basic approach of the model is to split the collector and ground in segments and calculate the incident radiation based on individual view factors for each segment. Figure 42 shows a division in 20 collector segments (C_1 to C_{20}) and 20 ground segments (G_1 to G_{20}) of equal length.

The number of segments can be chosen according to the needed precision. The model assumes that the length of the collector row is much larger than the height, i.e. the collector row is of infinite length. This allows to a two-dimensional representation of the array and the calculation of the view factor between two surfaces according the “Hottel’s crossed-string rule” [31]. The model uses the

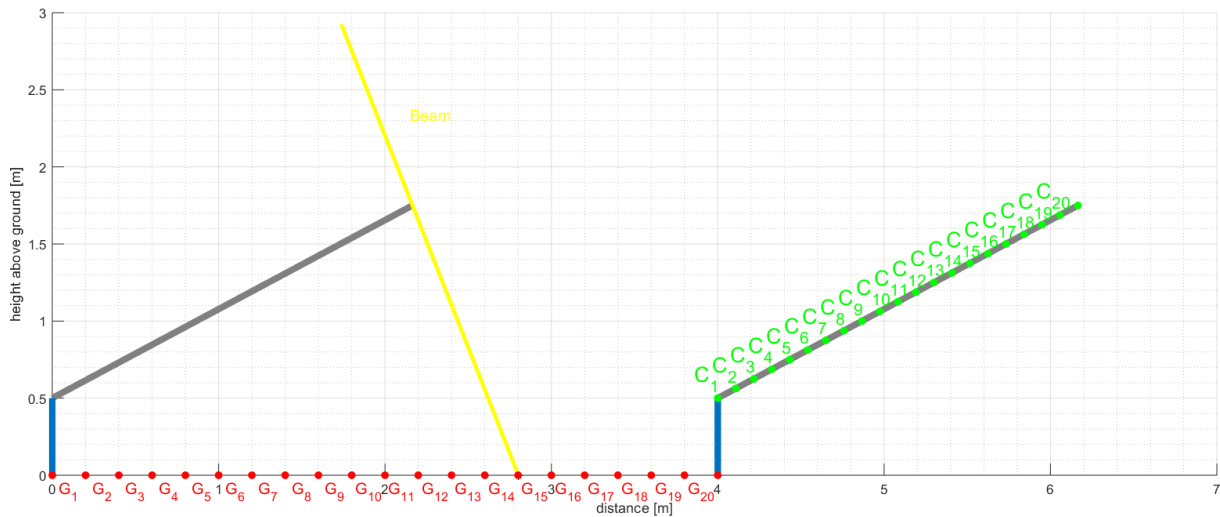


Figure 42: Radiation model with visualization of the discretization segments.

parameter collector tilt β , collector height h , row spacing c , height above ground a , azimuth γ and ground inclination ζ (in the same direction as the azimuth) as inputs. Additionally, a horizon view obstruction angle can be defined for external view obstructions. The reduction of the view factor along the collector height depends on the collector array geometry. Figure 43 shows the reduction of the sky view factor along the collector height from the top to bottom of the collector for 3 m and 6 m row spacing and 30° , 45° and 60° collector tilt angle with no view obstruction from the horizon.

If the horizon view obstruction angle is considered, then the upper parts of the collectors receive the same irradiance, as the dashed lines in figure 44 indicate, and then merge. The row spacing 3 m, collector tilt 30° and horizon view obstruction angle 7° (blue dashed line on the left) corresponds to the situation in the middle of the FHW plant. The sky view factor for these collectors is $F_{c-s} = 0.899$ at the top, stays the same until 60.7 cm from the top and then drops to $F_{c-s} = 0.607$ at the bottom. For an isotropic sky and 100 W/m^2 diffuse irradiance on the horizontal plane, where the collector only receives radiation from the sky, the top would receive 89.9 W/m^2 and the bottom 60.7 W/m^2 .

If the collector is split into m segments along the collector height and n ground segments, then the irradiance on collector segment i is given by

$$G_{T,i} = (G_{bH} + G_{dH} \cdot A_i) R_b + G_{dH} \cdot (1 - A_i) \cdot F_{c_i-s} + \sum_{j=1}^n (G_{bH} \rho_g S_j + G_{dH} \rho_g F_{g_j-s}) \cdot F_{c_i-g_j} \quad (24)$$

$$G_{bT,i} = G_{bH} \cdot R_b \quad (25)$$

$$G_{bT+cT,i} = (G_{bH} + G_{dH} \cdot A_i) R_b \quad (26)$$

Note that the beam and circumsolar radiation is treated the same as in equation (20). The circumsolar radiation is by definition diffuse radiation, but as it is assumed to come from the same direction as the beam radiation, collector array models could also use the sum of beam and circumsolar

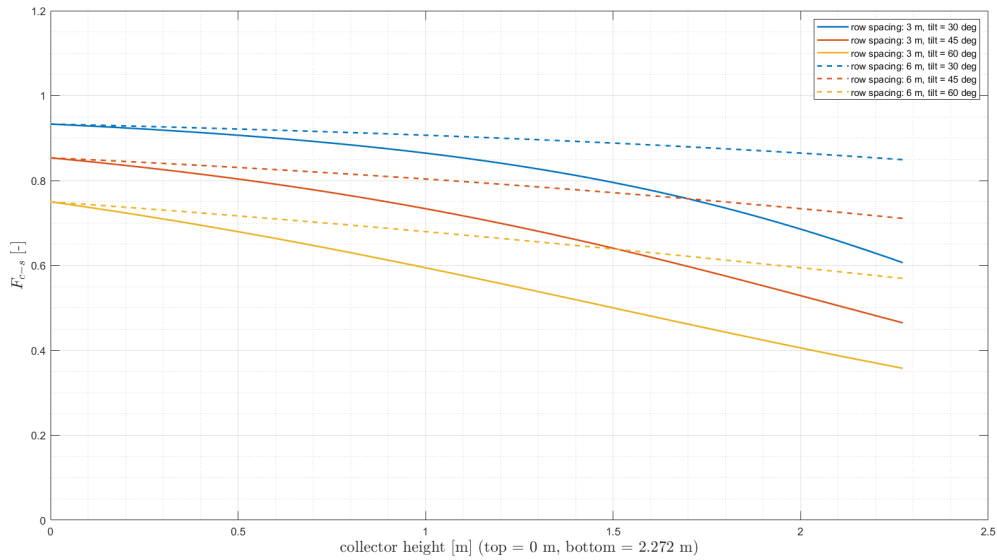


Figure 43: Reduction of the sky view factor along the collector height for 3 m and 6 m row spacing and 30°, 45° and 60° tilt (azimuth = 180° (south), height above ground = 43.5 cm, ground tilt = 0°, horizon view obstruction angle = 0°).

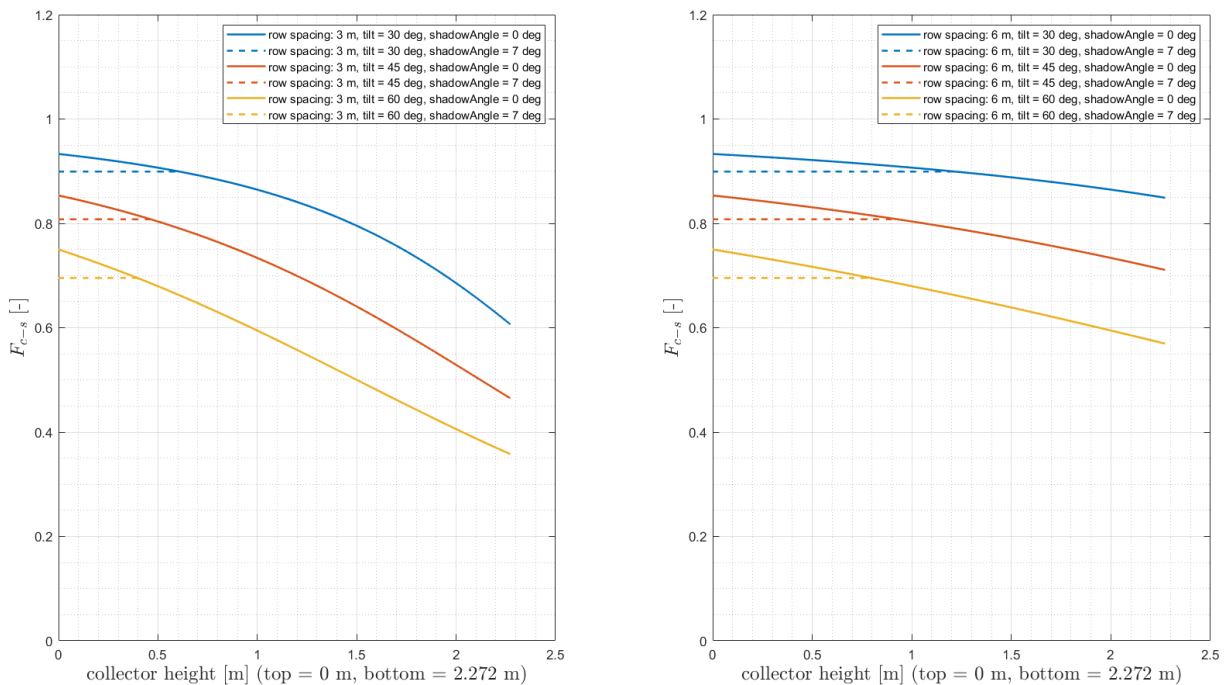


Figure 44: Reduction of the sky view factor along the collector height for 3 m row spacing (left) and 6 m row spacing (right) and 30°, 45° and 60° tilt, and 0° and 7° horizon view obstruction angle.

radiation G_{bT+cT} (equation 26) instead of beam radiation G_{bT} (equation 25) depending on the modeling purpose. The diffuse radiation is the difference between total tilted radiation and beam radiation (plus circumsolar radiation if it is treated like beam radiation). For the isotropic radiation from the sky, the view factor of the segment towards the sky is used. The radiation from the ground sums up the received radiation from each ground segment. The incident radiation on the ground treats beam and diffuse separately, where $S_j = 1$ if the beam reaches the segment and $S_j = 0$ otherwise. The shadow length on the ground can be calculated according to [71].

The calculation of the irradiance on a tilted pyranometer in the collector plane is done with equation (24), where the irradiance of segment i is used where the sensor is located. If the pyranometer is located above the top of the collector the formula can be used in a similar way. This model is called the **tilted sensor model (TSM)**. It is used in combination with the Erbs model when the total tilted radiation and beam radiation is measured (case A in figure 38) and alone if both total tilted and beam radiation are measured (case B in figure 38). Note that for a specific collector array and segment i , equation (18) is a function of G_{bH} and G_{dH}

$$G_{T,i} = f_i(G_{bH}, G_{dH}) \quad (27)$$

and together with the Erbs model (equation (19)) a function of G .

$$G_{T,i} = f_i(G_H \cdot (1 - E(G_H)), G_H \cdot E(G_H)) \quad (28)$$

The backward application then solves

$$\begin{aligned} G_{T,i,meas} - f_i(G_{bH}, G_{dH}) &= 0 & \text{case A} \\ G_{T,i,meas} - f_i(G_H \cdot (1 - E(G_H)), G_H \cdot E(G_H)) &= 0 & \text{case B} \end{aligned} \quad (29)$$

with an optimization procedure or matrix inversion for simple models. A unique solution requires that the forward calculation is an injective function.

The **tilted collector model (TCM)** calculates the average total irradiance as the average over all the segments

$$G_{T,avg} = \sum_{i=1}^m G_{T,i} \quad (30)$$

Results of the radiation modeling for the FHW plant are shown in chapter 9.3.

7.2 Heat exchanger model

The D-CAT 2-N model (see chapter 6.5) requires the capacity flow in the solar circuit, which is based on the primary volume flow, see equation (10). However, in some installations the volume flow is not available in the solar circuit, but only on the secondary side of a heat exchanger separating solar (primary) from secondary circuit. In this case, the primary-side capacity flow can still be calculated if the secondary-side volume flow is measured: With thermal power measured on the secondary side of the heat exchanger, and flow and return temperatures measured on the primary side (solar circuit), then a heat exchanger model is necessary to calculate the primary-side capacity flow. Secondary-side power measurements are usually available for solar thermal installations. Compared to primary-side measurements, secondary-side measurements are lower cost, technically simpler and more reliable if

water is the heat transfer fluid in the secondary side (well known fluid properties).

Heat exchangers can be classified according to several features (transfer process, number of fluids, surface compactness, construction features, flow arrangements, heat transfer mechanism) [83]. For large solar district heating systems, counter flow plate heat exchanger are most common [84]. Heat exchangers are usually insulated and thermal losses (first law losses) to the ambient can therefore be neglected [85] as well as capacity effects of the heat exchanger. The simplest heat exchanger model is

$$\dot{C}_f = \frac{\dot{Q}_{\text{sec}}}{\vartheta_{\text{pri,fl}} - \vartheta_{\text{pri,ret}}} \quad (31)$$

A possible deterioration of the heat transfer coefficient of the heat exchanger (e.g. because of fouling) increases the temperature difference ΔT between primary and secondary side [86]. This leads to higher operating temperatures of the solar circuit and a lower collector efficiency. This does not require additional modeling and does not distort the estimated collector array parameter as the collector heat losses are higher, but not the heat loss coefficient. The heat exchanger performance (heat transfer coefficient) can be tested separately if needed.

7.3 Pipe model

Pipe models in the D-CAT method can be used to calculate the temperature loss of the supply pipes and return pipes from the collector array to the heat exchanger or heat sink, if the flow and return temperatures are not measured directly at the entrance and exit of the collector array. Note that pipe losses within the array (connectors between collectors and connection pipes between rows) are not modeled, because they are very small compared to the heat losses of the collectors and modeling them would require a substantial additional effort. Also note that modeling the return temperature of the collector array is in the flow direction (the output temperature of the model is lower than the input temperature) and modeling of the outlet temperature is reverse to the flow direction (the output temperature of the model is higher than the input temperature). A simple model for the pipe losses is described in [87]

$$T_{\text{out}} = T_{\text{sur}} + (T_{\text{in}} - T_{\text{sur}}) \exp\left(\frac{-L \cdot K}{\dot{V} \cdot C \cdot \rho_f \cdot c_f}\right) \quad (32)$$

where T_{sur} is the temperature of the surroundings, K is the overall heat transfer coefficient (in $\text{W}/\text{m}^2\text{K}$), L is pipe length, \dot{V} is volume flow based on the average velocity through the pipe and C is the heat capacity per unit length of fluid in the pipe: $C = A \cdot \rho_f \cdot c_f$, if the solid part of the pipe is not included. The model can be rewritten in terms of the travelling time Δt through the pipe:

$$T_{\text{out}} = T_{\text{sur}} + (T_{\text{in}} - T_{\text{sur}}) \exp\left(\frac{-\Delta t \cdot K}{C}\right) \quad (33)$$

The model assumes that heat losses per unit pipe length are proportional to the temperature difference between the fluid in the pipe and the surroundings and that the temperature of the surroundings is constant. Diffuse heat transfer and the effects of pressure loss and wall friction are neglected. More detailed models can be found in [87].

8 Parameter estimation

8.1 System test and condition monitoring

As a key project result of the MeQuSo project, D-CAT is available as a fully automatic collector array test, from raw measurement data to final model parameters and system simulations based on these parameters. Automation is an important aspect as it increases the D-CAT scope of application: D-CAT can be used as a collector array test method, and by periodic and automatic application D-CAT can be used as a **model-based condition monitoring** method for large collector arrays. In the framework of condition monitoring for large solar thermal systems, a simple “stationary analysis” (described in chapter 2.3) can be used to see if the system roughly meets the expected performance. The D-CAT parameter estimation process provides a more thorough analysis, providing quantitative information about the collector field operation and possible causes of malfunctions or reduced energy yield. This parameter estimation process is based on the 2-N model (chapter 6.5) and estimates the parameters of this model in an inverse analysis. As a result of the D-CAT method, we have a detailed quantitative technical description of a collector array based on all modeled physical effects.

In the MeQuSo project, the D-CAT method has been developed and implemented in MATLAB®, including data pre-processing and data handling (see chapter 5.3), numeric solution of the dynamic collector array model (see chapter 6.7) and estimation of the model parameters (this chapter). In doing so, the D-CAT test method and collector array measurement data were kept separated: The method has an encapsulated design and implementation, allowing different collector arrays to be “plugged in” with their measurement data, and possibly even with adapted models.

The chosen approach makes the D-CAT method generally applicable to collector arrays (not only within the MeQuSo project), in very much the same way it has been applied to the FHW collector arrays within MeQuSo. The developed methodology can be applied to a variety of collector array geometries. Currently, the model is suitable for flat-plate collectors, as used in the vast majority of large solar thermal installations. The developed estimation method is designed to run as an offline / batch process. The parameter estimation is an extensive process taking several hours, but it runs in a fully automatic way and can thus be easily repeated at any time.

How to read chapter 8:

- Chapter 8.2 explains available data and how it is handled as input for the parameter estimation. It contains a somewhat more detailed description of a D-optimal data selection method that selects part of the experimental data for the estimation process.
- Chapter 8.3 has a formal formulation of the parameter estimation problem, including a brief description of how uncertainty in the experimental data is treated.
- The optimization process and choice of optimization algorithm are contained in chapter 8.4.

8.2 Optimal data selection

Overall, the goal of the automatic optimal data selection approach is the obtain **high quality parameter estimates**, **good generalization** to non-observed operating conditions and **improved optimization time**. At the time of proposal writing for the MeQuSo project, the idea was to deliberately vary some collector array operating conditions in order to obtain sufficient data variation for the parameter

estimation. For example, collector array volume flow could be temporarily reduced, or collector array inlet temperature could be temporarily increased, following active manipulation of the system control by the plant operator. Deliberately choosing system inputs (such as volume flow), e.g. with a PRBS signal as is done in [88], would be beneficial for the parameter estimation process. We have to take into account, though, that some of the major system inputs (return temperature, solar radiation) cannot be freely controlled. In the course of the MeQuSo project, the approach of deliberately varying input signals was rejected in favor of a procedure for automatic data selection. One reason is the already mentioned limitation in choosing input signals. Another reason is that the data selection approach needs not interfere with the system control, that is: No special test sequences need to be run, and the barriers to using the D-CAT method for practical LST plants are lowered.

The idea of optimal data selection is: Collect measurement data from the LST plant in a passive way (no manipulation of system control), then select the “best” subset of intervals among the entire set (around 500 1-hourly intervals per year), and use the selected subset for parameter estimation. In short, optimal data selection is the task to select a subset of the available measurement intervals based on the following criteria:

- **Good generalization:** The parameter estimation process yields model parameters that describe the condition of the collector array in a way that is valid for a wide range of operating conditions. This is particularly important for the FHW plant: Being a district heating supply system, the required outlet temperatures of the solar plant are within a narrow range, which is bad for parameter estimation. Since we want the D-CAT method to use measurement data available from normal system operation (without touching system control), it is even more important to carefully select diverse data for parameter estimation.
- **De-correlation:** Clustering and correlation in the subset should be kept minimal. The separability of the estimated model parameters based on the selected data subset should be as good as possible, or in other words: We want to include measurement data that yield the lowest possible variance in the estimated parameters.

Used measurement data

Measurement data have been acquired within the MeQuSo project in a field installation, the FHW plant in Graz, Austria (see chapter 3 for details). The measurement data cover **3 years of operation** and refer to 5 collector arrays, all operated and measured independently. Each collector array has a collector area of approx. 500 m², and all use large area flat-plate collectors of well-known and experienced manufacturers.

The measurement data of the collector arrays have been acquired in a 1-second sampling rate, averaged to 10 seconds during post-processing. The measurement channels used as input data in the parameter estimation process include:

- inlet and outlet temperature of each array (additionally, the outlet temperatures of each row were measured, but only the mixed outlet temperature is used in the parameter estimation, as single row measurements cannot be assumed to be frequently available)
- volume flow of each array
- beam and diffuse radiation in collector plane
- ambient temperature; other ambient conditions (wind and air humidity) were available for the FHW plant, but not used in the parameter estimation.

The measurement data listed above are used as inputs in the D-CAT method. Some measurement channels are not strictly required, for instance the beam radiation which can be approximated from other radiation measurements using radiation models, in case the measurement is not directly available.

As a result of the measurement process, we have detailed and high-quality measurement data covering the years from **2017**, **2018** and **2019**. The total volume of the collected measurement data is approximately 40 GB of raw data. The MATLAB[®] implementation based on AEE INTEC's ADA software [56] handles automatic pre-processing of the raw data, including steps like outlier detection, plausibility checks, ignored time intervals (e.g. maintenance work) and a calibration correction for some measurement instruments; chapter 5.3 has more details on the data pre-processing.

Interval length

Based on the reasonings concerning the validity domain of the collector array model (see chapter 6.6), measurement data are separated into chunks of usable data, where the model is valid. For the D-CAT method, all data intervals with a length of at least 1.5 hours of unshaded operation are included in the analysis. The 1.5 hours interval length consists of a 30-minutes pre-simulation interval (needed for model initialization, see chapter 6.8) plus a 1-hour main simulation interval. The choice of a 1-hour interval length is arbitrary. The main reasons for choosing 1 hour as an interval length are:

The same 1-hour interval length is used in the ISO standard (under preparation) for a simplified collector array performance check, hence using the same interval length improves comparability between results from the ISO standard and results from the D-CAT method.

The 1-hour interval length seems to be a good trade-off between two contrasting goals: On the one hand, shorter intervals increase data diversity in the intervals (increased overall information content), while longer intervals tend to average out the data (reduced overall information content). On the other hand, longer intervals are less susceptible to initialization errors, keeping in mind that although the model initialization works well for practical purposes, there is still some uncertainty due to heuristics used in the model initialization (see chapter 6.8 for details).

The time constant of water-driven flat plate collectors at a mass flow rate of $8 \text{ kg/m}^2\text{h}$ is approximately 15 minutes. The general choice (for a variety of different mass flow rates) of 1 hour corresponds to 4 times the 15-minutes time constant, which seems to be a reasonable choice in terms of the dynamic behavior of collector arrays.

We also tried to use the D-CAT method with shorter intervals, with a length of 15 and 30 minutes. This increases diversity in the data and might be an option to go if the D-CAT method is applied to shorter evaluation periods, for example a two week operation period.

Generalization

Based on the total interval length of 1.5 hours as described above, one year of measurement data yields **approx. 500 intervals** for each of the tested collector arrays at the FHW plant. The 500 intervals represent a large share of the collector array's operation. In principle, the measurement data from all these intervals could be used for the parameter estimation process. Nevertheless, taking all 500 intervals is not a very helpful approach for parameter estimation.

First, model runs (required by the optimizer to estimate the parameters) would become very expensive if all intervals are included in the analysis, since each optimization run would require to run each and every data interval. Second, the data have some unwanted properties (see figure 45):

- Data are **clustered**: A lot of intervals are very similar, in terms of model variables. E.g., as can be seen in figures 45, total collector array radiation is mostly clustered in the range of 800 –

1000 W/m², and collector array temperatures (collector mean minus ambient mean) is mostly around 60 K. There is considerably less data far away from this cluster. Figure 48 (page 87) provides insight into the full correlation structure of the model predictors.

- Data are **correlated**, as becomes clear by looking at figure 45 again: Such correlation in data is problematic since it introduces correlation to the model parameters, since several correlated sets of model parameters would be able to describe given measurement data.

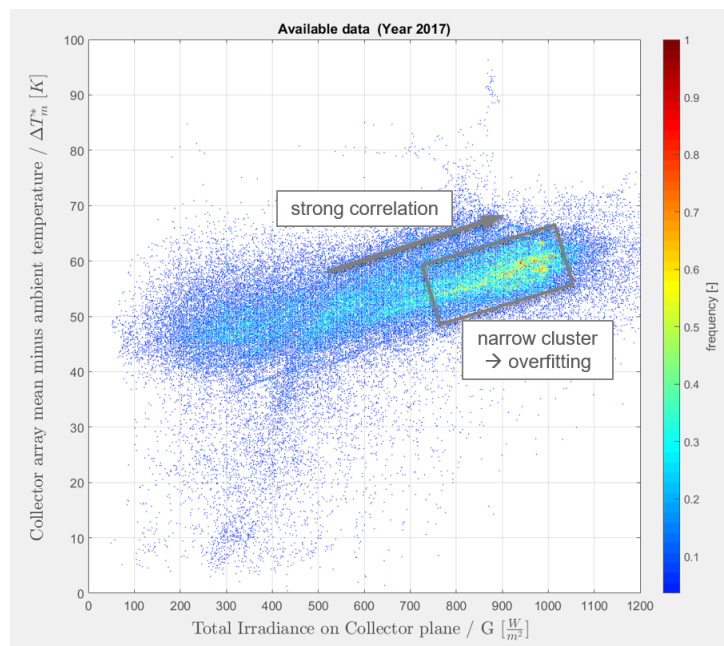


Figure 45: Problems with clustered and correlated measurement data, represented here by a cross-sectional plot of collector array temperature over total irradiance, based on 1-minute data for the year 2017.

D-Optimal data selection

In the ISO 9806 standard for single collector tests [10], the data selection approach consists in manually selecting data from 4 different “day types” (mostly clear sky, partly cloudy etc.). For the D-CAT method, the data intervals used for the parameter estimation are selected in an automated and optimal way, maximizing the information content of the data selection with regard to the collector array model.

A major advantage of this **automatic data selection** is that the D-CAT estimation process can operate as a passive test that requires no manipulation at all in the system control. Actively changing system control is potentially associated with safety problems and loss of energy yield. Furthermore, it would require the system operator, the control company and the researchers who perform the test, to agree on a common procedure. This would be a barrier to the application of the collector array test which disappears following automatic data selection in the D-CAT method. For the FHW collector arrays, we found that normal operating data provided good data variation, and we found that the data selection process successfully identified and selected the most diverse data.

The selection of the “best” subset of intervals is based on similar statistical foundations as **Design of Experiments** – but in this case we do not design experiments, we strive to optimally select data among already performed experiments. The statistical concept is the information content of the

measurement data in order to allow for **lowest-variance** parameter estimation and **best-separable** model parameters.

The information content of data with respect to the chosen collector array model can be formalized in the Fisher information. Based on the Fisher information, there are several concepts of “optimal” designs or data selections. One popular optimality criterion is called “D-optimality” : A data selection is D-optimal if it “spans the largest volume possible in the experimental region” [89]. Loosely speaking, several very similar intervals (e.g. warm and sunny) are less informative compared to a selection of intervals with different conditions (e.g. also cold and sunny, or warm and overcast etc.), because the variety in input data helps separating the physical effects described by the parameters in the collector array model.

The effect of the optimal data selection is illustrated in figure 46. The same dense cluster of data already seen in figure 45 above is displayed again in figure 46 (top subplot), this time in terms of 1-hourly mean (one dot for each of the approx. 500 yearly intervals). The result of the optimal data selection becomes visible in the bottom subplot, where 25 out of the 500 intervals have been selected following the D-optimality criterion.

It becomes evident that the data selection favors more extreme data, near the edges of the data region, while the dense cluster is not over-represented anymore. Figure 47 displays the days of the year with available and selected intervals. Loosely speaking, the data selection gives precedence to data intervals where the model prediction is most sensitive to parameter changes.

Simplified Approach for Nonlinear model

The D-CAT 2-N model is a nonlinear PDE model, and optimal data selection for nonlinear dynamic models is a complex and current research topic. Important recent publications include the review paper of [90], and more specifically about nonlinear systems [91], [92] and [93].

For linear models, the optimal design theory is based on the model matrix X , a matrix containing the model derivatives with respect to the model parameters. For the MeQuSo D-CAT method, a simplified approach is used, where each of the approx. 500 intervals is represented by the mean parameter sensitivities in that interval. In other words, each interval is represented as a single point in the parameter sensitivity space, or as a row in the model matrix X , a 500×9 matrix. The optimal interval selection task based on the D-optimality criterion described above is equivalent to maximizing the determinant of the information matrix $X'X$. This approach makes use of the fact that the collector array model is nonlinear in its states (temperatures), but linear in its parameters.

The concrete optimal data selection is based on the so-called **Fedorov algorithm**, developed in [94] and described in detail in [95]. The basic idea behind the Fedorov algorithm is to start with an initial interval design, and calculate a delta value for all other exchange intervals among the non-selected candidate intervals. Based on these delta values, one interval will be dropped from the interval selection in favor of another interval with a higher optimality value, calculated as determinant of the information matrix. For the given approx. 500 intervals per operating season, the MATLAB[®] implementation of the basic Fedorov optimization algorithm (doing an exhaustive search among all intervals) is fast enough to find the optimal interval design in a few seconds, so none of the more sophisticated algorithm variants had to be used.

In the development of the D-CAT method, we experimented with the **number of intervals** to be included in the optimal design. A higher number of intervals increases simulation time and ultimately deteriorates the generalization properties of the method to new, unseen operating or weather conditions. An indicative number is to include at least the two extremes (minimum and maximum sensitivity) corresponding to each of the model parameters. This would result in the number of 18 intervals, since

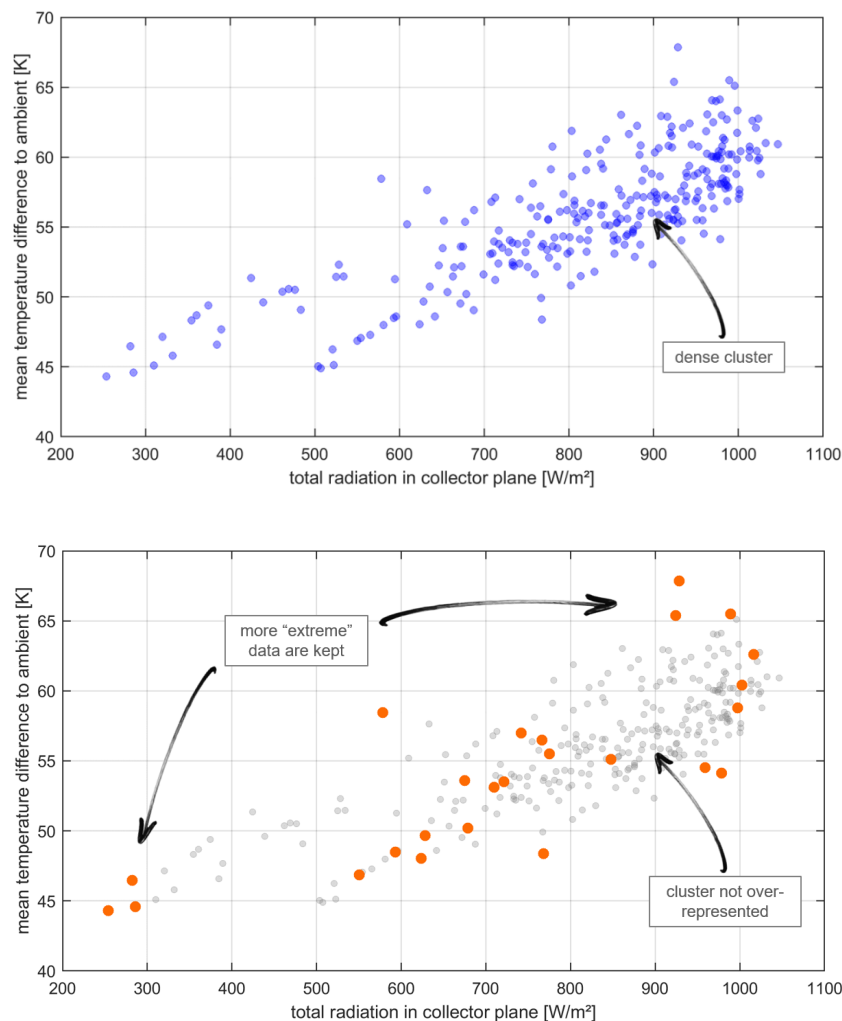


Figure 46: Top: Collector array temperature vs. total radiation (same data as in figure 45), condensed here as 1-hourly mean values, so there is one dot for each of the approx. 500 candidate intervals. Bottom: Exemplary result of the optimal data selection process, selecting 25 out of the approx. 500 available intervals. The data selection gives precedence to the more extreme data.

the D-CAT 2-N model has 9 parameters. Within MeQuSo, we experimented with different numbers of selected intervals (between 18 and 50). We found that with increasing number of intervals, the correlation coefficients between model predictors tended to increase, resulting in problems during parameter estimation, with model parameters becoming harder to separate. Not surprisingly, this mainly affected the separation of optical and thermal parameters (mainly a_1 and $(\tau\alpha)$). The authors would recommend keeping the number of intervals below 30. Due to the advantages in simulation time, we decided to go towards the lower limit and generally used between 20 and 25 intervals in the development of the D-CAT method. Figure 48 shows the correlation structure between the 2-N model predictors, comparing (a) all available intervals with (b) the optimally-selected intervals.

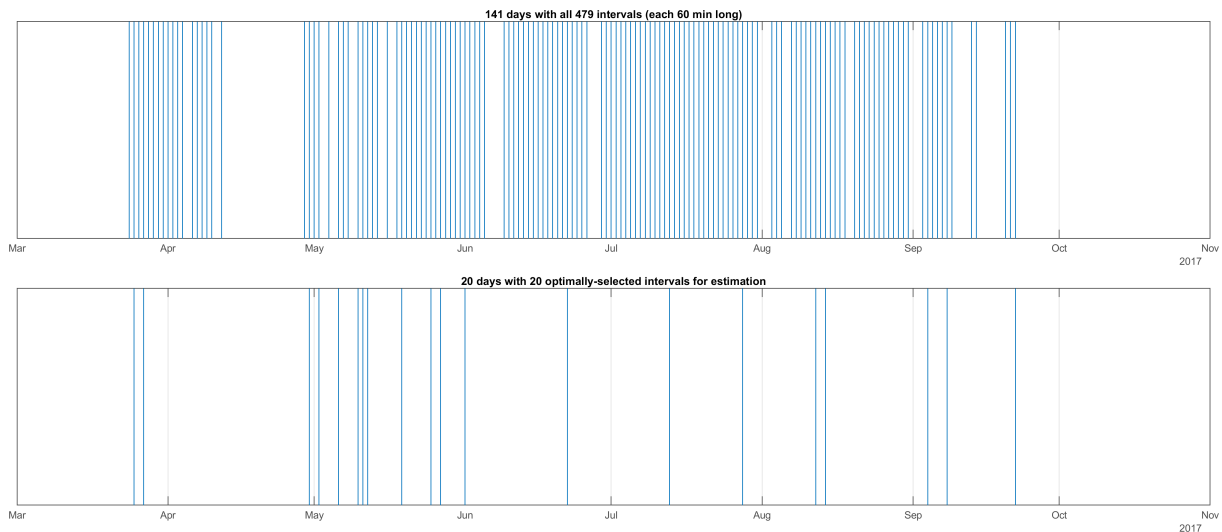


Figure 47: Top subplot: Distribution of days containing at least one valid 1.5-hour interval for the collector array test. The period from October to mid-March had to be excluded due to shading. Bottom subplot: Distribution of the days containing one or more optimally-selected intervals, as described in chapter 8.2.

8.3 Problem formulation

Given a model structure (the D-CAT 2-N model, see chapter 6.5) and experimental data (20 optimally-selected 1-hourly intervals, see chapter 8.2), the parameter estimation process consists in tuning or calibrating the 9 model parameters in order. The goal is that the model with the calibrated parameters shall best reproduce the experimental data. In the parameter estimation process, the quality of a specific set of model parameters is evaluated by means of a cost function which describes the *goodness of fit*, that is, a quantitative measure that compares the model prediction to the experimental data, over all 20 selected data intervals.

The N -dimensional vector of scalar model parameters (see chapter 6.5) is represented as θ . In the case of the D-CAT 2-N model we have $N = 9$ model parameters, so $\theta \in \mathbb{R}^N$. Given a set model parameters, the cost function $J(\theta)$ is the scalar real-valued function mapping a given set of model parameters to its goodness of fit: $J(\cdot) : \mathbb{R}^N \rightarrow \mathbb{R}$. The cost function $J(\cdot)$ may include uncertainty information about the parameters and about the measurement data (e.g. measurement noise, sensor accuracy), and the specific formulation of a cost function leads to different methods, such as least squares, weighted least squares, maximum likelihood or Bayesian estimation [96].

As described in chapter 6.7, the method of lines was used to discretize the D-CAT 2-N model, a PDE model (see chapter 6.5), to obtain an ODE system which can be formulated as a nonlinear deterministic state-space model. As explained in [97] and [98], and adopting a similar nomenclature, this state-space system can be formulated as

$$\frac{dT(t, \theta)}{dt} = f(t, T(x, t, \theta), v(t), \theta) \quad (34)$$

$$T_{out}(t, \theta) = g(T(x, t, \theta), \theta) \quad (35)$$

$$T(t_0) = T_0(\theta) \quad (36)$$

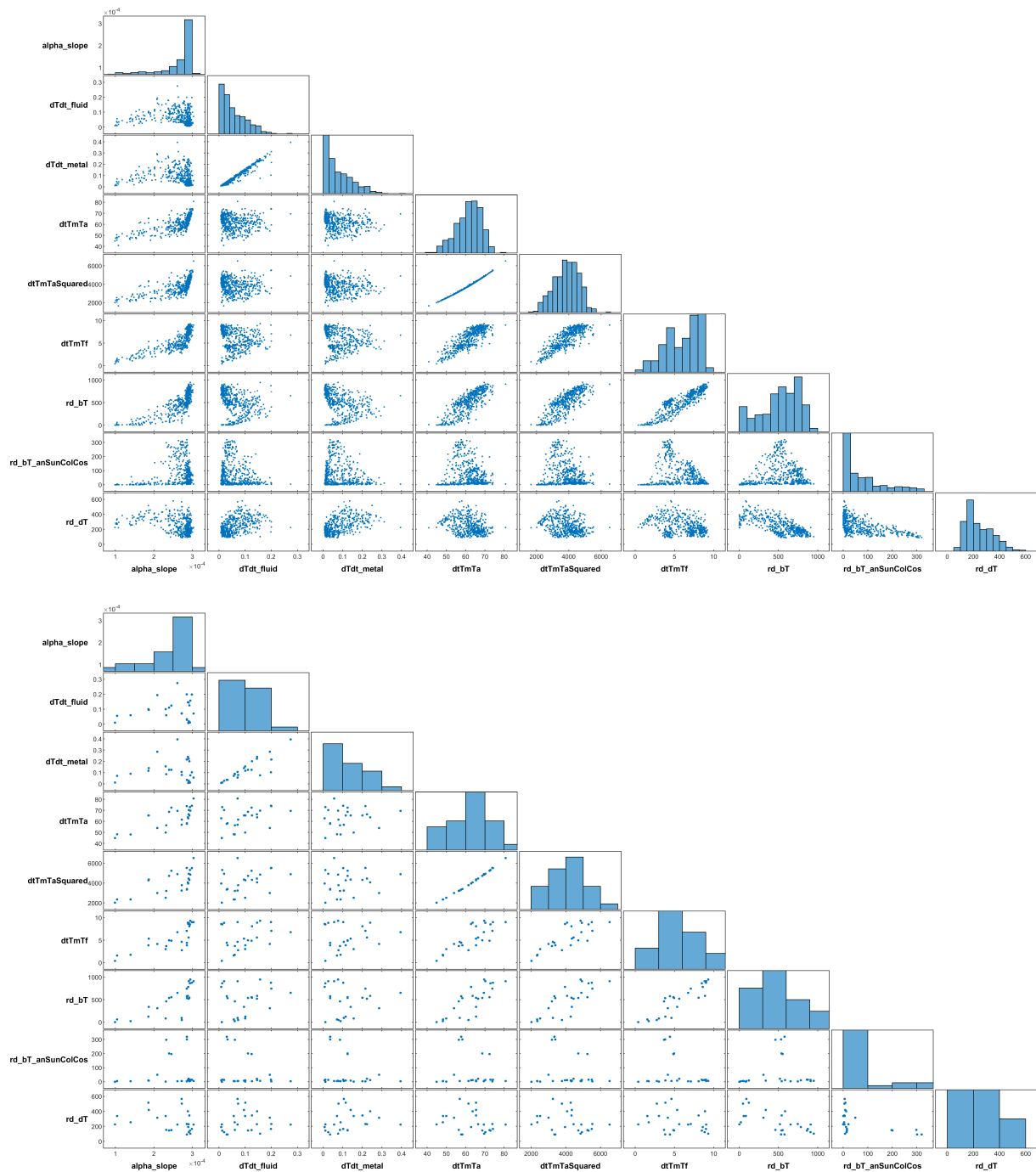


Figure 48: Distribution of the model predictors used in the D-CAT 2-N model, displayed as histograms and correlation plots. The top figure includes the full set of approx. 500 intervals available for one of the FHW collector arrays in one year of operation. The bottom figure includes the 20 optimally-selected intervals.

Note that being a state-space model, there is no dependence on position x in the time derivative term $dT(t, \theta)/dt$. In this more general formulation, the vector T is used as symbol for the state vector, concatenating the vectors of metal temperatures T_m and fluid temperatures T_f along a collector row/collector array. The function $f(\cdot)$ is the vector function resulting from the numerical discretization of the model equations (see chapter 6.7). The model predictors $v(t)$ enter the state-space model in function $f(\cdot)$. The collector array outlet temperature T_{out} , measured at position $x = 1$, is calculated from $T_f(x, t)$ by means of linear extrapolation, as explained in chapter 6.7. The extrapolation calculation is summarized in equation (35) as $g(\cdot)$.

For the parameter estimation, the outlet temperatures $T_{out}(t)$ are available as measurements for all optimally-selected intervals, at discrete time points. The time points depend on the chosen sampling rate, and were 10 seconds in the MeQuSo case. Let T_{ik} denote the outlet temperature at time $t = t_i$, in the k -th interval. As with all measurements, T_{out} can only be measured with some uncertainty. Assuming this uncertainty to be additive Gaussian white noise, the measured values \tilde{T}_{ik} can be represented as

$$\tilde{T}_{ik} = T_{ik}(x(t_i, \theta), \theta) + \epsilon_{ik} \quad (37)$$

The measurement uncertainty term ϵ_{ik} is characterized by the noise variance σ_{ik} , with

$$\epsilon_{ik} \sim \mathcal{N}(0, \sigma_{ik}^2), \quad (38)$$

i.e. the noise term is assumed to be normally-distributed, with some noise variance σ_{ik}^2 . In MeQuSo, we calculated these noise variances based on sensor data sheet specifications. In the general case, the noise variance can be time dependent, and this is generally the case for thermal models.

The problem of estimating the model parameters can now be formulated as a maximum likelihood problem. Under the assumptions of equation (38), maximizing the likelihood is equivalent to minimizing the weighted least squares expression:

$$J(\theta) = \sum_{k=1}^{N_k} \sum_{i=1}^{N_i} \left(\frac{T_{ik}(x(t_i, \theta), \theta) - \tilde{T}_{ik}}{\sigma_{ik}} \right)^2 \quad (39)$$

with N_i being the number of measurements available in one interval and N_k the number of optimally-chosen intervals (20, in our case, see chapter 8.2).

chapter 6.8 explains the reasonings used for initialization of the model parameters. Based on these same reasonings, it is straightforward to derive physically meaningful lower and upper bounds for the parameters, θ_{\min} and θ_{\max} . This is very helpful for the optimization process, and it turns the optimization problem from an unbounded into a bounded nonlinear programming problem. With the cost function from equation (39), the parameter estimation problem can be formulated as the nonlinear optimization problem. The calibrated model parameters are defined as the parameter set $\hat{\theta}$ that minimize $J(\theta)$ in the optimization problem. chapter 8.4 includes more practical details about the optimization.

$$\begin{aligned} & \arg \min_{\theta} J(\theta) \\ & \text{subject to } \theta_{\min} \leq \theta \leq \theta_{\max} \end{aligned} \quad (40)$$

One characteristic of the thermal measurement data of collector arrays is their good signal-to-noise ratio, allowing for simpler methodology in the cost function choice. For the D-CAT test method, a

weighted least squares (WLS) approach as stated in equation (39) is chosen for the cost function. WLS includes the measurement uncertainties of the outlet temperature measurements as extrinsic information in the estimation: The residual between model output and measured experimental value is weighted with the inverse of the measurement uncertainty of the measured outlet temperature $1/\sigma_{ik}$. In short, better experimental data (lower measurement uncertainty) get a higher weight in the calculation of the optimization cost function.

The inverse problem of parameter estimation in a numerically-solved nonlinear dynamic system, as is the case for the D-CAT method, is an ill-conditioned problem with many pitfalls; see [99] for a comprehensive discussion. Certainly not all aspects of the problem solution have been successfully solved in the MeQuSo project alone. The parameter estimation experiences we gained in MeQuSo indicate that some regularization methods might improve the parameter estimation process and results, e.g. variants of Tikhonov regularization as explained for a similar problem setup in [98]. A more comprehensive assessment of measurement and process noise would also deserve more attention, and more sophisticated estimation techniques could be used, as formulated for instance in [61] [100] [101].

The model parameters θ resulting from the parameter estimation are not deterministic numbers, but uncertain quantities to be treated as random variables. The outcome of the parameter estimation process, the final parameter estimate $\hat{\theta}$, are uncertain and correlated quantities. Since the model input variables have a clear correlation structure (see figure 48), it is interesting to investigate confidence regions and correlation structure of the model parameters resulting from the estimation process. In the case of linear models, the parameter confidence regions have elliptic shape in the parameter space, but as explained in [102] this is not true for nonlinear models, even if the measurement uncertainties are assumed to be normally-distributed (see equation (38)).

If we assume a Gaussian additive noise model (see equation (38)), we can construct confidence regions in the parameters space based on a Taylor expansion reasoning. As explained in [103], the parameters follow an F distribution with the degrees of freedom depending on the number of parameters and the number of measurement data. The following equation can be used for confidence regions with level $1 - \alpha$ and was first proposed by [104]

$$J(\theta) \leq J(\hat{\theta}) \left(1 + \frac{p}{n-p} F_{p, n-p}^{1-\alpha} \right) \quad (41)$$

with p being the number of parameters and n being the total number of data points, i.e. the number of sampled points over all of the selected data intervals. We used equation (41) to construct the parameter confidence regions and investigate the parameters' correlation structure. Figure 49 gives an example of such a plot.

Measurement Uncertainty

Uncertainties for sensors and data logging can be expressed as “standard uncertainty”, i.e. the standard deviation $\mu(x)$ for a measured value x based on data sheet specifications. Practical guidelines for in situ collector testing can be found in [105]. Uncertainties for some measurement points of the FHW plant are shown in chapter 3.5. For the parameter estimation, the measurement uncertainties can be used as “weights” in the optimization procedure (see chapter 8.4), where better data (lower measurement uncertainty) have more “weight”, i.e. a higher impact on the cost function which is minimized. In the most simple case, the measurement uncertainty of the outlet temperature (predicted variable) is used as a weight. A more comprehensive approach uses the combined measurement uncertainty of all measurement inputs (radiation, inlet temperature, ambient temperature, etc.) which influence

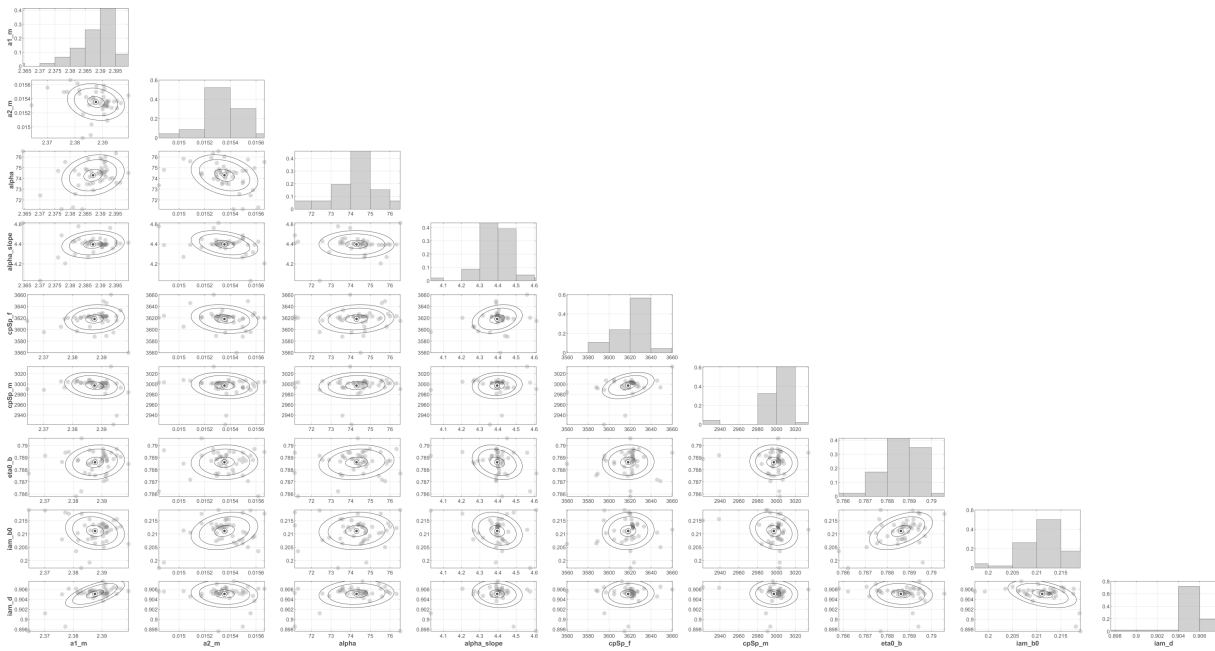


Figure 49: Histograms and covariances of the model parameters, based on the final estimation results for one collector array and one particular measurement season. The motivation and reasons behind this plot are explained in chapter 8.3. The confidence regions were calculated following equation (41).

the predicted outlet temperature. How these uncertainties are combined depends on the used model (D-CAT 1-N model or D-CAT 2-N model). For a model function f and a predicted variable Y

$$Y = f(X_1, X_2, \dots, X_N) \quad (42)$$

the combined uncertainties according to GUM [52] are calculated as follows

$$\mu(y) = \sqrt{\sum_{i=1}^N \left(\frac{\partial f}{\partial x_i} \right)^2 \mu(x_i)^2} \quad (43)$$

The GUM approach is based on a first-order Taylor series approximation of the model function f . A better approximation for the propagation of uncertainty through non-linear models is the **Unscented Transform (UT)**, which can be used for a non-linear projection of uncertainty mean and covariance and has become famous in the context of the Unscented Kalman Filter (UKF) [106] [107] [108] [109].

8.4 Optimization

The optimization problem consists in finding the best parameter set, that is the one which minimizes the chosen WLS cost function. The approach chosen in the D-CAT test, illustrated in figure 50, is known as initial value method or **single shooting**: The problem is solved as a nonlinear programming NLP problem, requiring the solution of an inner problem (numerical solution of the PDE model as an IVP initial value problem) for each of the 20 optimally-selected data intervals. The solution of the inner problem is described in chapter 6.7, the solution of the outer NLP is described in this chapter.

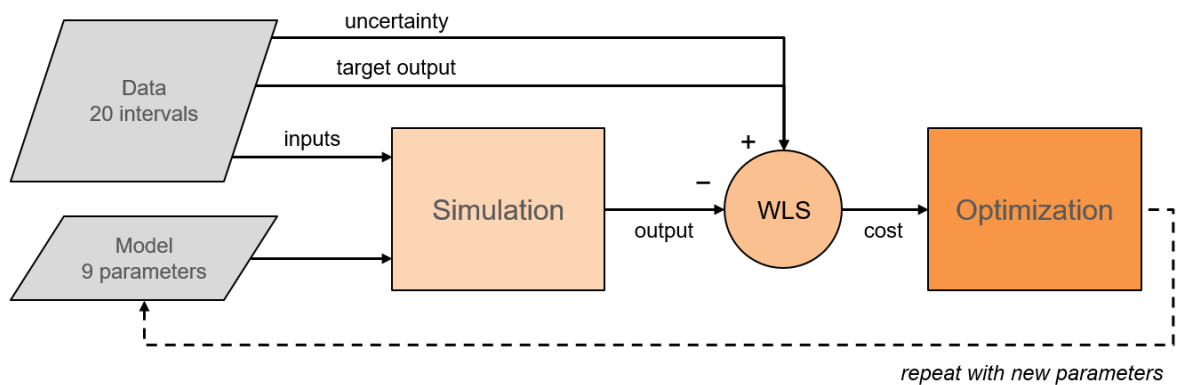


Figure 50: Illustration of the D-CAT parameter estimation process: Based on 9 model parameters, the collector array is simulated for each of the 20 optimally-selected measurement intervals. The WLS cost function is calculated using simulation output, target output and uncertainty from the experimental data. The optimizer proposes a new set of parameters and repeats the process until some cost minimum is found.

Optimization Algorithm

The parameter estimation problem of the D-CAT method is generally known as an inverse problem, and this kind of problems has been shown to be challenging. For instance, parameter estimation problems based on nonlinear dynamic models have been shown to be susceptible to getting stuck in spurious local minima, representing unphysical parameter sets; [99] states a number of issues and pitfalls that can arise in the parameter estimation of dynamic systems. [110] concluded that the early multi-start approaches (local optimization algorithms run multiple times from different starting points) were unsuccessful and highlighted that stochastic global optimization algorithms should be used instead. A practical guide about the choice of specific global optimization algorithms can be found in [111].

Within the MeQuSo project, a series of suitable optimization algorithms have been tested, including Genetic Algorithms (GA), Simulated Annealing (SA) and also surrogate methods. GA and SA have been found to perform well in terms of quality of the estimated parameters, but they were computationally very extensive. The tested surrogate optimization methods did not produce good quality parameter estimates.

Finally, a Particle Swarm Optimization (PSO) algorithm has been chosen, following good experiences of several authors for similar problems, as described for instance in [112] and in [103]. The PSO algorithm has somewhat better theoretical foundations compared to many other metaheuristics-based stochastic global optimization algorithms; in particular, convergence properties and the choice of meta-parameters of the PSO algorithm have been studied in some detail, for instance in [113] and [114]. The finally chosen optimization algorithm implementation is a hybrid stochastic-deterministic variant of the classical PSO algorithm, combining the good global optimization properties of PSO with faster local convergence. The algorithm is named PSWARM; it is described in [115] and can be downloaded from [116]. This algorithm has proven to be competitive for this type of problems, see for instance the review work of [117]. Further investigations on other optimization algorithms would, however, deserve further investigation and have the potential to lead to an overall improvement of the D-CAT method.

9 Application and validation

9.1 Practical optimization results

Figure 51 shows a visualization of the optimization process for one particular collector array and one particular measurement year (2018, in this case). The top left subplot shows the values of the cost function that is to be optimized. According to the used weighted least squares approach, this can be interpreted as a weighted RMSE value. Since the weights are not too different from 1, this value is close to an actual RMSE. The final **RMSE** value is around **0.6 K** as an overall deviation between model output and experimental data, based on collector array data of one particular season. The RMSE values obtained for other collector arrays and other measurement seasons were in a similar range. As a value characterizing the overall deviation between model and experiments over a broad variety of different operating conditions, 0.6 K can be regarded as a very satisfactory goodness of fit. This is particularly true if we keep in mind that the system, i.e. the condition of the collector array under consideration, changes over time, also within the same operating season. This induces some uncertainty into the estimated parameters.

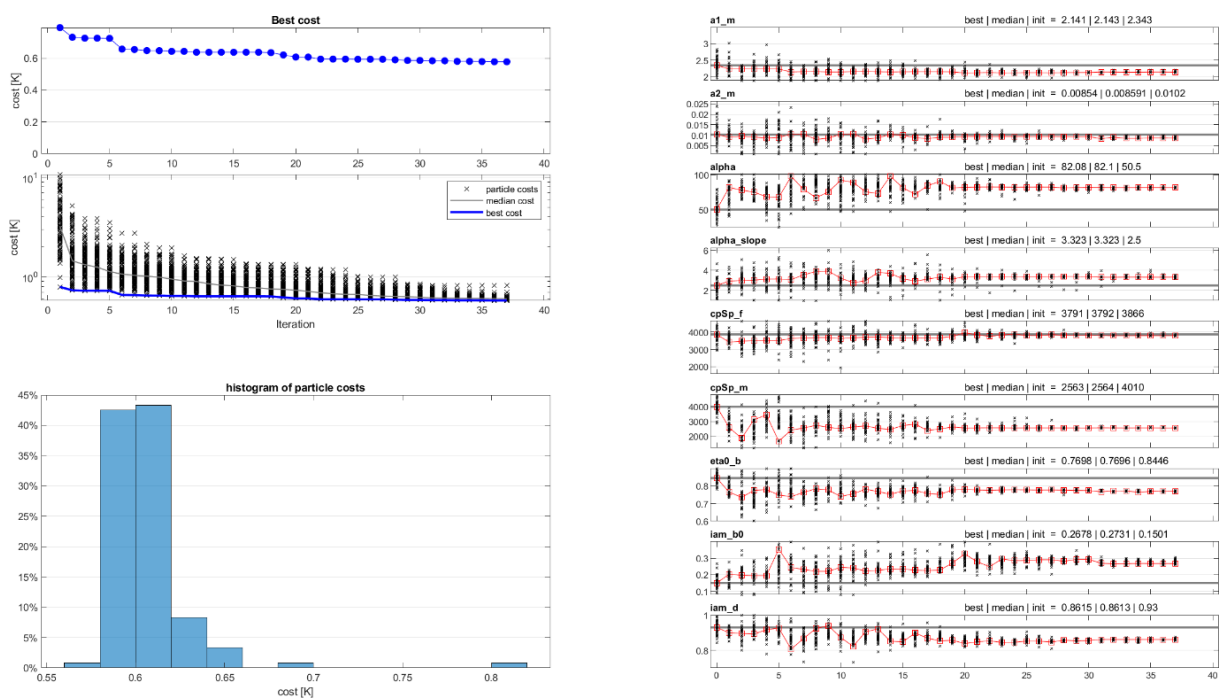


Figure 51: Visualization of the optimization process and estimated model parameters for one particular collector array, based on experimental data from one particular operating season.

Based on global optimization theory, we have no certainty that the parameters obtained from this optimization process do actually represent the global optimum. There are some hints, though, suggesting that the estimated parameters are quite **reliable**. For instance, let us consider the c_f value of the heat transfer fluid, the parameter named $cpSp_f$ in figure 51. For the FHW plant, the fluid heat capacity was determined in the lab (details in chapter 3.2.3). This is why, in principle, there is no need to estimate this parameter, for the FHW collector arrays. In the general case, however, the fluid property c_f is not known or not reliably known (some data sheet fluid property specifications are

not reliable). For this reason, we decided to include c_f as a parameter in the set of parameters to be estimated. As becomes clear from figure 51 (cpSp_f is in the 5th subplot from top on the right hand side), the estimated value of parameter cpSp_f is very close to the initial value which is the fluid property value as it was measured in the lab.

Table 12, page 94 has an overview **interpretation** of the estimated model parameters; these parameters are from an estimation of one particular collector array for the 2018 measurement season. The parameter values refer to the parameter subplots on the right-hand side of figure 51. Figure 52 and figure 53 visualize the parameter values in the well-known displays of collector efficiency curve and IAM curve. For an example plot of how the model output with calibrated parameters compares to the measured experimental data, please refer to figure 31 on page 62.

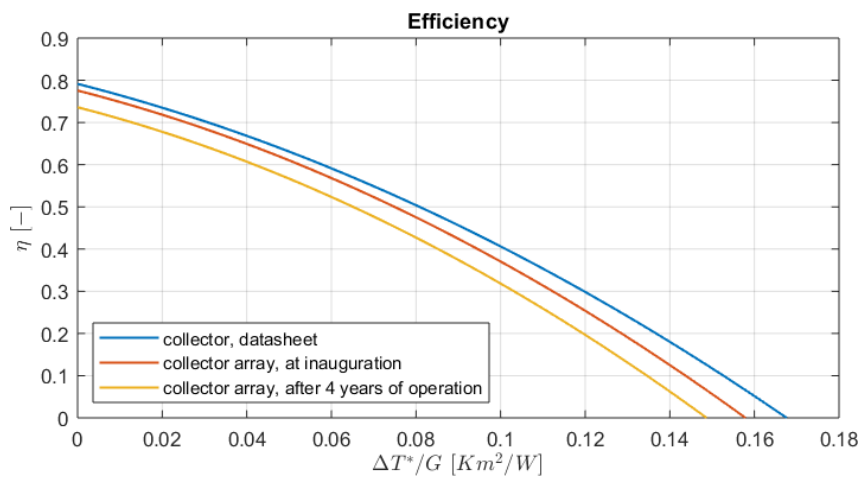


Figure 52: Example output of the condition monitoring using the D-CAT method, displayed in terms of a classical collector efficiency curve. The curves compare data sheet behavior with efficiency behavior at commissioning and after several years of operation.

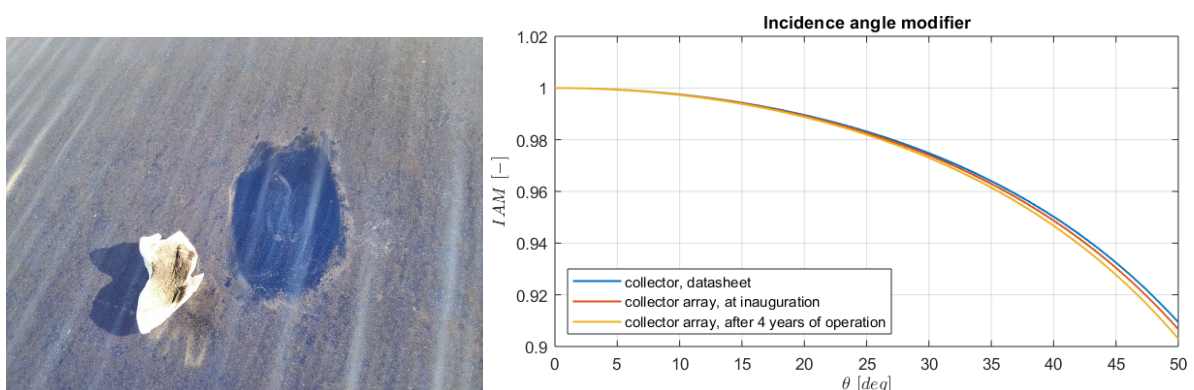


Figure 53: Dirt depositing on the outer collector cover is the main responsible for deteriorated incidence angle modifier (IAM) values. Right: Example output of IAM curves, comparing IAM values from the data sheet with the condition at plant commissioning and after 4 years operation, based on the estimated 2-N model parameter b_0 .

Table 12: Interpretation of the estimated model parameters, referring to figure 51.

<i>Parameter</i>	<i>Parameter description</i>	<i>Interpretation of estimated model parameter</i>
a_1, a_2	Heat transmission coefficient and temperature dependence of heat transmission coefficient; in the 2-N model, they refer to the solid, not fluid temperature	The initial guesses for a_1 and a_2 are calculated based on the data sheet values for the heat loss coefficients that refer to the mean fluid temperature, combined with some heuristics based on the collector's F' value. The optimization bounds are set quite loosely, allowing for big parameter variations during optimization. Both parameters reach physically meaningful values. The separation of a_1 and a_2 is problematic, because the model predictors for these parameters are highly correlated, as can be seen in figure 48; this is true even after optimal data selection, see figure 48. The separation of a_1 and a_2 was found to be problematic in some optimization runs.
α, α'	Convective heat transfer coefficient α between metal temperature T_m and fluid temperature T_f , and volume flow dependency of α .	The parameter α is closely related to the collector's F' value. Higher α values mean higher F' , which improves collector efficiency. α has been found to be an unproblematic parameter in model calibration. α' stays close to its initial value and improves model output in low volume flow regimes, but has limited overall influence on the model performance.
$(mc)_f, (mc)_m$	Heat capacity of the collector heat transfer fluid and of the solid part of the collector array.	Unlike the regression method used in [10], heat capacities can be reliably estimated using the D-CAT method. As mentioned above, $(mc)_f$ has been found to usually be an unproblematic parameter in the optimization. It can be estimated very reliably, comparing very well to the fluid property lab measurements. The estimations of $(mc)_m$ were almost always found to be considerably lower than the initial values based on data sheet information, but this is not too relevant since the data sheet uses a calculation method not directly applicable to the 2-N model. A lower value for the 2-N model solid heat capacity $(mc)_m$ is in line with previously reported findings, e.g. in [67].
$(\tau\alpha)$	Zero loss coefficient	The estimated $(\tau\alpha)$ is found to be lower than the initial value of clean collectors without operation hours. This is a clue to slight material degradation in the collectors' cover and/ or absorber material.
b_0	Incidence angle modifier	As expected, dirt depositing on the outer collector cover in field operation leads to increased optical losses at inclined solar incidence, and this becomes apparent in higher b_0 values compared to the initial data sheet value.
K_d	Incidence angle correction for diffuse radiation	K_d degrades in much the same way as b_0 , due to dirt on the collector cover. Overall, we found that the collectors in the field installation have can use approx. 5-7% less diffuse radiation compared to new and clean collectors as in the data sheet.

For the same collector array and the same operating season that was used to visualize the parameter results in the figures above, figure 54 shows a histogram of the **model residuals** (difference between modeled and measured flow temperature), including all 20 optimally-selected 1-hourly intervals. The mean value of all residuals is $\mu = 0.11$ K, the standard deviation $\sigma = 0.60$ K. A histogram of the model predictors of the D-CAT 2-N model is shown in figure 55, referring to one particular collector array of the FHW plant and to one particular operating season. The top subplot has histograms of all available 1-hourly 479 intervals that fulfill the model validity criteria, as described in chapter 6.6. The input data clustering described in chapter 8.2 is visible in figure 55: several predictors have skewed, non-uniform distributions. For instance, the plant mostly runs on a very reduced range of operating temperatures around 55..70 K (subplot titled dtTmTa). In the bottom plot with the optimally-selected intervals, the histograms are de-clustered and include more extreme data. This is important in order to avoid model overfitting and improve generalization of the estimated model parameters.

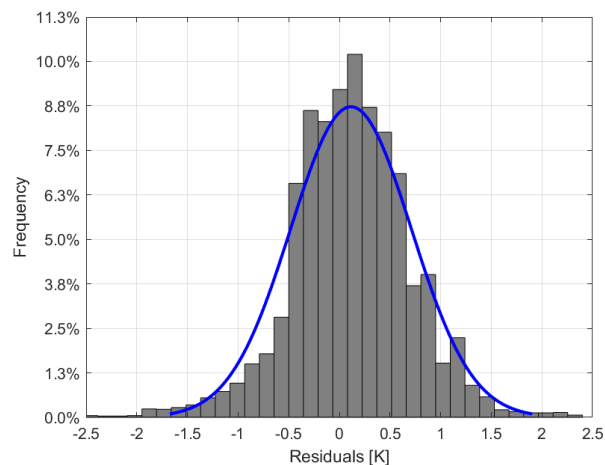
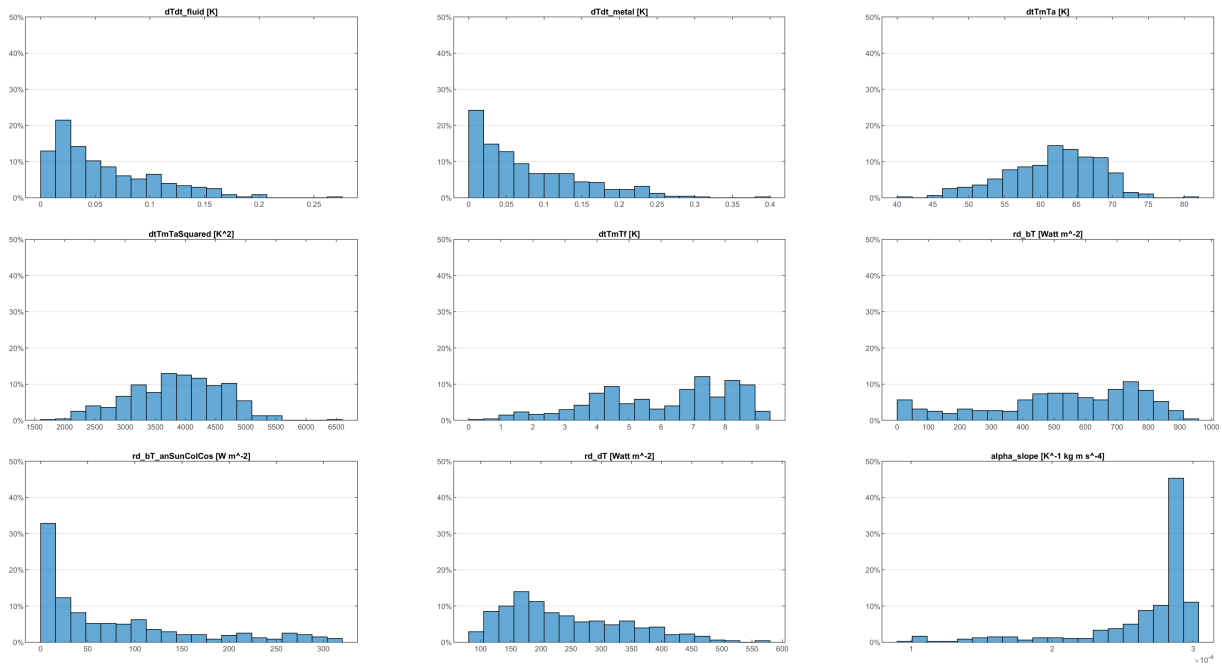


Figure 54: Histogram of model residuals, for one particular collector array and operating season, including all 20 selected optimal intervals. Mean and standard deviation are $\mu = 0.11$ K and $\sigma = 0.60$ K, respectively.

In an analysis of how residual values relate to model inputs (see figure 56), we found that typically, high residuals relate with sharp changes in beam radiation; such sharp changes are typical for weather conditions with intermittent clouds. We see little reason how this could be attributed to the model itself, as a model deficiency; we rather believe that this is a measurement representativity problem: Radiation measurement is done in only one particular spot of the collector array and does not necessarily represent the typical radiation over the entire array area, as is implicitly assumed by using the radiation measurements as model inputs. This mis-representation error is low in some situations (e.g. clear sky, homogeneously cloudy sky, dull or overcast sky), but the error is high in case there are intermittent small clouds on an otherwise clear sky with high beam radiation values. Overcoming this mis-representation problem would require a massively improved approach, possibly using optical measurement equipment to estimate cloud transition over an extended area (the collector array area) from spot measurements.

Histograms of filterIntervals mean values (479 intervals, each 60 min long)



Histograms of optimally-selected intervals (20 intervals, each 60 min long)

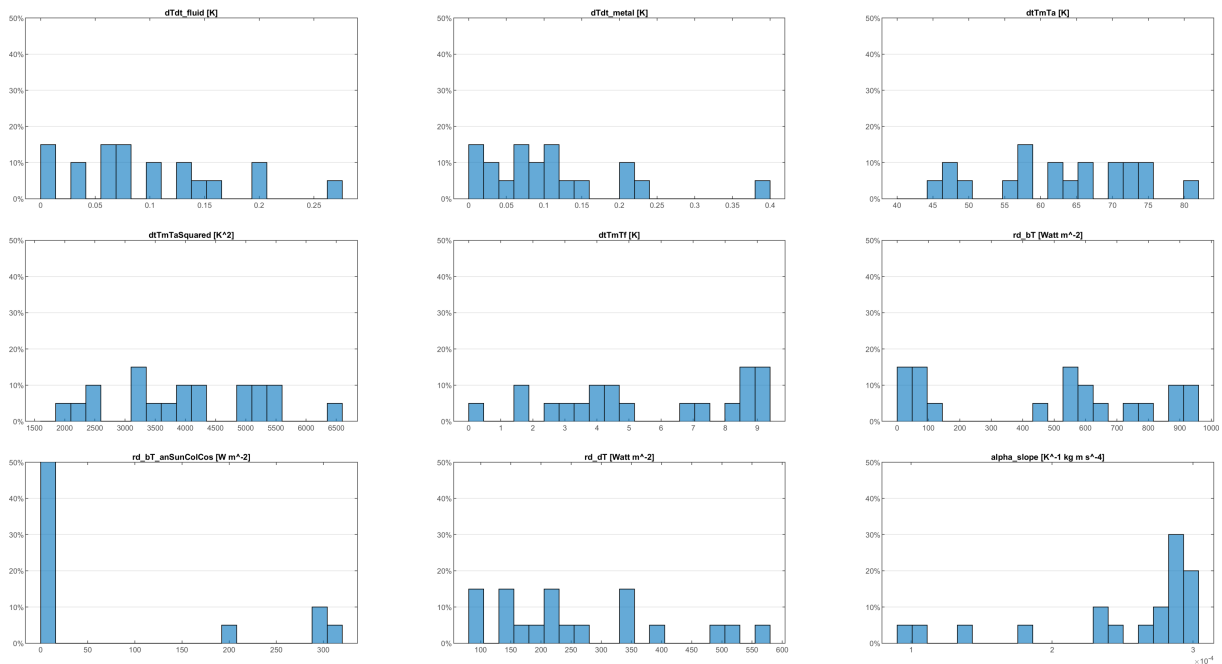


Figure 55: Histogram of model predictors of the D-CAT 2-N model. Top: All 479 available 1-hourly intervals for one collector array of the FHW plant, for one particular operating season. Bottom: Optimal data selection selects 20 out of the available intervals (see chapter 8.2). The clustering of input data (described in chapter 8.2) is visible in the top plot as non-uniform distributions. For instance, the top right histogram in the top plot has the temperature difference between collector metal and ambient temperature. Most intervals are around 55.70 K; the optimally-selected intervals are de-clustered and include more extreme data.

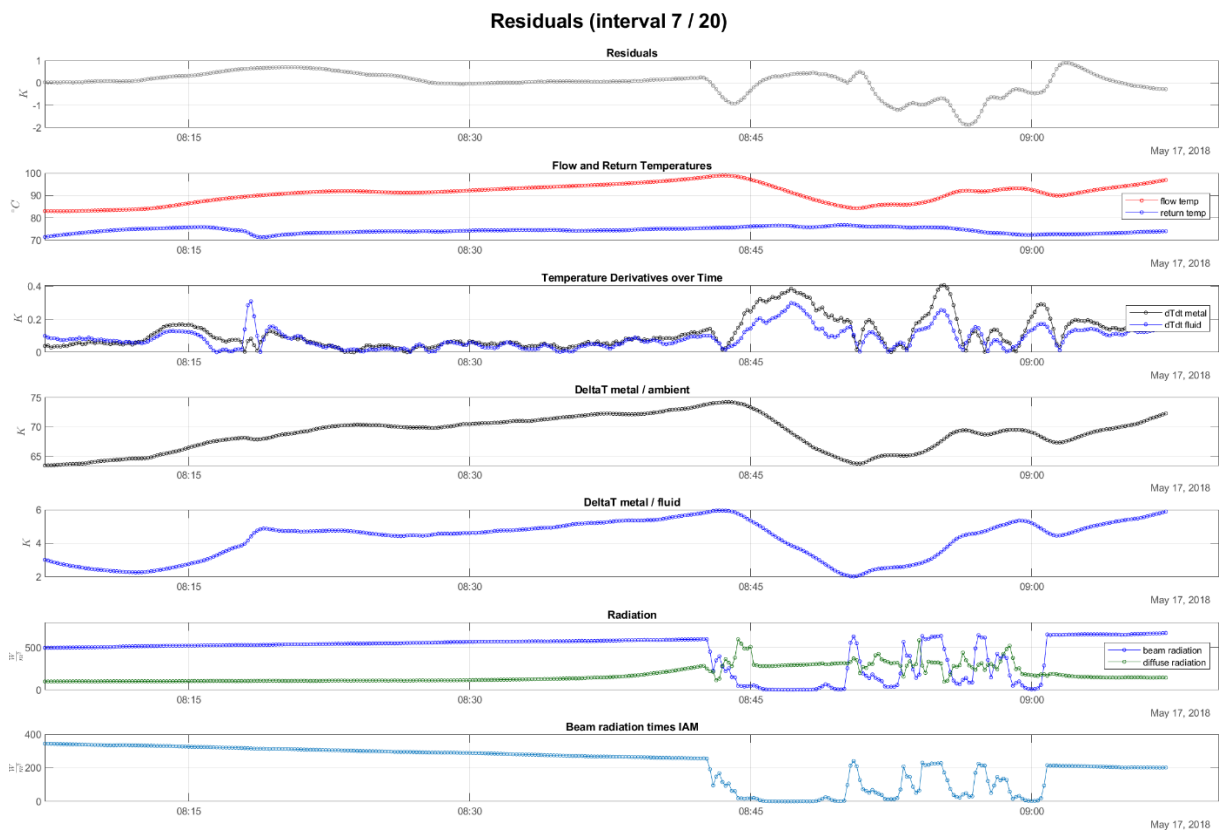


Figure 56: Plot of residuals vs. predictors (model inputs), for one particular collector array and one particular measurement data interval. The residuals plot shows the typical behavior, with higher residuals occurring mostly when radiation input has sharp changes coming from intermittent clouds.

9.2 Example results for model behavior

The intention of this chapter is to show illustrative examples that help getting an intuitive understanding of how the different collector array models behave, under different weather and operating conditions. The figures will contain a comparison of the behavior of the different models described so far (2-N model, 1-N model, QDT model – see chapter 6), compared to measurement data and compared to each other. Since the results contain insights into collector array behavior, they have to be handled as confidential, and accordingly the figures used in this chapter are anonymized. The shown figures are from the 2018 operating season and all relate to the same collector array.

For the 2-N model, the model parameters are those estimated with the parameter estimation method described in chapter 8 and chapter 9.1, based on the measurement data of 2018. For the 1-N model and the QDT model, the data sheet parameters are used. The chosen collector array consists of four collector rows, and the outlet temperature was measured both as mixed temperature and in each row individually; these measurements are compared to the 2-N model output.

The comparison in this chapter is based on three different cases; these have been selected to contain interesting phenomena such as varying radiation levels, fluctuating inlet temperatures and step changes in volume flow. All three presented intervals were not used for parameter estimation of the 2-N model, giving an impression of how the 2-N model behaves when applied to data that were not used for training. These are the three cases presented in this chapter:

- (A) Clear day with constant volume flow and small variations in inlet temperature (April 21st, 2018): figure 57, page 99.
- (B) Half-cloudy and half-clear day with some variability in volume flow and inlet temperature (April 18th, 2018): figure 58, page 100.
- (C) Very variable day with high variability in radiation, volume flow and outlet temperature (June 14th, 2018): figure 59, page 101.

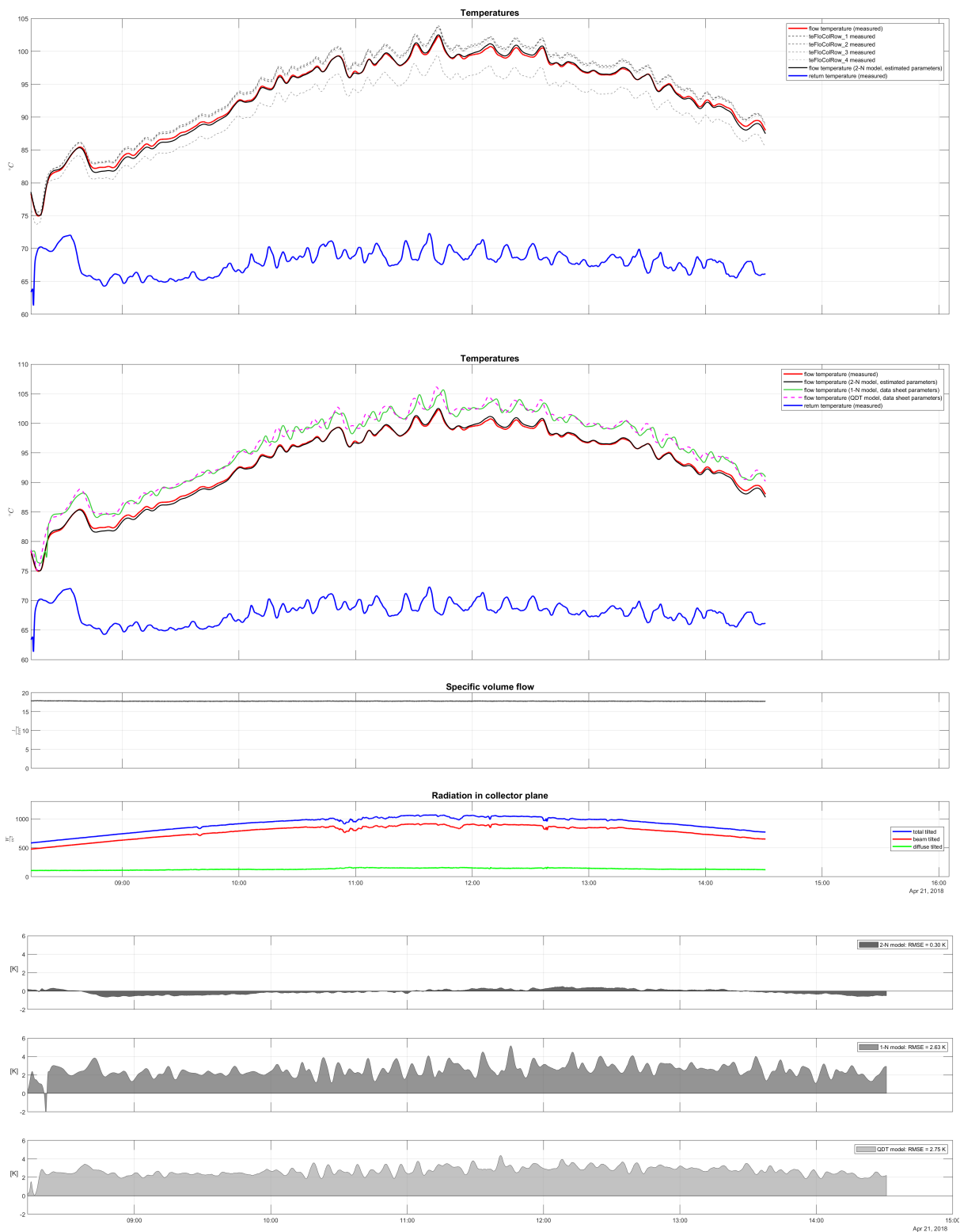


Figure 57: Case A: Clear day with constant volume flow and small variations in inlet temperature. (1) Top subplot: Output of the calibrated 2-N model (continuous black line) compared to measured outlet temperatures (continuous red line: mixed array temperature, dashed lines: individual collector row temperatures). (2) Middle temperature subplot: Comparison of mixed collector array outlet temperature with model outputs: calibrated 2-N model, 1-N model and QDT model with data sheet parameters. (3) The three bottom subplots hold the model residuals for the compared models. The plots show structural model deficiencies of the 1-N and QDT models as well as considerable residuals due to difference between data sheet and in-situ performance.

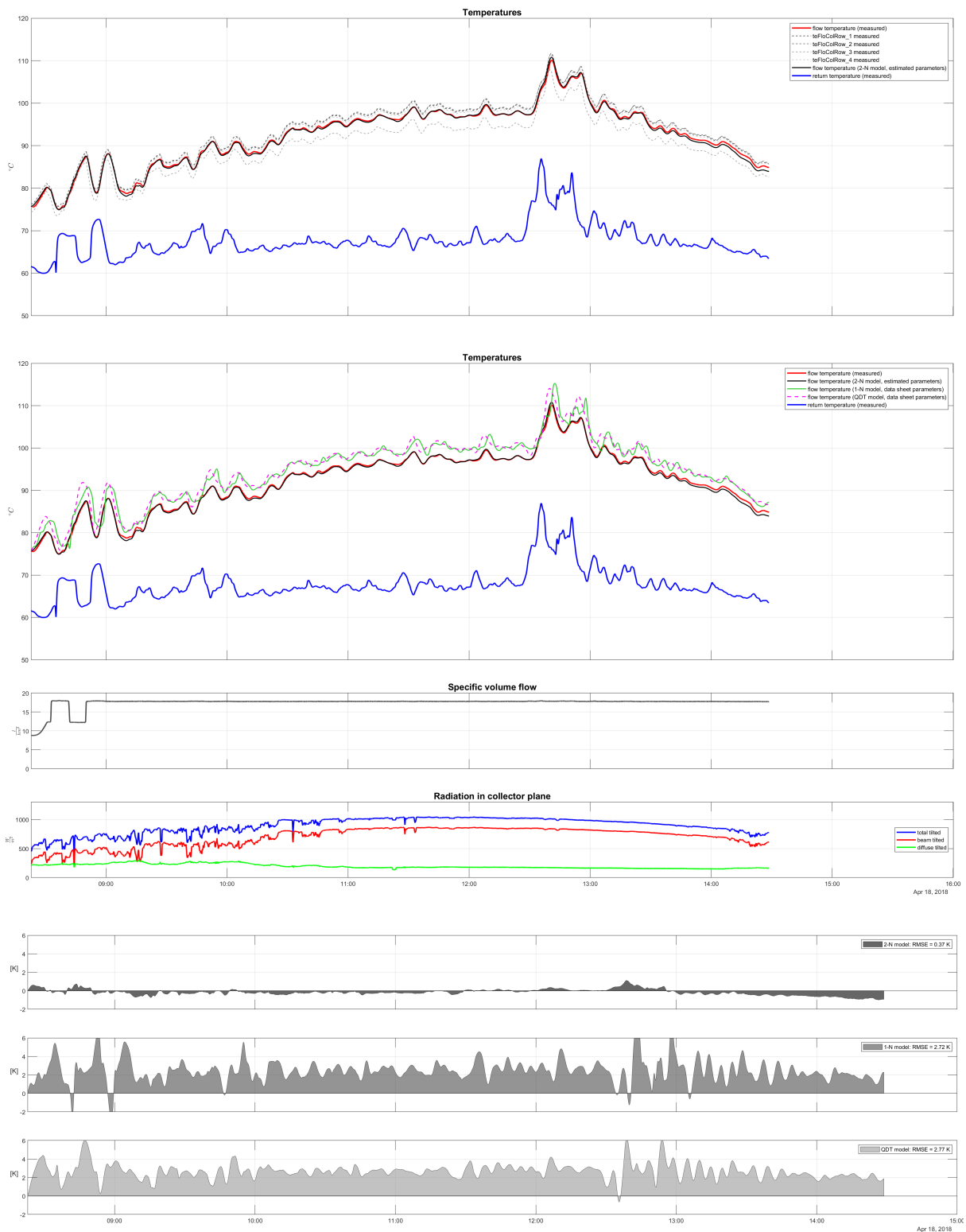


Figure 58: Case B: Half-cloudy and half-clear day with some variability in volume flow and inlet temperature. For a general description of the plots, please refer to figure 57. Model deficiencies of the 1-N model become apparent mainly around volume flow changes (before 9:00) and around temperature changes (before 13:00). The 2-N model with calibrated parameters (continuous black line) closely follows the measured collector array outlet temperature (continuous red line) with small residuals.

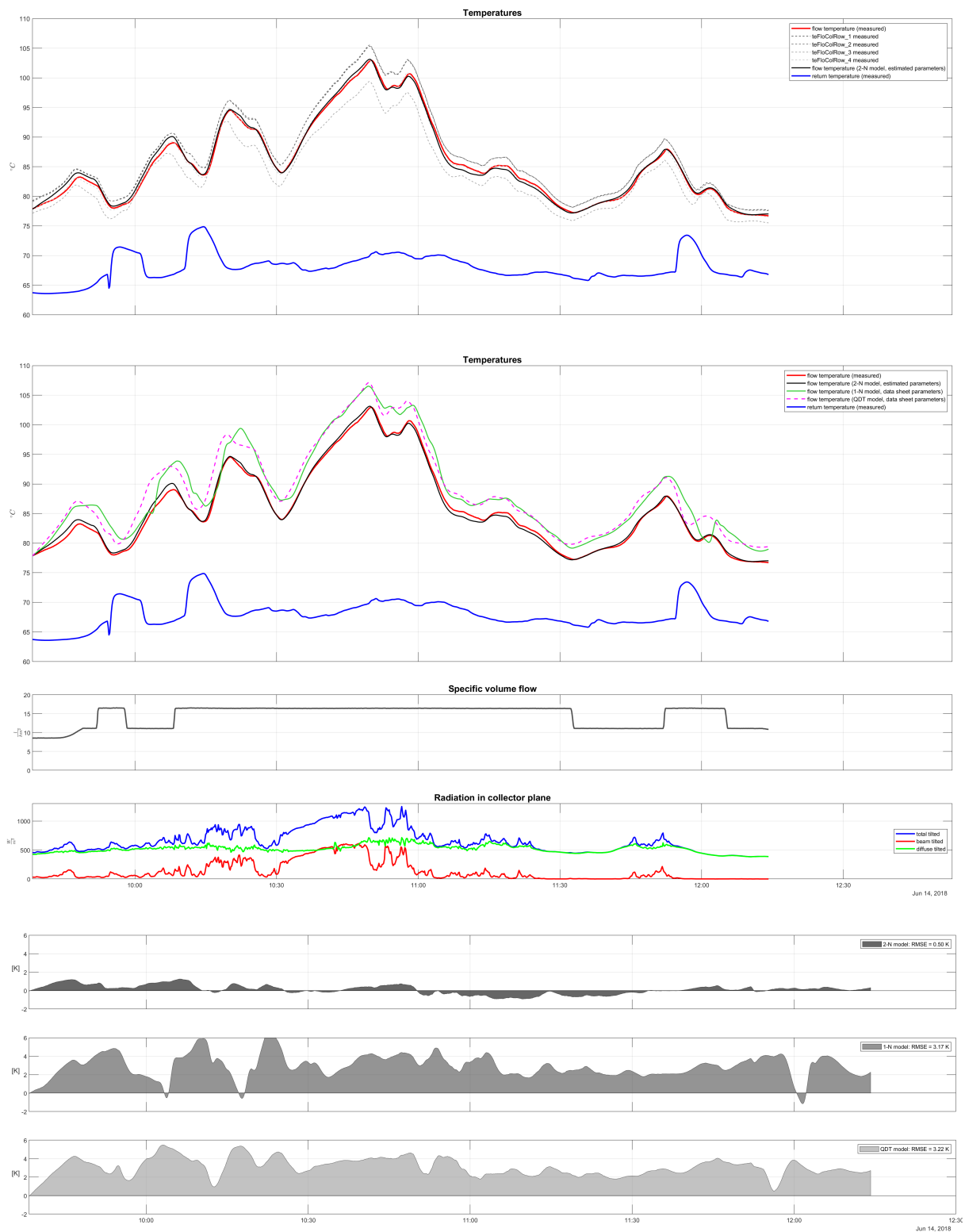


Figure 59: Case C: Very variable day with high variability in radiation, volume flow and outlet temperature. For a general description of the plots, please refer to figure 57. Radiation levels are very different, in the chosen interval, ranging from fully diffuse radiation to high total radiation levels above 1000 W/m². Measured outlet temperatures show high variations, described with a reasonable goodness of fit by the calibrated 2-N model. This indicates the potential of using the D-CAT procedure in the context of plant control, in order to achieve more constant outlet temperatures based on model-based or model-predictive control.

9.3 Example results for radiation modeling

The application of the radiation model (see chapter 7.1) to the FHW plant is shown this chapter. The differences between the measured irradiance on the top of collector and the modeled irradiance are shown in figure 60 for a sunny day and in figure 61 for a cloudy day. The modeled irradiance is the average total irradiance on the collectors, which accounts for the reduction of the diffuse irradiance along the collector height. Relevant are conditions with no shading (grey background color). The modeled irradiance is shown for the ISO and HD model with beam irradiance measurement (Tilted Sensor Model (TSM) + Tilted Collector Model (TCM)) and without beam irradiance measurement (Radiation Decomposition Model (RDM) + TSM + TCM). As can be seen in both figures, the difference of the measured irradiance minus the modeled irradiance is positive, which means the measured total irradiance is bigger than the modeled irradiance, i.e. the collectors are attributed a too high irradiance. For clear days (high share of beam irradiance), the differences are small, as the reduction of the diffuse irradiance does not affect the beam irradiance. A comparison between the ISO TSM + TCM and HD TSM + TCM model shows, that the HD model predicts an average total irradiance which is closer to the measured irradiance. The reason for this phenomenon is, that the HD model classifies some part of the diffuse irradiance as circumsolar diffuse irradiance, which is treated in the same way as beam irradiance with no reduction along the collector height. For clear skies, the combination with a radiation decomposition model (no beam measurement) shows a very similar prediction of the total titled irradiance both for the ISO and HD models. For a cloudy day, the differences between measured and modeled irradiance are larger in relative terms and often as well in absolute terms, as a comparison between figure 60 and figure 61 shows.

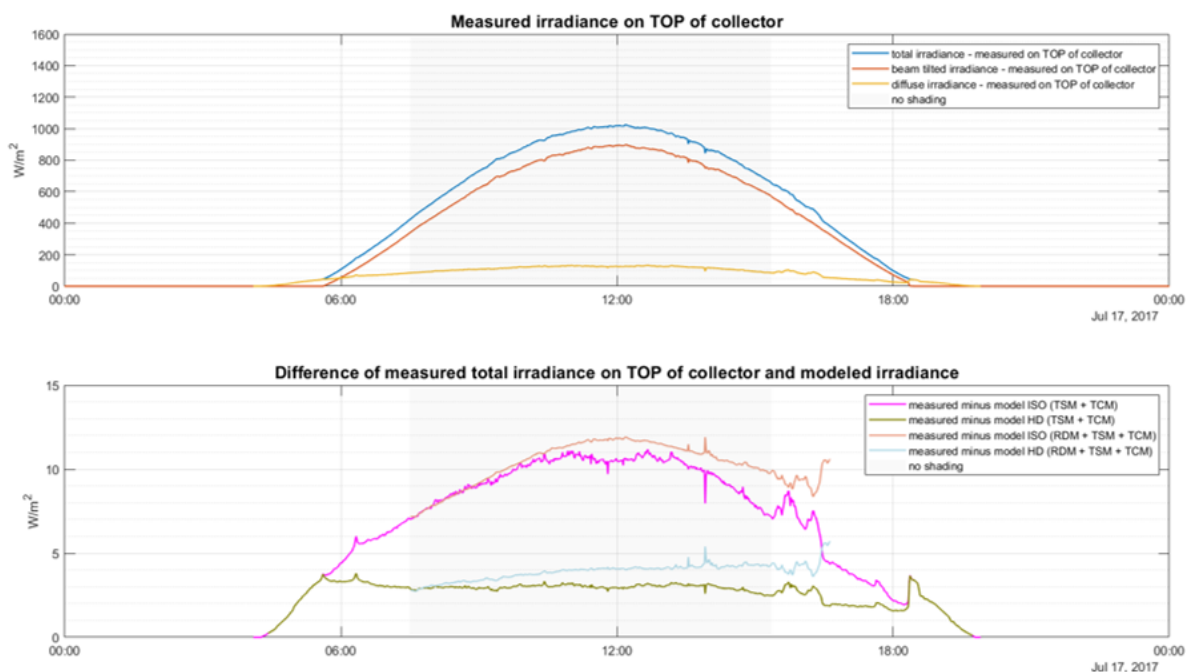


Figure 60: Measured and modeled radiations for a sunny day. Top: Measured irradiance with pyranometer placed on top of the collector for total irradiance and pyrhelimeter for beam irradiance. Bottom: Deviations of measured vs. modeled average irradiance on the collectors.

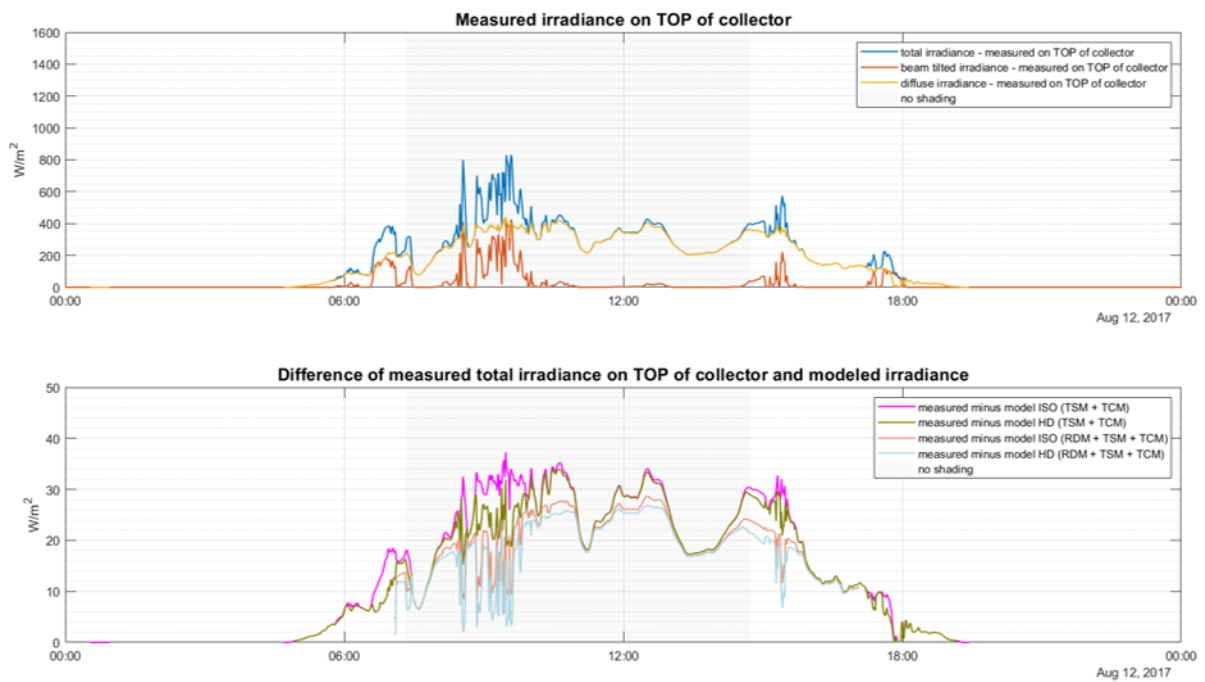


Figure 61: Measured and modeled radiations for a cloudy day. Top: Measured irradiance with pyranometer placed on top of the collector for total irradiance and pyrliometer for beam irradiance. Bottom: Deviations of measured vs. modeled average irradiance on the collectors.

Figure 62 shows a comparison for July 2017 for total daily irradiances, excluding conditions with external shading. The shares of the modeled irradiance in percent of the measured irradiance (bottom plot) shows differences of up to 9%. This is true for 2017-07-14, which is a cloudy day. For clear days with high irradiance, this is less of an issue. For example, for days with more than 4 kWh/(d m²) total irradiance in July 2017, average shares are 97.2% (ISO TSM + TCM), 98.3% (HD TSM + TCM) and 98.1% (ISO RDM + TSM + TCM) 98.8% (HD RDM + TSM + TCM) respectively.

The importance of radiation modeling for days with high diffuse irradiance is shown in figure 63, which displays a comparison for the daily diffuse irradiances. The ISO TSM + TCM and HD TSM + TCM are more exact, because they do not have to decompose the total radiation as do the ISO RDM + TSM + TCM and HD TSM + TCM models. In rare cases, the use of RDM models can lead to an overestimation of the diffuse irradiance (2017-13 and 2017-14).

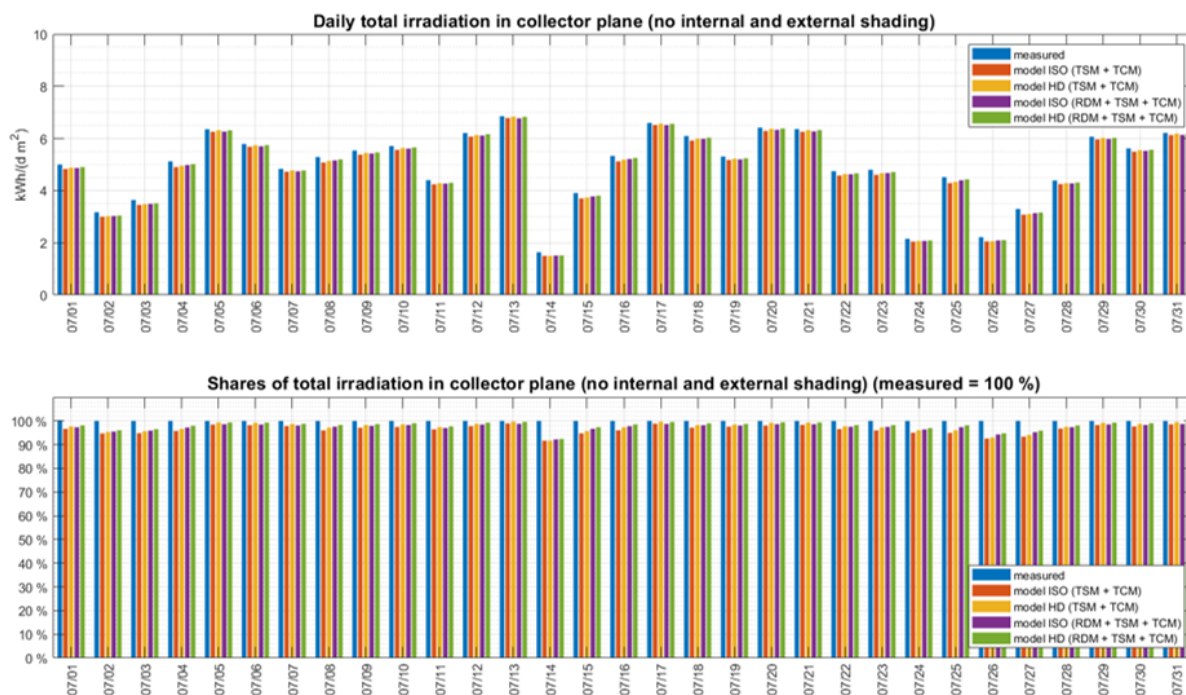


Figure 62: Measured and modeled total daily irradiance (no internal and external shading) absolute (top) and as a share of the measured irradiance (bottom).



Figure 63: Measured and modeled daily diffuse irradiance (no internal and external shading) absolute (top) and as a share of the measured irradiance (bottom).

The radiation modeling accounts for view obstructions. For the FHW plant with a row spacing of 3 m and collector tilt angle of 30° (see chapter 3.1), view obstructions due to collectors placed in front can be significant. Lower parts of the collectors receive less diffuse irradiance than the spot where the radiation is measured at the top of a collector in the middle of the field (the radiation setup is shown in chapter 3.2). If the modeled average diffuse irradiance instead of the measured diffuse irradiance at the top of the collector is used for G_d in the D-CAT 1-N equation (9) or D-CAT 2-N equation (12) respectively, the estimation of the diffuse radiation incidence angle modifier K_d can be more accurate.

Using the modeled average diffuse irradiance instead of the measured irradiance for target/actual comparisons allows a fairer comparison of the collector array performance. This is illustrated with the Performance Check (PC) method, the most widespread in-situ test method (see chapter 2.3, page 19) as shown in figure 64. One field of the FHW plant was evaluated with data from 2017. The limits of the operating conditions were set in accordance with equation (5), listed in the right column of table 2. The figure shows a comparison of the estimated thermal power output with equation (5), using (a) the measured diffuse irradiance (left) and (b) the modeled average diffuse irradiance (right) as the input for G_d . The evaluation shows that the collector array performance in case (a) is on average -6.6% below the performance estimated from the data sheet (with $f_{save} = 1$ in equation (5)), whereas in case (b) it is -4.7%, shifting the target/actual comparison in favor of the collectors. Note that the diffuse share is relatively low as the operating condition limits require $G_b > 600 \text{ W/m}^2$. The difference would be larger if operating conditions with a higher diffuse irradiance would be chosen.

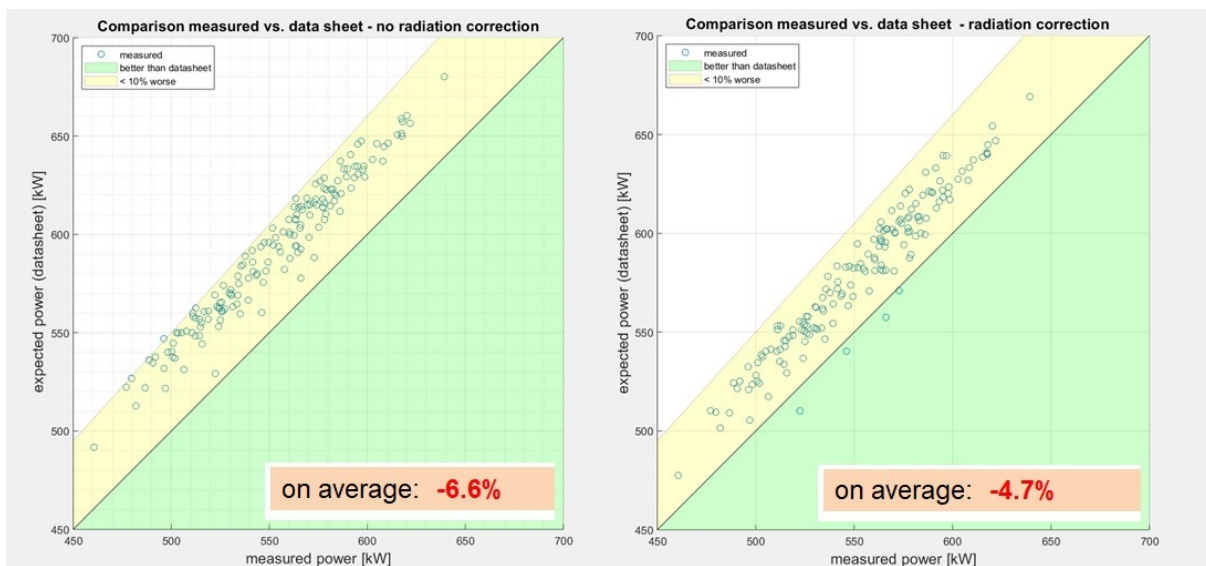


Figure 64: Comparisons of measured thermal power and estimated thermal power based on the PC method. Left: Measured diffuse irradiance is used for thermal power estimation (no correction due to view obstructions in the collector array). Right: Modeled diffuse irradiance is used for thermal power estimation (accounting for view obstructions), which shifts the target/actual comparison in favor of the collectors.

9.4 Solar yield guarantee

As explained in chapter 1.4, the solar yield is affected by multiple influencing factors like design, components, operation, load and environmental conditions. The D-CAT method allows an in-situ characterization of the collectors on a component level with the estimated collector parameters. These parameters can be used for a target/actual comparison or solar yield guarantee, where the collector manufacturer is not made liable for the way the collectors are actually operated. The basic idea is the same as in the ISTT method (see chapter 2.3, page 20): The annual solar yield is simulated with data sheet parameters (target) and estimated parameters (actual) with the following steps:

- Collector manufacturer certifies the collector and provides a data sheet with collector parameter (“data sheet parameter”)
- Collector parameter of the behavior of the collectors in the field (“estimated/in-situ parameter”) are retrieved by applying the D-CAT method to the collector array
- Simulations for the annual solar yield with the simulation tool are carried out with (a) “data sheet parameter” and (b) “estimated/in-situ parameter”
- The solar yield guarantee is fulfilled if the annual solar yield in case (b) is larger than case (a) minus safety factors (for uncertainties of the D-CAT procedure and other uncertainties)

To make such a procedure transparent and easy applicable, a standardized, pre-configured and preferably open source simulation tool with previously defined boundary conditions (e.g. weather data from test reference years of the location) should be used. This ensures that all parties can check the simulations on their own.

This procedure is shown illustratively for the FHW plant. The D-CAT 1-N model has the same collector parameter as the QDT model. Although the D-CAT 2-N model is superior for dynamic modeling, estimated parameters of the D-CAT 1-N model for one collector array of the year 2017 were used, as standardized simulation tools for the QDT model exist. As for the yield guarantee only the difference between two simulations matter, simple tools might be used as well, depending on the complexity of the plant and operation. A possibility is the tool ScenoCalc (Solar Collector Energy Output Calculator) [118], [119]. The tool is used by test institutes and certification bodies to enable them to convert collector model parameters determined through standardized tests into energy performance figures. ScenoCalc has been further developed for district heating applications, called ScenoCalcFW [120]. It includes heat exchanger, storage and the load curve of the district heating network.

ScenoCalcFW has been used to illustrate the solar yield guarantee. A screenshot of the simplified representation of an exemplary 1000 m² array of the FHW plant in ScenoCalc FW is shown in figure 65. Distribution pipes and the heat exchanger are included in the model. Weather data for Graz are from Meteonorm [121]. Flow and return temperatures of the district heat network are similar to the actual operation conditions.


Figure 66 shows the simulation results and its implications for the solar yield guarantee. The annual solar yield according to the simulation with data sheet parameters is 364 kWh/m²y (on the secondary side of the heat exchanger) and 351 kWh/m²y with estimated/in-situ parameters (-4.67%). If a tolerance of 5% is agreed on beforehand, than the guarantee is fulfilled. Note that both simulations will differ from the actual solar yield, but what counts is the difference.


ScenoCalc Fernwärme 2.0

Projektname: Projekt speichern

Standort und Betrachtungszeitraum anpassen Projektverwaltung


Standort: **Graz**
 Zeitraum: **1.1. - 31.12.**

Gefördert durch:
 Bundesministerium für Wirtschaft und Energie
 aufgrund eines Beschlusses des Deutschen Bundestages

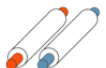
 **Berechnung**

Systemkonzept: Rohrleitungen Wärmeübertrager Solar Speicher Wärmeübertrager Netz Wärmenetz

Einstrahlung auf das Kollektorfeld
1387 MWh



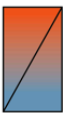
Kollektorfeld-ertrag
351 MWh
351 kWh/m²



Brutto-Kollektorfläche
1000 m²

Kollektortyp
Flachkollektor


Solare Wärmelieferung an das Wärmenetz
347 MWh
347 kWh/m²



Systemnutzungsgrad
99%

Solarer Nutzungsgrad
25%

Wärmenetz-Temperaturen
100 / 60 °C



Rohrleitungsverluste
4 MWh

Figure 65: Screenshot of FHW plant representation in ScenCalc FW.

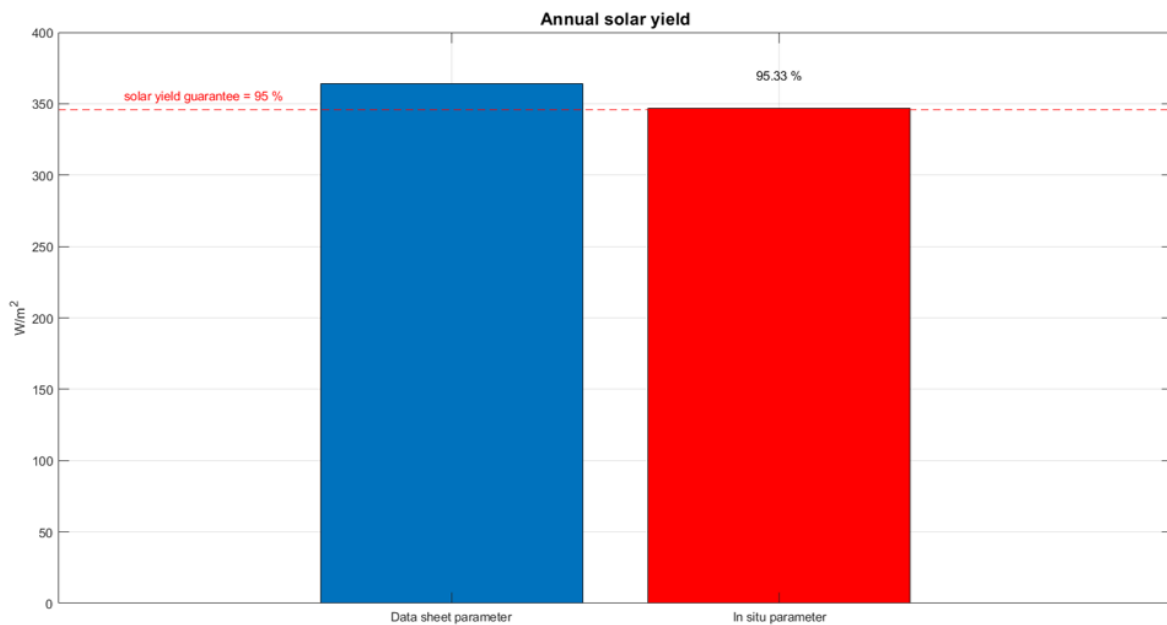


Figure 66: Annual yield comparison with data sheet parameter and estimated parameter.

10 Discussion and conclusion

10.1 Discussion and lessons learned

The following points are important from the perspective of the authors:

- **Importance of good modeling:** The findings of the MeQuSo project show that the QDT model and also a simple extension of it to collector rows (D-CAT 1-N model) are not able to satisfactorily explain the behavior of collector arrays under fully dynamic conditions. The D-CAT 2-N model is a simple extension, modeling fluid and metal temperatures separately, and is able to accurately describe the measured experimental data. Inappropriate models lead to biased and meaningless parameters; for the collector array test, we want reliable parameters, so using a good model is mandatory. The 2-N model can be formulated as a nonlinear state-space model, so the theory available for state-space models can be applied.
- **Radiation measurement:** Good quality radiation measurement is crucial, ideally providing beam and total/diffuse radiation as separate inputs. The importance of good radiation measurements is not a surprising result, but is not an easy task for in-situ measurements. Within the MeQuSo project, the DNI at the FHW plant was measured with a pyrliometer mounted on an active sun tracker; this is only possible within a research project and not in general due to economic restrictions. Sensor cleaning was done by hand. The pyrliometer was much more affected by soiling than the pyranometer, who was directly exposed to rain and had a ventilation unit. The installation of an “air shield” for pyrliometer soiling prevention (e.g. “AirShield® DNI” [122]) is worth considering. Another alternative is the use of a sensor that measures both direct and diffuse irradiance in one device (e.g. Sunshine Pyranometer SPN1 [10]) and does not require a sun-tracker. A much simpler alternative is to measure total radiation in the collector plane and use a model to calculate beam and diffuse from total radiation as it is possible with auxiliary models used in the D-CAT method (see chapter 7.1).
- **Between-collectors measurements:** In one of the collector rows of the investigated FHW plant, temperatures between collectors in one collector row have been measured. The goal was to possibly gain more insight about the collector efficiency at different temperature levels within an array. Although all temperature sensors were calibrated in the lab before being installed in the field, and although the installation and flow situation of the sensors was ideal, these measurements hardly provided new insights. This is because the sensor measurement uncertainty was simply too large, the temperature difference between single collectors small due to the large absolute volume flows in collector arrays. For collector arrays, it seems not to make sense to measure temperatures within a serially-connected row of collectors, unless different types of collectors are mixed.
- **Combination of methods:** Prior to applying D-CAT as a sophisticated method, pre-evaluation of the collector array performance with simpler methods is important. In particular, the Performance Check (PC) method (see chapter 2.3) seems to be a promising and simple way for a quick first analysis. While this method does not provide deeper insights into the physical effects causing the observed collector array behavior, having simple and reliable results at hand surely helps to understand and apply the more detailed but also more costly D-CAT method.
- **External shading:** In order to reduce the number of unknown or not well-known influencing factors, for the development of the D-CAT method external shading on the collector array

(shading from surrounding objects) was explicitly excluded. For a more widespread application of the method, external shading should be treated in a different and generally-applicable way, including already available methods [123] and possibly machine learning methods.

- **Validation and optimization:** In the MeQuSo project, the D-CAT method has been applied to several large-area collector arrays, with several different method setups and options. The outputs of the validation process revealed interesting and helpful insights, but overall not all unsuccessful applications of the test method could be resolved, and some remained hard to explain. The global optimization algorithm sometimes got stuck in a local minimum, despite trying a multitude of algorithms and adjusting their settings following literature advice; the optimization was a very lengthy process taking several hours to deliver the parameter estimates.
- **Framework and software implementation:** D-CAT is designed to run a fully automated collector array test, and this automation was proven in the MeQuSo project. The main drawback of the current implementation is that it requires a software tool which is able to perform the data handling automatically including pre-processing, filtering, parameter estimation and presentation of the results. All steps of the procedure are described in detail in the present document, such that solar companies, certification bodies or research institutes can implement the procedure on their own. But this requires programming skills and senior expertise in data handling. It is questionable whether it makes sense for many institutes to have their own software implementations, as there is always considerable freedom in how such methods are implemented as a software, and the final implementations would very probably not yield perfectly comparable results; see also the unsatisfactory experiences from the round-robin tests in [12].

10.2 Conclusion

Summary of the D-CAT method

The D-CAT method is a new test procedure for collector arrays, which allows a characterization of the deployed collectors in the field with a set of parameters, similar to the parameters delivered by the QDT method in Solar Keymark/ISO 9806 for single collectors. The collector parameters of the D-CAT method describe the collectors' behavior based on measurements of the collector array taken from normal system operation. The in-situ collector parameters capture the current condition of the collector array and their actual, "real-world" performance. In this sense, the D-CAT test provides a detailed and realistic characterization of collector arrays as a technical component in energy systems and extends the QDT method to collector arrays.

Performance reductions that concern the collectors on a component level (such as soiling, broken insulation, faulty foil tension etc.) are reflected in the estimated parameters: For instance, heavy soiling of the outer collector cover will be reflected in worse optical parameter values, compared to clean collectors. Collectors with broken insulation or faulty foil tension will have higher heat loss coefficients. On the other hand, performance relevant factors which do not accrue to the collectors are separated and not attributed to the collectors on a component level. Examples for such factors include system control, weather conditions, collector array geometry and hydraulic setup. The assessment (and responsibility) of the performance of the deployed collectors (that the collectors were in the appropriate condition when installed on-site and after some time in operation) and the performance of the whole array can thus be separated. Having in-situ collector parameters as test outcome combined with an appropriate collector array model is the most general way to perform in-situ testing. The following use cases are possible for the D-CAT method:

- 1) **Commissioning:** Target/ actual comparison with guaranteed thermal power output/yield. This brings clarity into the risk sharing between manufacturer and plant operator. The D-CAT method can both be used for thermal power output and yield guarantees.
- 2) **Surveillance:** Detecting trends by running the D-CAT test repeatedly, in a model-based condition monitoring setting. Changes in the collectors can be observed on a detailed single-parameter level, allowing to understand the observed system behavior. The parameters allow a direct physical interpretation that can be used to take predictive maintenance actions.
- 3) **Control:** The D-CAT yields a calibrated collector array model which can be used for model-based or model-predictive control for collector arrays. Collector arrays have high latency due to long fluid travel times, so model-based control has the potential to improve control quality resulting in constant outlet temperatures and increased efficiency.
- 4) **Testing at different locations:** Transparent comparison of collector arrays, independent of local weather and operational differences such as control or temperature levels (the D-CAT model helps separate these “extrinsic” factors from the collector performance on a component level).

Innovations and unique features of the D-CAT method

What makes the D-CAT method unique is the combination of the following features, developed in the MeQuSo project:

- In order to have a LST collector array tested with D-CAT, the first step is to configure a few basic parameters (collector area, tilt angle etc.); this is a one-off and straightforward step. Once this configuration is done, the test procedure runs automatically including data pre-processing, optimal selection of measurement intervals and parameter estimation. As final result, D-CAT can deliver KPIs (thermal power guarantee fulfilled, energy yield forecast) as well as model parameters that characterize the collector array (optical and thermal parameters, heat losses, thermal capacities etc., see table 12 on page 94).
- D-CAT allows performance assessment for both thermal power output and solar energy yield by providing collector parameters which reflect the current condition of the LST system.
- Clear separation between the performance of the collectors on a component level from their use in the field, by correcting for local weather conditions, pipe losses, heat exchanger performance, control strategy, row spacing, etc. for which the collector manufacturer or maintainer does not bear responsibility. This setup allows for a fair assessment of the collectors under “real operating conditions”.
- D-CAT is applicable with measurement instrumentation as it is commonly available in LST collector arrays: Inlet and outlet temperature, volume or capacity flow, total radiation in collector plane. Sensor positioning, number of sensors and sensor accuracy as they are commonly available are sufficient to apply the D-CAT test. Of course, as usual when measurements are done, lower quality input data deliver lower quality test results.

In the MeQuSo project we used high precision measurement instrumentation in order to exclude measurement uncertainty from the method development. Temperatures and volume flow were measured in the solar circuit, and solar radiation was measured separately as direct and diffuse radiation. This is not a necessary requirement for applying D-CAT: In case temperature and

volume or capacity flow measurements are not directly measured in the solar circuit, piping and heat exchanger have to be included in the analysis; this is described in chapters 7.2 and 7.3. In case radiation is measured only as total radiation (horizontally or in collector plane, as commonly available for LST), additional models can be used to obtain direct and diffuse irradiance as split measurements. This is described in chapter 7.1.

- Dynamic collector array models have been developed as PDE-based dynamic models that extend the QDT model to the needs of collector arrays. Choice between different collector array models: (1) Either the 1-N model (chapter 6.4) to have comparability with parameters obtained by the QDT laboratory test according to QDT/ISO 9806 [10]. (2) Or the 2-N model (chapter 6.5) to have a model without structural deficiencies and better agreement with the measurement data of large collector arrays.
- Use of the developed dynamic models in a grey-box setting to calibrate the models by estimating their parameters from measurement data. Use of a global optimization based parameter estimation method including treatment of measurement uncertainty to some extent.
- D-CAT can make use of fully dynamic measurement inputs, i.e. data from the normal plant operation can be used with very little restrictions. The QDT test substantially restricts the dynamic range of measurement data to be used as test inputs; that makes sense, but is a limitation due to the fact that the QDT model can only explain such data. For the D-CAT method, much more data compared to the QDT test can be used for the parameter estimation because the developed dynamic models have a large range of validity. There is no need to run special test sequences or to use only data with quasi-dynamic or quasi-stationary operating conditions.
- A new data selection methodology has been developed, following Design of Experiments principles: A statistically optimal data selection procedure selects the most informative chunks of input data for the parameter estimation problem and avoids overfitting.
- As a collector array test method, D-CAT can be run periodically for long term performance evaluations and surveillance, providing a possibility to detect long term trends and to evaluate maintenance measures (e.g. cleaning of collectors, adjusting foil tensions etc.), since changes of collector characteristics are reflected in the test parameters. The method is multi-purpose and can be applied for commissioning, surveillance, control and comparison of collector arrays, even at different geographic locations.
- The D-CAT method can be used for performance monitoring (“model-based condition monitoring”) and detailed assessment of LST plants: The estimated model parameters, obtained as a multivariate random variable, reflect the current condition of the tested LST plant. The parameters have a straightforward physical interpretation: In particular, the D-CAT approach enables one to separate weather influence from the behavior of the collector array, seen as a technical component. This yields a clear and concise answer to risk sharing among involved stakeholders, e.g. investor, plant operator and collector manufacturer.

11 Outlook

As a result of the MeQuSo project, the D-CAT method is currently in a proof of concept state. The D-CAT method has the potential to be established as a central tool that enables clear risk sharing among the stakeholders involved in the realization of LST plants, such as investors, plant designers, operators and collector manufacturers. A stringent quality assessment and performance guarantee method like the D-CAT method eventually improves trust and financial security in large solar thermal projects; the long-term reliability of the technology can be proven to decision makers and investors.

However, the method has not yet been deployed on a broad scale. Below is an outlook of promising further developments, structured into three groups: (1) Widespread validation, (2) Further method development and (3) Software tool development.

Widespread validation

- **Comparison of in-situ methods:** A long-term perspective is to standardize the method. Current developments regarding standardization are targeting in-situ performance. Since 2018, the ISO 9806 [10] method for single collector test is allowed to be performed either in the laboratory or in-situ. In the ISO/TC 180 standard under preparation [124] there is a new work item with a proposal for a simple method for checking collector array performance. The D-CAT method distinguished itself from the ISO 9806 [10] method by being applicable to the whole collector arrays rather than a single collector and from the ISO/TC 180 method by estimating parameters. Although these two methods in general are good approaches to in-situ testing, the use case not covered by these methods is a solar yield guarantee of the whole collector array, which is what really matters to investors. Standardization is a long-term perspective and first requires more practical experience and validation. A systematic comparison and possibly merge of in-situ test procedures for collector arrays would be a necessary and promising next step.
- **Application to more LST plants:** To spread the application and to validate the method, it is necessary to gain more practical experience with the method in terms of applying it a broader variety of plants. These plants should have different flat plate collector types, array geometries and hydraulic configurations, climatic conditions, operating strategies, measurement setups, etc. Given the current TRL level, this should be done within scientific research projects, where measurement data of large scale solar thermal plants have already been collected, like the project “Begleitforschung” for large solar thermal plants in Austria [125] [126]. However, initiatives on a European level would be preferable in order to include more data, widespread technologies and different climates. A web-based dissemination of solar thermal plants like solarheatdata.eu [47] could increase the transparency of in-situ performance, allow a transparent comparison of deployed collector arrays and increase the trust in the solar thermal technology.
- **Integration of other collector types:** In the current state of development, the D-CAT method is limited to flat plate collectors. This restriction was linked to the fact that for the MeQuSo project only measurements from flat-plate collector arrays at the FHW plant were available. The framework of the D-CAT method allows the extension to other collector types such as evacuated tube or CPC collectors. To do so, the the 2-N model (equations (12) and (13) in chapter 6.5) need to be adjusted with terms adapted to the respective collector types. This might require two-axis incidence angle modifiers, radiative heat losses, etc.

Further method development

- **External shading:** Another topic is the selection of operating conditions without external shading. If there is a software tool available to apply the D-CAT test, this might be the main effort in applying the method. Possible solutions might be (1) to use GIS tools, (2) automated detection of shading pattern by a camera mounted on site, or (3) an estimation of external shading pattern solely based on measurement data (reduced thermal power output) with a non-parametric model and the subsequent exclusion of these data, as described in [123]; a distinction between performance reductions by shading or other factors, however, might pose some challenges.
- **Parameter estimation:** The D-CAT method is based on parameter estimation in a numerically-solved nonlinear dynamic model; a multitude of difficulties are commonly reported in literature for such models (see [99], for instance). Overall, we can confirm these difficulties: Our experiences with the parameter estimation process indicate that some regularization methods might be required to improve the parameter estimation process and results, for instance variants of Tikhonov regularization as explained for a similar problem setup in [98]. A more comprehensive assessment of measurement and process noise would also deserve more attention, to state the D-CAT model as a stochastic state-space model. More sophisticated estimation maximum-likelihood or Bayes-based estimation techniques could be used, as formulated for instance in [61] [100] [101]. Further development of the method towards online application would be a very interesting extension, towards application in a real-time plant surveillance setting and online parameter estimation; the expertise in this field was limited within the MeQuSo project consortium. In order to do so, appropriate parameter estimation techniques, e.g. Kalman filter based methods, would be required. The methods explained in Sarkka [127] are based on the Unscented Kalman Filter (UKF) for state estimation of nonlinear systems and would be an improvement of the currently used technique in the D-CAT method.
- **Plant control:** As an outcome of a system test, D-CAT provides a reliable calibrated collector array model based on in-situ parameters. While model-based (predictive) control of solar plants is a somewhat studied field (see, for instance, [128] [129] [60] [130]), the outcomes of a D-CAT collector array test add knowledge and information that can be used to improve the control of LST systems: The use of a nonlinear model with calibrated parameters from in-situ operation for model-based (predictive) control is a new field of application yet to be established. Model-based control strategies typically use data sheet parameters which can be off. Using in-situ parameterization instead of data sheet parameters better represents the collector array and its outlet temperature. This could be used for model based (predictive) control, leading to more stable temperature output and increased energy yield. For control purposes, osne basic options is to use a nonlinear model such as the D-CAT 2-N model (see chapter 6.5), as described in de Andrade [131]. Another option is to linearize the nonlinear D-CAT 2-N model around the current operating point, or to use a more advanced approach such as multilinear model approximations as described in Pangalos [132].

Software tool development

- **Open source:** To arrive from a proof of concept to a widely-adopted test method, the authors recommend the development of a publicly available open source software tool. A central open source tool would decrease the overall implementation cost, make the method consistent, improve

software and method quality and ease the application. Such a tool also has the potential to improve the core software part (e.g. compiled, parallelized code) and to include improved modeling and parameter estimation theory.

- **Improved implementation:** The implementation of the D-CAT requires a common framework, which needs to cover data handling, modeling, optimal data selection and parameter estimation as main parts. While all these steps have been addressed and implemented in the MeQuSo project, an improved implementation relying on open source packages to be shared in the community would add value to the project results. To apply the D-CAT method, considerable computational effort is required, in particular for the global optimization. The main steps include data pre-processing and validation, pre-modeling data (e.g. radiation model), implementing the dynamic model, selecting test intervals and performing the parameter estimation. A more widespread application requires more expertise, mainly for improving the software part.

Nonlinear system identification is an active research topic, as documented in the 120-page document [133]. A central tool has the potential to include advances in the field, e.g. combinations of parameter estimation and machine learning [134]. The central tool should be based on an open source language like R or Python, and the implementation should rely on state-of-the-art and well-maintained open source software packages, particularly for the parameter estimation and uncertainty estimation parts. Among the options to be considered is the R package dMod [135]. Python has important packages like statsmodels [136] and PyMC3 [137], currently being released as PyMC4 and rebased on Tensorflow. The optimization part can rely on reliable packages like Pyomo [138] [139]. GEKKO [140] is emerging as a promising modeling and optimization suite. The software Dakota [141], developed by Sandia National Laboratories, is an open source software and was used by ISE in [142]; it is a feature-rich software but has a small user community compared to the options stated above.

Another option would be to implement the system in Modelica combined with one of the many optimization approaches such as JModelica or Optimica [143] [144] [145] [146]. Several authors have been working on parameter estimation approaches based on the general FMI standard; this is an active international research field with numerous approaches developed in the recent years [147] [148]. Bonvini [149] developed a UKF-based parameter estimation framework, Bonilla [150] an open source package called Optifmus, Vanfretti [151] the RaPIId toolbox. The state of development and maturity of these approaches and tools is very different, some have compatibility issues, some were merely prototypes, some have been abandoned at all. One of the more recent developments, ModestPy [152] – under development – seems to be a promising approach.

- **Graphical user interface (GUI):** A GUI for the D-CAT test would certainly help spread the method, enabling users with basic computer knowledge to apply the procedure. A GUI would also ease the standard task of configuring a collector array to apply the test. Another topic might be the development of an integrated software tool covering the life cycle of dimensioning, operation and monitoring of LST plants. This would allow to configure the tool just once; in order to apply the plant monitoring, it would be enough to just add the measurement data.
- **KPI calculation:** As an outcome of the D-CAT method, we have a calibrated physical model representing the plant operation over a very wide range of operating conditions. The calibrated model can be used in a simple forecasting tool (such as ScenoCalcFW [120], for instance), to calculate forecast KPIs such as solar energy yield and energy cost (LCOE). The model parameters estimation additionally delivers the uncertainty structure of the parameters. This information can be used together with an uncertainty propagation method (such as the Unscented Transform

[109], for instance) to quantify the uncertainty of an energy yield or other KPI forecast in terms of confidence intervals. This is a step of major importance: Being able to quantify forecast KPI uncertainty allows stakeholders to take informed, reliable decisions based on observed real-life operation of LST plants.

12 Appendix

12.1 List of abbreviations

<i>Abbreviation</i>	<i>Description</i>
D-CAT	Dynamic Collector Array Test
DNI	Direct normal irradiance
DSC	Dynamic solar collector (test method)
ESCo	Energy Service Company
FHW	Fernheizwerk (plant)
GUM	Guide to the expression of uncertainty in measurement
HD	Hay-Davies (model)
IAM	Incidence angle modifier
ICC	In-situ Collector Certification (test method)
ICCP	In-situ Check of Collector Array Performance (test method)
ICFT	In-situ Solar Collector Field Test (test method)
ISO	Isotropic (model) / International organization for standardization
ISTT	In-situ Short Term Testing (test method)
KPI	Key performance indicator
LCOE	Levelized cost of energy
LCOH	Levelized cost of heat
LST	Large solar thermal system
MLR	Mulitple linear regression
NDM	New dynamic method (test method)
ODE	Ordinary differential equation
O&M	Operation and maintenance
PDE	Partial differential equation
PC	Performance Check (test method)
RMSE	Root-mean-square error
QDT	Quasi-dynamic test
RDM	Radiation decomposition model
SDH	Solar district heating
TCM	Tilted collector model
TSM	Tilted sensor model
WLS	Weighted least squares

12.2 List of symbols

<i>Symbol</i>	<i>Description</i>	<i>Unit</i>
A	area	m^2
A_G	gross area of collector array	m^2
$A_{G,col}$	gross area of collector as defined in ISO 9488	m^2
A_i	anisotropy index	—
$A_{P,col}$	aperture area / absorber plate area of collector	m^2
a_1	<i>1-N model</i> : Collector heat loss coefficient at $\bar{T} - T_a = 0$ (as in QDT model of ISO 9806:2017 [10]) <i>2-N model</i> : Heat transfer coefficient from absorber to ambient at $T_m - T_f = 0$	$W/(m^2K)$ $W/(m^2K)$
a_2	<i>1-N model</i> : Temperature dependence of collector heat loss coefficient (as in QDT model of ISO 9806:2017 [10]) <i>2-N model</i> : Temperature dependence of heat transfer coefficient from absorber to ambient	$W/(m^2K^2)$ $W/(m^2K^2)$
a_3	wind speed dependence of the collector heat loss coefficient	$J/(m^3K)$
a_4	sky temperature dependence of the collector heat loss coefficient	—
a_5	effective thermal capacity of the collector	$J/(m^2K)$
a_6	wind speed dependence of the zero loss efficiency of the collector	s/m
a_7	wind speed dependence of infrared radiation exchange of the collector	$W/(m^2K^4)$
a_8	radiation losses of the collector	$W/(m^2K^4)$
ASL	sea level	m
b_0	incidence angle modifier (IAM)	—
c_f	specific heat capacity of fluid	$J/(kg K)$
D_{row}	row spacing of collector array	m
d_{sens}	distance of radiation sensor from collector plane	m
E_L	longwave irradiance, $\lambda > 3\mu m$	W/m^2
f_{save}	safety factor (for PC method)	—
F'	collector efficiency factor	—
F_{c-g}	view factor collector to ground	—
F_{c-s}	view factor collector to sky	—
F_R	collector heat removal factor	—
G, G_T	total / hemispherical solar irradiance on collectors (measured or corrected with radiation model)	W/m^2
G_H	total / hemispherical solar irradiance on horizontal plane	W/m^2
G_b, G_{bT}	direct solar irradiance on collectors	W/m^2
G_{bH}	direct solar irradiance on horizontal plane	W/m^2
G_c, G_{cT}	circumsolar irradiance on collectors	W/m^2
G_d	diffuse solar irradiance on collectors (measured or corrected with radiation model)	W/m^2

Table 14 – continued from previous page

Symbol	Description	Unit
$G_{d,avg}$	modeled average diffuse solar irradiance on the collectors, accounting for the obstructed sky and ground view for collectors within the array	W/m^2
G_{dH}	diffuse solar irradiance on horizontal plane	W/m^2
G_o	extraterrestrial radiation	W/m^2
H_{col}	collector height	m
H_{ground}	height of collectors above ground	m
H_s	shading height	m
h_{sens}	position of sensor relative to top of collector	m
K_b	incidence angle modifier for direct solar radiation	—
K_d	incidence angle modifier for diffuse radiation	—
k_T	clearness index	—
L	length	m
L_{col}	length of collector	m
L_{row}	length of collector row	m
L_s	length of shadow on collector row	m
\dot{m}	mass flow rate	kg/s
\dot{m}_l	mass flow rate through one absorber tube	kg/s
\dot{m}_{pri}	mass flow rate primary side (solar circuit)	kg/s
\dot{m}_{sec}	mass flow rate secondary side	kg/s
\dot{m}_{sp}	specific mass flow rate per collector area	$kg/(m^2s)$
(mc)	effective heat capacity of collector per collector area	$J/(m^2K)$
$(mc)_f$	effective heat capacity of collector heat transfer fluid per collector area	$J/(m^2K)$
$(mc)_m$	effective heat capacity of solid part of collector (array) per collector area	$J/(m^2K)$
(Mc)	total effective heat capacity of collector	J/K
$(Mc)_{fin}$	total effective heat capacity of one absorber fin per unit area	$J/(m^2K)$
$(Mc)_{\Delta x}$	total effective heat capacity of collector element	J/K
n_{col}	number of collectors in the collector array	—
n_{front}	number of front rows	—
n_{back}	number of back rows	—
\dot{Q}_{sp}	specific power output of collector (array)	W/m^2
\dot{Q}_{est}	estimated thermal power output of collector array (for PC method)	W/m^2
\dot{Q}_{sec}	power output on secondary side	W/m^2
R_b	ratio between beam radiation on the horizontal and the tilted surface	—
S, S_b	shading coefficient / shading share for beam radiation	—
S_d	shading coefficient / shading share for diffuse radiation	—
t	time	s
u	surrounding air speed	m/s
u'	reduced surroundings air speed: $u' = u - 3 \text{ m/s}$	m/s
\bar{T}	collector (array) mean temperature	$^{\circ}C$
T_a	ambient air temperature	$^{\circ}C$

Table 14 – continued from previous page

<i>Symbol</i>	<i>Description</i>	<i>Unit</i>
T_f	fluid temperature	$^{\circ}C$
$T_f(x, t)$	fluid temperature at position x in the collector array	$^{\circ}C$
$T_m(x, t)$	solid (metal) temperature at position x in the collector array	$^{\circ}C$
T_{in}	inlet temperature (of collector / collector array)	$^{\circ}C$
T_{out}	outlet temperature (of collector / collector array)	$^{\circ}C$
U_L	overall collector heat loss coefficient	$W/(m^2K)$
V_f	collector array fluid volume	m^3
\dot{V}	volume flow	m^3/s
\dot{V}_{sp}	specific volume flow per collector area	$m^3/(m^2s)$
w	distance between absorber tubes	m
W_{col}	collector thickness	m
x	axial co-ordinate along the flow direction	m
<i>Greek letters</i>		
α	convective heat transfer coefficient between T_m and T_f	$W/(m^2K)$
α'	volume flow dependence of convective heat transfer	$kg/(s^2m^3)$
β	tilt angle of collectors in array	rad
γ	azimuth of collector array	rad
ΔT	temperature difference	K
Δx	length of collector element	m
ζ	ground tilt angle	rad
$\eta_{0,b}$	peak collector efficiency ($\eta_{0,b}$ at $\bar{T} - T_a = 0$ K) on beam irradiance G_b	—
$\eta_{0,hem}$	peak collector efficiency ($\eta_{0,hem}$ at $\bar{T} - T_a = 0$ K) on hemispherical irradiance G	—
θ	parameter vector	—
θ_{col}	angle of incidence between sun and collector plane	rad
θ_z	incidence angle on horizontal surface	rad
κ_{sens}	external shadow angle	rad
λ	latitude	$^{\circ}$
ρ_f	fluid density	kg/m^3
ρ_g	ground reflectance coefficient	—
σ	standard deviation	—
σ_{SB}	Stefan-Boltzmann constant	$W/m^2 \cdot K^4$
$(\tau\alpha)$	effective transmittance absorptance product	—
ϕ	longitude	$^{\circ}$
ϕ_{st}	longitude of standard meridian	$^{\circ}$

12.3 List of figures

1	Risk sharing in large solar thermal projects: The main parties involved in the realization and operation of a large solar thermal plant (operator, investor, heat consumer etc.) interact in many ways along the project steps from planning phase to ongoing operation. This figure displays their interests and responsibilities.	11
2	System boundaries for test methods. The D-CAT method has the system boundaries “Collector array without distribution pipes”.	16
3	Comparison of monthly solar yield over 10 years. For one installation, the monthly solar yields are plotted over 10 years of operation. Grouping by month reveals outliers (e.g. May 2019) which need to be systematically analysed. Source: SOLID.	22
4	Thermal power output of a solar collector array vs. incoming radiation: The specific power output [W/m ²] (left axis) is plotted over one day and compared with the radiation on the collector array [W/m ²] (right axis). Source: SOLID.	22
5	Input-Output diagram [47] evaluation of the large scale solar thermal installation at Silkeborg.	23
6	Collector array of FHW plant with ground-mounted collectors. Source: SOLID, Picfly.at Thomas Eberhard.	26
7	Collector mountings at the FHW plant.	26
8	Measurement setup of the FHW plant, with sensor positions, position of solar tracker and webcam (adapted from <i>Google Maps</i>).	30
9	The volume flow sensors require settling sections upstream and downstream of the sensor.	31
10	Temperature measurement at the mixed outlet of all rows of one collector array (left). Temperature measurement between collectors (right).	31
11	Pyranometer (top left), ambient temperature sensor with ventilation unit (middle left), wind sensor (bottom left) and radiation platform including pyrhelimeter and unshaded and shaded pyranometer (right).	32
12	Mounting of webcam at FHW plant (left) and sample picture (right).	33
13	Thermodynamic properties of the FHW heat transfer fluid, compared to Tyfocor L [®] : density (left) and heat capacity (right).	34
14	View towards south with transport distribution pipe (left) and view towards west (right) of FHW plant.	34
15	Screenshot of the SketchUp 3D model for the FHW plant.	35
16	Periods with no external shading (top) and daily hours with shading-free periods (bottom) for the FHW plant.	36
17	Soiling of pyrhelimeter in winter (top left), broken glass of collector shortly after inauguration (top right), soiled collector (bottom).	37
18	Performance boundaries.	41
19	Calculation of model inputs for different measurement points.	42
20	Overview of the D-CAT method.	43
21	Low precision measurement setup.	45
22	High precision measurement setup.	46
23	Representation of FHW plant (with main vertices) as a graph in ADA.	49
24	Ambient temperature as an example of how RawDatapoints are implemented in ADA. Left: command window view with clickable links. Right: properties of the RawDatapoint object.	50

25	Model parameters of the QDT model depend on the chosen averaging time: Quadratic heat loss coefficient (a_2 , top) and heat capacity coefficient (a_5 , bottom) resulting from MLR regression are plotted over the chosen averaging time (x axis).	55
26	Exemplary application of the 1-N model to a 1-hour interval of data from one of the FHW collector arrays. While the modeled flow temperature roughly follows the measured temperature (upmost subplot), the model output shows some clear structural deficiencies (e.g. around 9:30).	57
27	Volume flow dependence of the convective heat transfer coefficient α on volume flow through a collector array. A simple linear correction model has been used in the present D-CAT 2-N model.	58
28	Histogram of wind speeds at the site of the FHW plant in Graz for the year 2018. Wind speeds are consistently in a very low range with practically no high wind speed data available at the FHW site; the same is true for the other two measured years, 2017 and 2019.	59
29	Schematic drawings of hydraulic setup of large-area harp collector (left) and exemplary collector array using harp collectors (right) [49]. The exact dimensions are not important here and are just exemplary values.	61
30	Comparison of collector row outlet temperatures and the mixed collector array outlet temperature. For one of the FHW collector arrays consisting of four collector rows, the four collector row outlet temperatures are plotted in the top subplot (dotted lines). The solid line is the array outlet temperature, measured after the four collector row mass flows are mixed; this is the temperature modeled by the D-CAT 2-N model. The subplot in the middle depicts the total collector array volume flow that results in fluctuating return temperatures. For less dynamic operating conditions, the travel time differences among the collector rows are much less significant.	62
31	Exemplary application of the 2-N model to the same collector array and the same 1-hour interval as in figure 26. Apparently, the 2-N model (with 100 numeric discretization compartments in flow direction) does not show the same structural deficiencies as the 1-N model and is capable of an accurate enough description of the flow temperature.	62
32	Domain of model validity for the D-CAT 2-N model: The requirements are that there is no shading on the tested collector array, and that the pump has been in operation for at least 5 min. All other dynamics (in radiation, volume flow and inlet temperature) are accepted.	63
33	Internal and external shading of FHW plant. The core area labelled “no shading” marks the data intervals that can be used with the D-CAT method for data selection and parameter estimation of the FHW collector arrays.	64
34	Uniform spatial grid along the collector array main flow direction, represented by the x axis (0 = collector array inlet, 1 = collector array outlet). Note the non-uniform grid at inlet and outlet of collector array.	66
35	Visual representation of the fluid temperatures (hidden states) along the main flow direction of a collector array, from inlet temperature (bottom) to outlet temperature (top)	67
36	Histogram of α , the convective heat transfer coefficient between metal and fluid part in the D-CAT 2-N model, calculated using the calculation drafted above.	69
37	Example of internal shading at the FHW plant and irradiance reductions (left) compared to a pyranometer placed on top of a collector row (right) lead to non-uniform irradiance distribution.	71

38	Overview radiation modeling.	72
39	Internal shading calculation [71].	73
40	Internal shading of the FHW plant.	73
41	Erbs correlation.	74
42	Radiation model with visualization of the discretization segments.	76
43	Reduction of the sky view factor along the collector height for 3 m and 6 m row spacing and 30°, 45° and 60° tilt (azimuth = 180° (south), height above ground = 43.5 cm, ground tilt = 0°, horizon view obstruction angle = 0°).	77
44	Reduction of the sky view factor along the collector height for 3 m row spacing (left) and 6 m row spacing (right) and 30° , 45° and 60° tilt, and 0° and 7° horizon view obstruction angle.	77
45	Problems with clustered and correlated measurement data, represented here by a cross-sectional plot of collector array temperature over total irradiance, based on 1-minute data for the year 2017.	83
46	Top: Collector array temperature vs. total radiation (same data as in figure 45), condensed here as 1-hourly mean values, so there is one dot for each of the approx. 500 candidate intervals. Bottom: Exemplary result of the optimal data selection process, selecting 25 out of the approx. 500 available intervals. The data selection gives precedence to the more extreme data.	85
47	Top subplot: Distribution of days containing at least one valid 1.5-hour interval for the collector array test. The period from October to mid-March had to be excluded due to shading. Bottom subplot: Distribution of the days containing one or more optimally-selected intervals, as described in chapter 8.2.	86
48	Distribution of the model predictors used in the D-CAT 2-N model, displayed as histograms and correlation plots. The top figure includes the full set of approx. 500 intervals available for one of the FHW collector arrays in one year of operation. The bottom figure includes the 20 optimally-selected intervals.	87
49	Histograms and covariances of the model parameters, based on the final estimation results for one collector array and one particular measurement season. The motivation and reasonings behind this plot are explained in chapter 8.3. The confidence regions were calculated following equation (41).	90
50	Illustration of the D-CAT parameter estimation process: Based on 9 model parameters, the collector array is simulated for each of the 20 optimally-selected measurement intervals. The WLS cost function is calculated using simulation output, target output and uncertainty from the experimental data. The optimizer proposes a new set of parameters and repeats the process until some cost minimum is found.	91
51	Visualization of the optimization process and estimated model parameters for one particular collector array, based on experimental data from one particular operating season.	92
52	Example output of the condition monitoring using the D-CAT method, displayed in terms of a classical collector efficiency curve. The curves compare data sheet behavior with efficiency behavior at commissioning and after several years of operation.	93
53	Dirt depositing on the outer collector cover is the main responsible for deteriorated incidence angle modifier (IAM) values. Right: Example output of IAM curves, comparing IAM values from the data sheet with the condition at plant commissioning and after 4 years operation, based on the estimated 2-N model parameter b_0	93

54	Histogram of model residuals, for one particular collector array and operating season, including all 20 selected optimal intervals. Mean and standard deviation are $\mu = 0.11$ K and $\sigma = 0.60$ K, respectively.	95
55	Histogram of model predictors of the D-CAT 2-N model. Top: All 479 available 1-hourly intervals for one collector array of the FHW plant, for one particular operating season. Bottom: Optimal data selection selects 20 out of the available intervals (see chapter 8.2). The clustering of input data (described in chapter 8.2) is visible in the top plot as non-uniform distributions. For instance, the top right histogram in the top plot has the temperature difference between collector metal and ambient temperature. Most intervals are around 55..70 K; the optimally-selected intervals are de-clustered and include more extreme data.	96
56	Plot of residuals vs. predictors (model inputs), for one particular collector array and one particular measurement data interval. The residuals plot shows the typical behavior, with higher residuals occurring mostly when radiation input has sharp changes coming from intermittent clouds.	97
57	Case A: Clear day with constant volume flow and small variations in inlet temperature. (1) Top subplot: Output of the calibrated 2-N model (continuous black line) compared to measured outlet temperatures (continuous red line: mixed array temperature, dashed lines: individual collector row temperatures). (2) Middle temperature subplot: Comparison of mixed collector array outlet temperature with model outputs: calibrated 2-N model, 1-N model and QDT model with data sheet parameters. (3) The three bottom subplots hold the model residuals for the compared models. The plots show structural model deficiencies of the 1-N and QDT models as well as considerable residuals due to difference between data sheet and in-situ performance.	99
58	Case B: Half-cloudy and half-clear day with some variability in volume flow and inlet temperature. For a general description of the plots, please refer to figure 57. Model deficiencies of the 1-N model become apparent mainly around volume flow changes (before 9:00) and around temperature changes (before 13:00). The 2-N model with calibrated parameters (continuous black line) closely follows the measured collector array outlet temperature (continuous red line) with small residuals.	100
59	Case C: Very variable day with high variability in radiation, volume flow and outlet temperature. For a general description of the plots, please refer to figure 57. Radiation levels are very different, in the chosen interval, ranging from fully diffuse radiation to high total radiation levels above 1000 W/m ² . Measured outlet temperatures show high variations, described with a reasonable goodness of fit by the calibrated 2-N model. This indicates the potential of using the D-CAT procedure in the context of plant control, in order to achieve more constant outlet temperatures based on model-based or model-predictive control.	101
60	Measured and modeled radiations for a sunny day. Top: Measured irradiance with pyranometer placed on top of the collector for total irradiance and pyrhelimeter for beam irradiance. Bottom: Deviations of measured vs. modeled average irradiance on the collectors.	102
61	Measured and modeled radiations for a cloudy day. Top: Measured irradiance with pyranometer placed on top of the collector for total irradiance and pyrhelimeter for beam irradiance. Bottom: Deviations of measured vs. modeled average irradiance on the collectors.	103

62	Measured and modeled total daily irradiance (no internal and external shading) absolute (top) and as a share of the measured irradiance (bottom).	104
63	Measured and modeled daily diffuse irradiance (no internal and external shading) absolute (top) and as a share of the measured irradiance (bottom).	104
64	Comparisons of measured thermal power and estimated thermal power based on the PC method. Left: Measured diffuse irradiance is used for thermal power estimation (no correction due to view obstructions in the collector array). Right: Modeled diffuse irradiance is used for thermal power estimation (accounting for view obstructions), which shifts the target/actual comparison in favor of the collectors.	105
65	Screenshot of FHW plant representation in ScenCalc FW.	107
66	Annual yield comparison with data sheet parameter and estimated parameter.	107

12.4 List of tables

1	Criteria for test procedure classification (D-CAT specifications in red italics).	15
2	Restrictions on operating conditions according to the PC method.	20
3	Overview of all collector types installed at the FHW plant.	27
4	Tilt, row spacing and height above ground for the measured collector arrays.	28
5	Sensors and data logging.	29
6	Measurement uncertainties for selected operating conditions.	38
7	Inputs for collector array model (core model).	42
8	Description of measurement setups.	46
9	Plant parameters.	48
10	Overview of the parameters used in the D-CAT 2-N model, equations (12) and (13).	60
11	Model parameter initialization approaches for the D-CAT 2-N model.	68
12	Interpretation of the estimated model parameters, referring to figure 51.	94

13 References

- [1] W. Weiss and M. Spörk-Dür, “Solar Heat Worldwide - Global Market Development and Trends in 2018 - Detailed Market Figures 2017,” 2019.
- [2] F. Mauthner, “Technical Report Subtask C – Part C,” p. 30,
- [3] I. E. Agency, *Recommendation: Converting solar thermal collector area into installed capacity (m² to kWh)*. Available online: https://www.iea-shc.org/Data/Sites/1/documents/statistics/Technical_Note-New_Solar_Thermal_Statistics_Conversion.pdf, 2004.
- [4] A. INTEC, *Calculation based on ‘Solar Heat Worldwide’ Editions 2012 - 2019*, 2019.
- [5] S. Fahr, D. Tschopp, J. E. Nielsen, K. Kramer, and P. Ohnewein, “Review of in situ Test Methods for Solar Thermal Installations,” 2019.
- [6] A. Müller, “Solargrids, Solarenergie und Wärmenetze: Optionen und Barrieren in einer langfristigen, integrativen Sichtweise,” Endbericht Projektnummer: FFG Nr. 834552, Nov. 29, 2014.
- [7] B. Perers, H. Zinko, and P. Holst, *Analytical Model for the Daily Energy Input Output Relationship for Solar Collector Systems*. Stockholm: Swedish Council for Building Research, 1985.
- [8] *TRNSYS 17. A transient system simulation program*. Solar Energy Laboratory, Univ. of Wisconsin-Madison, Madison, 2012.
- [9] *Polysun*, Winterthur: Vela Solaris AG, 2019.
- [10] *EN ISO 9806 Solar energy — Solar thermal collectors — Test methods*, 2017.
- [11] E. S. T. I. F. (ESTIF), “Solar Keymark Scheme Rules. SKN N0444R3. Edition 2019-12-12,” ESTIF, Brussels, 2019.
- [12] S. Fischer, “Europäischer Ringversuch von Sonnenkollektoren und Solaranlagen,” presented at the OTTI - 22. Symposium Thermische Solarenergie, Regensburg: Ostbayerisches Technologie-Transfer-Institut e.V. (OTTI), 2012.
- [13] C. A. Gueymard, “A review of validation methodologies and statistical performance indicators for modeled solar radiation data: Towards a better bankability of solar projects,” *Renewable and Sustainable Energy Reviews*, vol. 39, pp. 1024–1034, 2014.
- [14] J. A. Duffie and W. A. Beckman, *Solar Engineering of Thermal Processes*, 4th ed. Hoboken: John Wiley, 2013, 910 pp.
- [15] B. Perers, P. Kovacs, and U. Pettersson, “Experiences and lessons learned from 30 years of dynamic collector testing, modelling and simulation,” in *ISES Solar World Congress 2011*, 2011. [Online]. Available: http://orbit.dtu.dk/fedora/objects/orbit:71449/datastreams/file_6263097/content (visited on 2017-05-01).
- [16] T. Beikircher, N. Benz, M. Gut, P. Kronthaler, C. Oberdorf, W. Schölkopf, and H. Drück, “A short term test method for large installed solar thermal systems,” in *Proc. ISES Solar World Congress*, vol. 4, Citeseer, 1999. [Online]. Available: <http://citeseerx.ist.psu.edu/viewdoc/download?doi=10.1.1.460.9138&rep=rep1&type=pdf> (visited on 2017-02-22).
- [17] D. Thevenard and S. Pelland, “Estimating the uncertainty in long-term photovoltaic yield predictions,” *Solar Energy*, vol. 91, pp. 432–445, May 2013. DOI: [10.1016/j.solener.2011.05.006](https://doi.org/10.1016/j.solener.2011.05.006).

- [18] C. Kaltenecker, “Deriving a Minimum Acceptable Rate of Return on Equity for a Wind Farm from a Comprehensive Risk Model Using Monte Carlo Simulation,” TU Wien, Wien, 2012.
- [19] J.-O. Dalenbäck and S. Werner, “Solar District Heating - Boundary Conditions and Market Obstacles,” CIT Energy Management AB, Gothenburg, 2012.
- [20] PlanEnergi, *Solar District Heating - Inspiration and Experiences from Denmark*, 2018. [Online]. Available: <http://task55.iea-shc.org/Data/Sites/1/publications/SDH%20Inspiration%20Experience%20DK%20v5.pdf> (visited on 2019-05-29).
- [21] ISO/IEC, *ISO/IEC Directives. Part 2. Edition 8.0. 2018-05*, 2018.
- [22] D. C. Montgomery, *Design and Analysis of Experiments*, Eighth edition. Hoboken, NJ: John Wiley & Sons, Inc, 2013, 730 pp.
- [23] J. Fan, Z. Chen, S. Furbo, B. Perers, and B. Karlsson, “Efficiency and lifetime of solar collectors for solar heating plants,” in *ISES Solar World Congress 2009*, 2009, pp. 331–340. [Online]. Available: http://orbit.dtu.dk/fedora/objects/orbit:56322/datastreams/file_4035765/content (visited on 2017-04-04).
- [24] E. S. T. I. F. (ESTIF), “SOLAR KEYMARK Scheme Rules. SKY-1.5pt_-1.5ptNO444R1. Edition 2019-03-07,” ESTIF, Brussels, 2019.
- [25] (). Global Solar Certification Network (GSCN), [Online]. Available: <http://gscn.solar> (visited on 2020-02-22).
- [26] K. Kramer, S. Mehnert, K. Geimer, M. Reinhardt, S. Fahr, C. Thoma, P. Kovacs, and P. Ollas, “GUIDE TO STANDARD ISO 9806:2017 A Resource for Manufacturers, Testing Laboratories, Certification Bodies and Regulatory Agencies,” Fraunhofer ISE, Freiburg, 2017. [Online]. Available: <http://rgdoi.net/10.13140/RG.2.2.30241.30562> (visited on 2020-02-22).
- [27] J. Nayak and E. Amer, “Experimental and theoretical evaluation of dynamic test procedures for solar flat-plate collectors,” *Solar Energy*, vol. 69, no. 5, pp. 377–401, 2000. DOI: [10.1016/S0038-092X\(00\)00108-0](https://doi.org/10.1016/S0038-092X(00)00108-0).
- [28] B. Perers and H. Wallethun, “Dynamic collector models for 1 hr time step derived from measured outdoor data,” in *Energy Conservation in Buildings*, Elsevier, 1991, pp. 199–204. DOI: [10.1016/B978-0-08-037215-0.50041-9](https://doi.org/10.1016/B978-0-08-037215-0.50041-9).
- [29] B. Perers, “Dynamic method for solar collector array testing and evaluation with standard database and simulation programs,” *Solar Energy*, vol. 50, no. 6, pp. 517–526, Jun. 1, 1993. DOI: [10.1016/0038-092X\(93\)90114-4](https://doi.org/10.1016/0038-092X(93)90114-4).
- [30] B. Perers, “An improved dynamic solar collector test method for determination of non-linear optical and thermal characteristics with multiple regression,” *Solar Energy*, Selected Proceeding of ISES 1995: Solar World Congress. Part IV, vol. 59, no. 4, pp. 163–178, Apr. 1, 1997. DOI: [10.1016/S0038-092X\(97\)00147-3](https://doi.org/10.1016/S0038-092X(97)00147-3).
- [31] S. Fischer, W. Heidemann, H. Müller-Steinhagen, B. Perers, P. Bergquist, and B. Hellström, “Collector test method under quasi-dynamic conditions according to the European Standard EN 12975-2,” *Solar Energy*, vol. 76, no. 1-3, pp. 117–123, Jan. 2004. DOI: [10.1016/j.solener.2003.07.021](https://doi.org/10.1016/j.solener.2003.07.021).

- [32] S. Mehnert, F. Ise, S. Fischer, U. Fritzsche, M. J. Carvalho, C. Stadler, K. Vehring, and C. Lampe, "SKN-1.5pt_-1.5ptN0444-1.5pt_-1.5ptAnnex P5.5-1.5pt_-1.5ptIn-Situ Collector Certification-1.5pt_-1.5ptR0," Fraunhofer ISE, Freiburg im Breisgau, 2019.
- [33] E. Amer, J. Nayak, and G. Sharma, "A new dynamic method for testing solar flat-plate collectors under variable weather," *Energy Conversion and Management*, vol. 40, no. 8, pp. 803–823, May 1999. DOI: [10.1016/S0196-8904\(98\)00145-9](https://doi.org/10.1016/S0196-8904(98)00145-9).
- [34] W. Kong, B. Perers, J. Fan, S. Furbo, and F. Bava, "A new Laplace transformation method for dynamic testing of solar collectors," *Renewable Energy*, vol. 75, pp. 448–458, Mar. 2015. DOI: [10.1016/j.renene.2014.10.026](https://doi.org/10.1016/j.renene.2014.10.026).
- [35] B. Perers, P. Holst, and H. Zinko, "The Södertörn Solar District Heating Test Plant. Results 1982 - 1985. BFR 810939-4," Studsvik Energiteknik AB, Sweden, 1987.
- [36] J. Muschaweck and W. Spirkl, "Dynamic solar collector performance testing," *Solar Energy Materials and Solar Cells*, vol. 30, no. 2, pp. 95–105, 1993. DOI: [10.1016/0927-0248\(93\)90011-Q](https://doi.org/10.1016/0927-0248(93)90011-Q).
- [37] J. Nayak, E. Amer, and S. Deshpande, "Comparison of three transient methods for testing solar flat-plate collectors," *Energy Conversion and Management*, vol. 41, no. 7, pp. 677–700, May 2000. DOI: [10.1016/S0196-8904\(99\)00142-9](https://doi.org/10.1016/S0196-8904(99)00142-9).
- [38] P. Almeida, M. Carvalho, R. Amorim, J. Mendes, and V. Lopes, "Dynamic testing of systems – Use of TRNSYS as an approach for parameter identification," *Solar Energy*, vol. 104, pp. 60–70, Jun. 2014. DOI: [10.1016/j.solener.2014.02.010](https://doi.org/10.1016/j.solener.2014.02.010).
- [39] S. Fahr, U. Gumbel, A. Zirkel-Hofer, and K. Kramer, "In Situ Characterization of Thermal Collectors in Field Installations," in *Proceedings of EuroSun 2018*, Rapperswil, CH: International Solar Energy Society, 2018, pp. 1–10. DOI: [10.18086/eurosun2018.12.01](https://doi.org/10.18086/eurosun2018.12.01).
- [40] D.-T. D. Ltd, "User Manual for the Sunshine Pyranometer type SPN1. Version: 4.2. Download: https://www.delta-t.co.uk/wp-content/uploads/2019/06/SPN1_User_Manual_4.2.pdf," 2019.
- [41] M. Bosanac and J. E. Nielsen, "In situ check of collector array performance," *Solar Energy*, Selected Proceeding of ISES 1995: Solar World Congress. Part IV, vol. 59, no. 4–6, pp. 135–142, Apr. 1997. DOI: [10.1016/S0038-092X\(96\)00138-7](https://doi.org/10.1016/S0038-092X(96)00138-7).
- [42] W. Kong, S. Furbo, and B. Perers, "Development and validation of an in situ solar collector field test method," p. 28, 2019.
- [43] J. E. Nielsen and D. Trier, *Guaranteed power output. IEA-SHC TECH SHEETS 45.A.3.1. Available online: <http://task45.iea-shc.org/fact-sheets>*, 2014.
- [44] B. Epp. (2015). Germany: Solar District Heating Tenders with 3-Year Solar Yield Guarantee, [Online]. Available: <https://www.solarthermalworld.org/news/germany-solar-district-heating-tenders-3-year-solar-yield-guarantee> (visited on 2020-02-24).
- [45] T. Beikircher, N. Benz, M. Gut, C. Schwenk, and W. Schölkopf, "Entwicklung eines standardisierten Abnahmeverfahrens für solarthermische Großanlagen," Abschlussbericht, Feb. 2000.
- [46] P. Isaakson and L. O. Eriksoon, "MFC 1.0B. Matched Flow Collector Model for simulation and testing. User's manual. August 1993. Some errors corrected September 1994," Kungl Tekniska Högskolan, Stockholm, 1994.

- [47] (2020). Solarheatdata.eu, [Online]. Available: <http://solarheatdata.eu/> (visited on 2020-02-24).
- [48] I. Dresden, “Bestimmung von Dichte, Wärmekapazität, pH-Wert und Reservealkalität einer Kühlsole. Protokoll Nr.: 18-487.,” ILK Dresden, Dresden, 2019.
- [49] P. Ohnewein, R. Hausner, and D. Preiß, *ParaSol, Hydraulikdesign von parallelen Kollektormodulen in solarthermischen Großanlagen. Final project report*, 2015.
- [50] M. Fährlich, “Messen und Testen von Solarkollektorfeldern. Verhalten, Unsicherheiten und Abhängigkeiten von relevanten physikalischen Messgrößen im Solarkollektorfeld und deren Auswirkungen auf die Wärmeleistungsbestimmung,” Master thesis, Karl-Franzens-Universität, Graz, 2018.
- [51] (). GIS-Steiermark, [Online]. Available: <https://gis.stmk.gv.at> (visited on 2017-11-24).
- [52] I. G. 98-3:2008, *Uncertainty of Measurement - Part 3: Guide to the Expression of Uncertainty in Measurement*. Geneva: ISO, 2008.
- [53] J.-O. Dalenbäck, “Success Factors in Solar District Heating. WP 2- Micro Analyses Report. Deliverable D2.1,” CIT Energy Management AB, Gothenburg, Tech. Rep., 2010.
- [54] S. Furbo, J. Dragsted, B. Perers, E. Andersen, F. Bava, and K. P. Nielsen, “Yearly thermal performances of solar heating plants in Denmark – Measured and calculated,” *Solar Energy*, vol. 159, pp. 186–196, Jan. 1, 2018. DOI: [10.1016/j.solener.2017.10.067](https://doi.org/10.1016/j.solener.2017.10.067).
- [55] F. Vignola, J. Michalsky, and T. Stoffel, *Solar and Infrared Radiation Measurements*. CRC press, 2012.
- [56] P. Ohnewein, D. Tschopp, M. Hamilton-Jones, and H. Schrammel, *ADA Advanced Data Analysis*, AEE INTEC, 2017–2020.
- [57] P. Ohnewein, D. Tschopp, H. Schrammel, B. Gerardts, H. Poier, S. Krammer, A. Köstinger, and A. Weinappl, “METHODIQA. Methodik-Entwicklung zur Qualitätssicherung für Erneuerbare Wärme Systeme durch intelligentes Betriebsmonitoring,” AEE INTEC, Gleisdorf, 2016.
- [58] P. Ohnewein, H. Schrammel, D. Tschopp, S. Krammer, H. Poier, B. Gerardts, A. Köstinger, and A. Weinappl, “METHODIQA - Development of a Quality Assurance Methodology for Renewable Heat Systems Based on Intelligent Operational Monitoring,” *Energy Procedia*, vol. 91, pp. 376–383, Jun. 2016. DOI: [10.1016/j.egypro.2016.06.285](https://doi.org/10.1016/j.egypro.2016.06.285).
- [59] S. Kalogirou, E. Mathioulakis, and V. Belessiotis, “Artificial neural networks for the performance prediction of large solar systems,” *Renewable Energy*, vol. 63, pp. 90–97, Mar. 2014. DOI: [10.1016/j.renene.2013.08.049](https://doi.org/10.1016/j.renene.2013.08.049).
- [60] E. Camacho, F. Rubio, M. Berenguel, and L. Valenzuela, “A survey on control schemes for distributed solar collector fields. Part II: Advanced control approaches,” *Solar Energy*, vol. 81, no. 10, pp. 1252–1272, Oct. 2007. DOI: [10.1016/j.solener.2007.01.001](https://doi.org/10.1016/j.solener.2007.01.001).
- [61] L. J. Frölke, *Grey-box models for prediction and control of solar district heat plants*, 2018.
- [62] J. M. Lemos, R. Neves-Silva, and J. M. Igreja, *Adaptive Control of Solar Energy Collector Systems*, ser. Advances in Industrial Control. Cham: Springer International Publishing, 2014. [Online]. Available: <http://link.springer.com/10.1007/978-3-319-06853-4> (visited on 2017-06-14).
- [63] T. Tesfamichael and E. Wäckelgård, “Angular solar absorptance of absorbers used in solar thermal collectors,” *Applied Optics*, vol. 38, no. 19, p. 4189, Jul. 1, 1999. DOI: [10.1364/AO.38.004189](https://doi.org/10.1364/AO.38.004189).

- [64] W. Kamminga, “Experiences of a solar collector test method using fourier transfer functions,” *International Journal of Heat and Mass Transfer*, vol. 28, no. 7, pp. 1393–1404, 1984. DOI: [10.1016/0017-9310\(85\)90170-X](https://doi.org/10.1016/0017-9310(85)90170-X).
- [65] N. E. Wijesundera, M. N. A. Hawlader, and K. Y. Foong, “Estimation of Collector Performance Parameters From Daily System Tests,” *Journal of Solar Energy Engineering*, vol. 118, no. 1, pp. 30–36, Feb. 1, 1996. DOI: [10.1115/1.2847922](https://doi.org/10.1115/1.2847922).
- [66] J. Deng, R. Ma, G. Yuan, C. Chang, and X. Yang, “Dynamic thermal performance prediction model for the flat-plate solar collectors based on the two-node lumped heat capacitance method,” *Solar Energy*, vol. 135, pp. 769–779, Oct. 2016. DOI: [10.1016/j.solener.2016.06.060](https://doi.org/10.1016/j.solener.2016.06.060).
- [67] W. Kong, Z. Wang, J. Fan, P. Bacher, B. Perers, Z. Chen, and S. Furbo, “An improved dynamic test method for solar collectors,” *Solar Energy*, vol. 86, no. 6, pp. 1838–1848, Jun. 2012. DOI: [10.1016/j.solener.2012.03.002](https://doi.org/10.1016/j.solener.2012.03.002).
- [68] P. Ohnewein and R. Hausner, “A Novel Approach to the Analysis of Hydraulic Designs in Large Solar Collector Arrays,” *Engy Proced*, 2014. [Online]. Available: http://www.academia.edu/download/38735469/_ParaSol_SHC_paper_FINAL_2013-09-20.pdf (visited on 2017-03-24).
- [69] A. Vande Wouwer, P. Saucez, and C. Vilas, *Simulation of ODE/PDE Models with MATLAB®, OCTAVE and SCILAB*. Cham: Springer International Publishing, 2014. [Online]. Available: <http://link.springer.com/10.1007/978-3-319-06790-2> (visited on 2019-06-06).
- [70] P. Pierson and J. Padet, “Time constant of solar collectors,” *Solar Energy*, vol. 44, no. 2, pp. 109–114, 1990. DOI: [10.1016/0038-092X\(90\)90072-K](https://doi.org/10.1016/0038-092X(90)90072-K).
- [71] J. Bany and J. Appelbaum, “The effect of shading on the design of a field of solar collectors,” *Solar cells*, vol. 20, no. 3, pp. 201–228, 1987. [Online]. Available: <http://www.sciencedirect.com/science/article/pii/0379678787900299> (visited on 2017-02-23).
- [72] D. G. Erbs, S. A. Klein, and J. A. Duffie, “Estimation of the diffuse radiation fraction for hourly, daily and monthly-average global radiation,” *Solar energy*, vol. 28, no. 4, pp. 293–302, 1982. [Online]. Available: <http://www.sciencedirect.com/science/article/pii/0038092X82903024> (visited on 2017-02-27).
- [73] J. Orgill and K. Hollands, “Correlation equation for hourly diffuse radiation on a horizontal surface,” *Solar Energy*, vol. 19, no. 4, pp. 357–359, 1977. DOI: [10.1016/0038-092X\(77\)90006-8](https://doi.org/10.1016/0038-092X(77)90006-8).
- [74] D. Reindl, W. Beckman, and J. Duffie, “Diffuse fraction correlations,” *Solar Energy*, vol. 45, no. 1, pp. 1–7, 1990. DOI: [10.1016/0038-092X\(90\)90060-P](https://doi.org/10.1016/0038-092X(90)90060-P).
- [75] A. Skartveit, J. A. Olseth, and M. E. Tuft, “An hourly diffuse fraction model with correction for variability and surface albedo,” *Solar Energy*, vol. 63, no. 3, pp. 173–183, 1998.
- [76] J. Torres, M. De Blas, A. García, and A. de Francisco, “Comparative study of various models in estimating hourly diffuse solar irradiance,” *Renewable Energy*, vol. 35, no. 6, pp. 1325–1332, Jun. 2010. DOI: [10.1016/j.renene.2009.11.025](https://doi.org/10.1016/j.renene.2009.11.025).
- [77] J. E. Hay, “Calculation of monthly mean solar radiation for horizontal and inclined surfaces,” *Solar Energy*, vol. 23, no. 4, pp. 301–307, 1979. [Online]. Available: <http://www.sciencedirect.com/science/article/pii/0038092X79901233> (visited on 2017-02-27).

- [78] R. Perez, R. Seals, P. Ineichen, R. Stewart, and D. Menicucci, “A new simplified version of the Perez diffuse irradiance model for tilted surfaces,” *Solar energy*, vol. 39, no. 3, pp. 221–231, 1987. [Online]. Available: <http://www.sciencedirect.com/science/article/pii/S0038092X87800312> (visited on 2017-02-27).
- [79] R. Perez, R. Stewart, R. Seals, and Guertin, Ted, “The development and verification of the Perez diffuse radiation model. SAND88- 7030 Report.,” Sandia National Laboratories, Albuquerque and Livermore, SAND88-7030, 7024029, 1988. DOI: [10.2172/7024029](https://doi.org/10.2172/7024029).
- [80] R. Perez, P. Ineichen, R. Seals, J. Michalsky, and R. Stewart, “Modeling daylight availability and irradiance components from direct and global irradiance,” *Solar energy*, vol. 44, no. 5, pp. 271–289, 1990.
- [81] M. Lave, W. Hayes, A. Pohl, and C. W. Hansen, “Evaluation of Global Horizontal Irradiance to Plane-of-Array Irradiance Models at Locations Across the United States,” *IEEE Journal of Photovoltaics*, vol. 5, no. 2, pp. 597–606, Mar. 2015. DOI: [10.1109/JPHOTOV.2015.2392938](https://doi.org/10.1109/JPHOTOV.2015.2392938).
- [82] Z. Tian, B. Perers, S. Furbo, J. Fan, J. Deng, and J. Dragsted, “A Comprehensive Approach for Modelling Horizontal Diffuse Radiation, Direct Normal Irradiance and Total Tilted Solar Radiation Based on Global Radiation under Danish Climate Conditions,” *Energies*, vol. 11, no. 5, pp. 1–19, 2018. DOI: [10.3390/en11051315](https://doi.org/10.3390/en11051315).
- [83] Shah, Ramesh K. and Sekulic, Dusan P., *Fundamentals of Heat Exchanger Design*. Hoboken: John Wiley & Sons, 2003.
- [84] Borovský, David and Trier, Daniel, “Solar district heating guidelines. Fact sheet 7.4,” SDH, 2014.
- [85] J. E. Hesselgreaves, R. Law, and D. A. Reay, *Compact Heat Exchangers. Selection, Design and Operation. Second Edition*. Oxford: Butterworth-Heinemann, 2016.
- [86] T. R. Bott, *Fouling of Heat Exchangers*, ser. Chemical Engineering Monographs vol. 26. Amsterdam ; New York: Elsevier, 1995, 524 pp.
- [87] I. Gabrielaitiene, B. Bøhm, and B. Sunden, “Evaluation of Approaches for Modeling Temperature Wave Propagation in District Heating Pipelines,” *Heat Transfer Engineering*, vol. 29, no. 1, pp. 45–56, Jan. 2008. DOI: [10.1080/01457630701677130](https://doi.org/10.1080/01457630701677130).
- [88] M. Pasamontes, J. Álvarez, J. Guzmán, M. Berenguel, and E. Camacho, “Hybrid modeling of a solar-thermal heating facility,” *Solar Energy*, vol. 97, pp. 577–590, Nov. 2013. DOI: [10.1016/j.solener.2013.09.024](https://doi.org/10.1016/j.solener.2013.09.024).
- [89] L. Eriksson and U. AB, Eds., *Design of Experiments: Principles and Applications ; [IID 1016 ; Training Course]*, Umetrics Academy - Training in Multivariate Technology, Umea: Umetrics AB, 2000, 329 pp.
- [90] G. Franceschini and S. Macchietto, “Model-based design of experiments for parameter precision: State of the art,” *Chemical Engineering Science*, vol. 63, no. 19, pp. 4846–4872, Oct. 2008. DOI: [10.1016/j.ces.2007.11.034](https://doi.org/10.1016/j.ces.2007.11.034).
- [91] Y. Chu and J. Hahn, “Parameter set selection for estimation of nonlinear dynamic systems,” *AIChE Journal*, vol. 53, no. 11, pp. 2858–2870, Nov. 2007. DOI: [10.1002/aic.11295](https://doi.org/10.1002/aic.11295).
- [92] J. R. Banga, K. J. Versyck, and J. F. Van Impe, “Computation of Optimal Identification Experiments for Nonlinear Dynamic Process Models: A Stochastic Global Optimization Approach,” *Industrial & Engineering Chemistry Research*, vol. 41, no. 10, pp. 2425–2430, May 2002. DOI: [10.1021/ie010183d](https://doi.org/10.1021/ie010183d).

- [93] A. R. G. Mukkula and R. Paulen, “Optimal Experiment Design in Nonlinear Parameter Estimation with Exact Confidence Regions,” *Journal of Process Control*, S0959152419300241, Mar. 2019. DOI: [10.1016/j.jprocont.2019.01.004](https://doi.org/10.1016/j.jprocont.2019.01.004).
- [94] V. Fedorov, *Theory of Optimal Experiments (Review)*, ser. Biometrika 59(3). 1972.
- [95] F. Triefenbach, *Design of Experiments: The D-Optimal Approach and Its Implementation As a Computer Algorithm*, 2008.
- [96] L. Ljung, “System identification. Theory for the User,” *Prentice Hall*, 1999. [Online]. Available: http://www.academia.edu/download/34822687/Ljung_L_System_Identification_Theory_For_User.pdf (visited on 2017-07-18).
- [97] R. Isermann and M. Münchhof, *Identification of Dynamic Systems*. Berlin, Heidelberg: Springer Berlin Heidelberg, 2011. [Online]. Available: <http://link.springer.com/10.1007/978-3-540-78879-9> (visited on 2017-02-05).
- [98] A. Gábor and J. R. Banga, “Robust and efficient parameter estimation in dynamic models of biological systems,” *BMC Systems Biology*, vol. 9, no. 1, p. 74, Dec. 2015. DOI: [10.1186/s12918-015-0219-2](https://doi.org/10.1186/s12918-015-0219-2).
- [99] K. Schittkowski, *Numerical Data Fitting in Dynamical Systems: A Practical Introduction with Applications and Software*. 2002. [Online]. Available: <https://public.ebookcentral.proquest.com/choice/publicfullrecord.aspx?p=3073764> (visited on 2020-02-11).
- [100] H. Madsen, *Time Series Analysis*. CRC Press, 2007. [Online]. Available: <http://henrikmadsen.org/books/time-series-analysis/> (visited on 2017-03-24).
- [101] J. L. Crassidis and J. L. Junkins, “Optimal Estimation of Dynamic Systems,” p. 750, 2012.
- [102] J. R. Donaldson and R. B. Schnabel, “Computational experience with confidence regions and confidence intervals for nonlinear least squares,” *Technometrics*, vol. 29, no. 1, pp. 67–82, 1987.
- [103] M. Schwaab, E. C. Biscaia Jr., J. L. Monteiro, and J. C. Pinto, “Nonlinear parameter estimation through particle swarm optimization,” *Chemical Engineering Science*, vol. 63, no. 6, pp. 1542–1552, Mar. 2008. DOI: [10.1016/j.ces.2007.11.024](https://doi.org/10.1016/j.ces.2007.11.024).
- [104] E. M. L. Beale, “Confidence regions in non-linear estimation,” *Journal of the Royal Statistical Society: Series B (Methodological)*, vol. 22, no. 1, pp. 41–76, 1960.
- [105] A. Zirkel-Hofer, S. Perry, S. Fahr, K. Kramer, A. Heimsath, S. Scholl, and W. Platzer, “Improved in situ performance testing of line-concentrating solar collectors: Comprehensive uncertainty analysis for the selection of measurement instrumentation,” *Applied Energy*, vol. 184, pp. 298–312, Dec. 2016. DOI: [10.1016/j.apenergy.2016.09.089](https://doi.org/10.1016/j.apenergy.2016.09.089).
- [106] S. Julier, “A General Method for Approximating Nonlinear Transformations of Probability Distributions,” p. 27, 1996.
- [107] S. J. Julier and J. K. Uhlmann, “New extension of the Kalman filter to nonlinear systems,” in *Signal Processing, Sensor Fusion, and Target Recognition VI*, vol. 3068, International Society for Optics and Photonics, Jul. 28, 1997, pp. 182–194. DOI: [10.1117/12.280797](https://doi.org/10.1117/12.280797).
- [108] E. A. Wan and R. Van Der Merwe, “The unscented Kalman filter for nonlinear estimation,” in *Adaptive Systems for Signal Processing, Communications, and Control Symposium 2000. AS-SPCC. The IEEE 2000*, Ieee, 2000, pp. 153–158. [Online]. Available: <http://ieeexplore.ieee.org/abstract/document/882463/> (visited on 2017-06-09).

- [109] S. Julier and J. Uhlmann, “Unscented Filtering and Nonlinear Estimation,” *Proceedings of the IEEE*, vol. 92, no. 3, pp. 401–422, Mar. 2004. DOI: [10.1109/JPROC.2003.823141](https://doi.org/10.1109/JPROC.2003.823141).
- [110] C. G. Moles, “Parameter Estimation in Biochemical Pathways: A Comparison of Global Optimization Methods,” *Genome Research*, vol. 13, no. 11, pp. 2467–2474, Nov. 1, 2003. DOI: [10.1101/gr.1262503](https://doi.org/10.1101/gr.1262503).
- [111] I. Boussaïd, J. Lepagnot, and P. Siarry, “A survey on optimization metaheuristics,” *Information Sciences*, vol. 237, pp. 82–117, Jul. 2013. DOI: [10.1016/j.ins.2013.02.041](https://doi.org/10.1016/j.ins.2013.02.041).
- [112] M. Rodriguez-Fernandez, P. Mendes, and J. R. Banga, “A hybrid approach for efficient and robust parameter estimation in biochemical pathways,” *Biosystems*, vol. 83, no. 2-3, pp. 248–265, Feb. 2006. DOI: [10.1016/j.biosystems.2005.06.016](https://doi.org/10.1016/j.biosystems.2005.06.016).
- [113] F. Marini and B. Walczak, “Particle swarm optimization (PSO). A tutorial,” *Chemometrics and Intelligent Laboratory Systems*, vol. 149, pp. 153–165, Dec. 2015. DOI: [10.1016/j.chemolab.2015.08.020](https://doi.org/10.1016/j.chemolab.2015.08.020).
- [114] R. Eberhart and J. Kennedy, “Particle swarm optimization,” in *Proceedings of the IEEE International Conference on Neural Networks*, vol. 4, Citeseer, 1995, pp. 1942–1948.
- [115] A. I. F. Vaz and L. N. Vicente, “A particle swarm pattern search method for bound constrained global optimization,” *Journal of Global Optimization*, vol. 39, no. 2, pp. 197–219, Sep. 4, 2007. DOI: [10.1007/s10898-007-9133-5](https://doi.org/10.1007/s10898-007-9133-5).
- [116] I. Vaz. (Feb. 11, 2020). PSwarm Solver Homepage, [Online]. Available: <http://www.norg.uminho.pt/aivaz/pswarm/> (visited on 2020-02-11).
- [117] L. M. Rios and N. V. Sahinidis, “Derivative-free optimization: A review of algorithms and comparison of software implementations,” *Journal of Global Optimization*, vol. 56, no. 3, pp. 1247–1293, Jul. 2013. DOI: [10.1007/s10898-012-9951-y](https://doi.org/10.1007/s10898-012-9951-y).
- [118] (). ScenoCalc tool, description on the ESTIF webpage about the Solar Keymark.
- [119] *ScenoCalcFW Handbuch*. [Online]. Available: <https://www.scfw.de/> (visited on 2020-02-25).
- [120] (). ScenoCalc Fernwärme, Ertragsvorhersagetool für Solarthermieanlagen in Wärmenetzen, [Online]. Available: <https://www.scfw.de/> (visited on 2020-02-25).
- [121] (). Meteonorm Software, [Online]. Available: <https://meteonorm.com/> (visited on 2020-02-25).
- [122] *AirShield® DNI. Soiling Prevention System for Pyrheliometer*, 2020. [Online]. Available: <https://www.kippzonen.com/Download/965/AirShield-Handout> (visited on 2020-02-25).
- [123] P. Bacher and H. Madsen, “Models for efficient integration of solar energy,” 2012.
- [124] ISO, *ISO/TC 180/SC Solar energy - Collector fields - Check of Performance. Version 07.1a*, 2019.
- [125] C. Fink, S. Knabl, R. Stelzer, B. Windholz, and F. Helminger, “Aggregierte Ergebnisse aus der wissenschaftlichen Begleitung des Förderprogramms „Solare Großanlagen“ in Österreich,” presented at the OTTI 27. Symposium Thermische Solarenergie, Bad Staffelstein, Deutschland, 2017.
- [126] C. Fink, S. Knabl, W. Wagner, R. Stelzer, B. Windholz, P. Schöffmann, and M. Hartl, “Aggregierte Ergebnisse zum Projekt WISSENSCHAFTLICHE BEGLEITFORSCHUNG ZUM FÖRDERPROGRAMM „SOLARTHERMIE – SOLARE GROßANLAGEN “ 2010-2014,” AEE INTEC, Gleisdorf, 2015.
- [127] S. Sarkka, “On Unscented Kalman Filtering for State Estimation of Continuous-Time Nonlinear Systems,” *IEEE Transactions on Automatic Control*, vol. 52, no. 9, pp. 1631–1641, Sep. 2007. DOI: [10.1109/TAC.2007.904453](https://doi.org/10.1109/TAC.2007.904453).

- [128] E. F. Camacho, M. Berenguel, F. R. Rubio, and D. Martínez, *Control of Solar Energy Systems*, ser. Advances in Industrial Control. London: Springer London, 2012. [Online]. Available: <http://link.springer.com/10.1007/978-0-85729-916-1> (visited on 2017-02-01).
- [129] M. Berenguel and F. R. Rubio, *Advanced Control of Solar Plants*. Springer Science & Business Media, 2012.
- [130] E. Camacho, F. Rubio, M. Berenguel, and L. Valenzuela, “A survey on control schemes for distributed solar collector fields. Part I: Modeling and basic control approaches,” *Solar Energy*, vol. 81, no. 10, pp. 1240–1251, Oct. 2007. DOI: [10.1016/j.solener.2007.01.002](https://doi.org/10.1016/j.solener.2007.01.002).
- [131] G.A. de Andrade, J. Álvarez, D. Pagano, and M. Berenguel, “Nonlinear controllers for solar thermal plants: A comparative study,” *Control Engineering Practice*, vol. 43, pp. 12–20, Oct. 2015. DOI: [10.1016/j.conengprac.2015.06.002](https://doi.org/10.1016/j.conengprac.2015.06.002).
- [132] G. Pangalos, G. Lichtenberg, and H. Werner, *Model-based controller design methods for heating systems*, in collab. with T. U. Hamburg-Harburg and T. U. Hamburg-Harburg. Berlin: epubli, 2016, 174 pp.
- [133] J. Schoukens and L. Ljung, “Nonlinear System Identification: A User-Oriented Roadmap,” Feb. 2, 2019. arXiv: [1902.00683](https://arxiv.org/abs/1902.00683) [cs]. [Online]. Available: <http://arxiv.org/abs/1902.00683> (visited on 2019-12-11).
- [134] A. Svensson, “Machine learning with state-space models, Gaussian processes and Monte Carlo methods,” p. 240,
- [135] D. Kaschek, W. Mader, M. Fehling-Kaschek, M. Rosenblatt, and J. Timmer, “Dynamic Modeling, Parameter Estimation, and Uncertainty Analysis in R,” *Journal of Statistical Software*, vol. 88, no. 10, 2019. DOI: [10.18637/jss.v088.i10](https://doi.org/10.18637/jss.v088.i10).
- [136] C. Fulton, “Estimating time series models by state space methods in Python: Statsmodels,” p. 78,
- [137] J. Salvatier, T. V. Wiecki, and C. Fonnesbeck, “Probabilistic programming in Python using PyMC3,” *PeerJ Computer Science*, vol. 2, e55, Apr. 6, 2016. DOI: [10.7717/peerj-cs.55](https://doi.org/10.7717/peerj-cs.55).
- [138] W. E. Hart, C. D. Laird, J.-P. Watson, D. L. Woodruff, G. A. Hackebeil, B. L. Nicholson, and J. D. Siirola, *Pyomo-Optimization Modeling in Python*. Springer, 2017, vol. 67.
- [139] K. A. Klise, B. L. Nicholson, A. Staid, and D. L. Woodruff, “Parmest: Parameter Estimation Via Pyomo,” in *Computer Aided Chemical Engineering*, ser. Proceedings of the 9 International Conference on Foundations of Computer-Aided Process Design, S. G. Muñoz, C. D. Laird, and M. J. Realff, Eds., vol. 47, Elsevier, Jan. 1, 2019, pp. 41–46. DOI: [10.1016/B978-0-12-818597-1.50007-2](https://doi.org/10.1016/B978-0-12-818597-1.50007-2).
- [140] L. Beal, D. Hill, R. Martin, and J. Hedengren, “GEKKO Optimization Suite,” *Processes*, vol. 6, no. 8, p. 106, Jul. 31, 2018. DOI: [10.3390/pr6080106](https://doi.org/10.3390/pr6080106).
- [141] M. S. Eldred, K. R. Dalbey, W. J. Bohnhoff, B. M. Adams, L. P. Swiler, P. D. Hough, D. M. Gay, J. P. Eddy, and K. H. Haskell, “DAKOTA : A multilevel parallel object-oriented framework for design optimization, parameter estimation, uncertainty quantification, and sensitivity analysis. Version 5.0, user’s manual.,” SAND2010-2183, 991842, May 1, 2010, SAND2010–2183, 991 842. [Online]. Available: <http://www.osti.gov/servlets/purl/991842-xggRJI/> (visited on 2019-05-22).
- [142] A. Hofer, D. Büchner, K. Kramer, S. Fahr, A. Heimsath, W. Platzer, and S. Scholl, “Comparison of Two Different (Quasi-) Dynamic Testing Methods for the Performance Evaluation of a Linear Fresnel Process Heat Collector,” *Energy Procedia*, vol. 69, pp. 84–95, May 2015. DOI: [10.1016/j.egypro.2015.03.011](https://doi.org/10.1016/j.egypro.2015.03.011).

- [143] A. Modelon, “JModelica.org user guide: Version 1.17. 175 pp,” 2016. [Online]. Available: <http://www.jmodelica.org/api-docs/usersguide/JModelicaUsersGuide-1.17.pdf>.
- [144] J. Åkesson, K.-E. Årzén, M. Gäfvert, T. Bergdahl, and H. Tummescheit, “Modeling and optimization with Optimica and JModelica.org—Languages and tools for solving large-scale dynamic optimization problems,” *Computers & Chemical Engineering*, vol. 34, no. 11, pp. 1737–1749, Nov. 2010. DOI: [10.1016/j.compchemeng.2009.11.011](https://doi.org/10.1016/j.compchemeng.2009.11.011).
- [145] G. Schweiger, H. Runvik, F. Magnusson, P.-O. Larsson, and S. Velut, “Framework for dynamic optimization of district heating systems using Optimica Compiler Toolkit,” presented at the The 12th International Modelica Conference, Prague, Czech Republic, May 15-17, 2017, Jul. 4, 2017, pp. 131–139. DOI: [10.3384/ecp17132131](https://doi.org/10.3384/ecp17132131).
- [146] E. Palmkvist, “Implementation of Grey-Box Identification in JModelica.org,” 2014. [Online]. Available: <http://lup.lub.lu.se/student-papers/record/4465456> (visited on 2017-03-28).
- [147] S. Gedda, C. Andersson, J. Åkesson, and S. Diehl, “Derivative-free Parameter Optimization of Functional Mock-up Units,” in *Proceedings of the 9th International MODELICA Conference; September 3-5; 2012; Munich; Germany*, Linköping University Electronic Press, 2012, pp. 819–828. [Online]. Available: <http://www.ep.liu.se/ecp/076/084/ecp12076084.pdf> (visited on 2017-04-25).
- [148] R. Kampfmann, N. Menager, and D. Mösch, “Parameter Estimation based on FMI,” presented at the 12th International Modelica Conference, Prague, May 15, 2017.
- [149] M. Bonvini, M. Wetter, and M. D. Sohn, “An FMI-based Framework for State and Parameter Estimation,” Mar. 10, 2014, pp. 647–656. DOI: [10.3384/ecp14096647](https://doi.org/10.3384/ecp14096647).
- [150] J. Bonilla, M. Berenguel, J. A. Carballo, and L. Roca, “Development of an open source multi-platform software tool for parameter estimation studies in FMI models,” presented at the 12th International Modelica Conference, Prague, May 15, 2017.
- [151] L. Vanfretti, M. Baudette, A. Amazouz, T. Bogodorova, T. Rabuzin, J. Lavenius, and F. J. Gómez-López, “RaPIId: A modular and extensible toolbox for parameter estimation of Modelica and FMI compliant models,” *SoftwareX*, vol. 5, pp. 144–149, 2016. DOI: [10.1016/j.softx.2016.07.004](https://doi.org/10.1016/j.softx.2016.07.004).
- [152] K. Arendt, M. Jradi, M. Wetter, and C. T. Veje, “Modesty: An open-source python tool for parameter estimation in functional mock-up units,” in *Proceedings of The American Modelica Conference 2018, October 9-10, Somberg Conference Center, Cambridge MA, USA*, Linköping University Electronic Press, 2019, pp. 121–130.

14 Contact

Project manager

DI Philip Ohnewein

p.ohnewein@aee.at

Phone: +43 (0) 3112-5886-0, ext. 255

Institute

AEE – Institute for Sustainable Technologies (AEE INTEC)

Feldgasse 19, A-8200 Gleisdorf

Fax: +43 (0) 3112-5886-18

<https://www.aee-intec.at/>

Project partners

GREENoneTEC Solarindustrie GmbH

KBB Kollektorbau GmbH

ÖkoTech Solarkollektoren GmbH

SOLID Solar Energy Systems GmbH (formerly S.O.L.I.D. Gesellschaft für Solarinstallation und Design mbH)